Development and Application of Analytical Derivative Methods in Ab Initio Crystal Orbital Theory

So Hirata

Doctor of Philosophy

Department of Structural Molecular Science
School of Mathematical and Physical Science
The Graduate University for Advanced Studies

1998

Contents

List of publication

So Hirata, Hajime Torii, and Mitsuo Tasumi, "Density-functional crystal orbital study on the structures and energetics of polyacetylene isomers," Phys. Rev. B, **57**(19), 11994–12001 (1998).

So Hirata and Suehiro Iwata, "Density functional crystal orbital study on the normal vibrations of polyacetylene and polymethineimine," J. Chem. Phys., **107**(23), 10075–10084 (1997).

So Hirata and Suehiro Iwata, "Density functional crystal orbital study on the normal vibrations and phonon dispersion curves of all-*trans*-polyethylene," J. Chem. Phys., **108**(18), 7901–7908 (1998).

So Hirata and Suehiro Iwata, "Ab initio Hartree–Fock and density functional studies on the structures and vibrations of an infinite hydrogen fluoride polymer," J. Phys. Chem. A, in press.

So Hirata and Suehiro Iwata, "Analytical second derivatives in ab initio Hartree–Fock crystal orbital theory of polymers," J. Mol. Struct. (THEOCHEM) (Special issue for Prof. Shigeru Huzinaga), in press.

So Hirata and Suehiro Iwata, "Analytical energy gradients in second-order Møller–Plesset perturbation theory for extended systems," J. Chem. Phys., in press.

Other publication

So Hirata, Hiroshi Yoshida, Hajime Torii, and Mitsuo Tasumi, "Vibrational analyses of *trans,trans*-1,3,5,7-octatetraene and all-*trans*-1,3,5,7,9-decapentaene based on ab initio molecular orbital calculations and observed infrared and Raman spectra," J. Chem. Phys., **103**(20), 8955–8963 (1995).

So Hirata, Hajime Torii, and Mitsuo Tasumi, "Vibrational analyses of *trans*-poly-acetylene based on ab initio second-order Møller–Plesset perturbation calculations of *trans*-oligoenes," J. Chem. Phys., **103**(20), 8964–8979 (1995).

So Hirata, Hajime Torii, Yukio Furukawa, Mitsuo Tasumi, and John Tomkinson, "Inelastic neutron scattering from *trans*-polyacetylene," Chem. Phys. Lett., **261**, 241–245 (1996).

So Hirata, Hajime Torii, and Mitsuo Tasumi, "Stereostructural and vibrational analyses of *cis*-polyacetylene based on density functional calculations of oligoenes," Bull. Chem. Soc. Jpn., **69**(11), 3089–3106 (1996).

Chapter 1

General introduction

The importance of the analytical-derivative methods [1–6] has been widely recognized by the computational quantum chemistry community since Pulay [7] first implemented the analytical first derivatives of the Hartree–Fock (HF) energy with respect to nuclear coordinates. The negatives of first derivatives correspond to the forces exerted on the nuclei by the presence of electrons and other nuclei, and they are essential in locating stationary points on the potential energy surfaces. The analytical-derivative method developed by Pulay enabled the evaluation of the forces on the nuclei with increased computational efficiency and increased numerical precision as compared to the earlier finite-difference method.

Inherent efficiency and accuracy of the analytical-derivative methods as demonstrated by Pulay have propelled computational quantum chemists to develop analytical methods for evaluating the higher-order energy derivatives and derivatives of correlation energies. Second and higher derivatives of energy are essential in studying the internal motions of molecular systems in the vicinity of their equilibrium geometries. In many problems, nuclear displacements are not very large around the equilibrium geometry, and the potential energy surface can be suitably expanded in a Taylor series, the coefficients of which are the energy derivatives with respect to nuclear coordinates. The energy second derivatives correspond to the quadratic force constants and are used in determining the normal modes of molecular vibrations in the harmonic approximation. Higher-order derivatives such as cubic and quartic force constants provide direct information about the anharmonic contributions to the vibrational frequencies.

The first practical implementation of the analytical second derivatives of the HF energy was reported by Pople *et al.* [8]. The derivatives of molecular orbital coefficients, which are required in the analytical evaluation of the energy second derivatives, are obtained as solutions to the coupled perturbed Hartree–Fock (CPHF) equation first derived by Gerratt and Mills [9]. The use of analytical second derivatives has turned out to be less expensive than the use of finite differences, contrary to earlier skepticism [1]. So far the analytical third derivatives of the HF energy have already been implemented by Gaw *et al.* [10].

One of the representative methods which are widely used in describing dynamical electron correlation is based on second-order Møller–Plesset perturbation theory [11–15]. This method, which is frequently abbreviated to MP2, accounts for typically 90 % of the dynamical correlation energy and has correct scaling with the size of systems ("size-

Table 1.1 Energy derivatives with respect to external parameters and related molecular properties.

Energy derivatives[a]	Property	
$\partial E/\partial Q$	Forces	Geometry optimization
$\partial^2 E/\partial Q_i \partial Q_j$	Force constants	Harmonic vibrational frequencies
		Geometry optimization
		Characterization of stationary points
$\partial^3 E/\partial Q_i \partial Q_j \partial Q_k$	Cubic force constants	Anharmonic vibrational frequencies
$\partial^4 E/\partial Q_i \partial Q_j \partial Q_k \partial Q_l$	Quartic force constants	Anharmonic vibrational frequencies
$\partial^2 E/\partial Q_i \partial F_\alpha$	Dipole moment derivatives	Infrared intensities
$\partial^2 E/\partial Q_i \partial F_\alpha \partial F_\beta$	Polarizability derivatives	Raman intensities

[a] E denote the energy and Q_i and F_α represent a nuclear coordinate and an electric field component, respectively.

extensivity") [15,16]. The first implementation of the MP2 first derivatives is due to Pople *et al.* [8], and an analytical-second-derivative scheme has also been developed by Handy *et al.* [17]. Analytical first derivatives are available also for higher-order Møller–Plesset perturbation theories [18,19] and other conventional correlated theories such as configuration interaction [20,21] and coupled cluster [22] theories. In the last decade, density functional theory has proven a very promising correlated method for describing the properties of molecules in the ground electronic states [23–25]. Density functional theory can take into account electron correlation with relatively small computational costs, which are in the same order of magnitude as the costs needed for HF calculations. Analytical first derivatives of density functional energy were implemented by Satoko [26], who employed $X\alpha$ functional. Later Johnson *et al.* [27,28] developed an analytical-first-derivative scheme for local, gradient-corrected, and hybrid exchange-correlation functionals. Analytical second derivatives of the density functional energy were implemented by Johnson and Frisch [29,30].

These analytical-derivative methods constitute an essential part of modern molecular orbital theory, and the structures, dynamics, reactions, and other properties of various molecular systems are now routinely studied with them. Correlation between the energy derivatives with respect to external parameters and molecular properties is summarized in Table 1.1, where electric field components are included among the external parameters.

Constant efforts have been made to extend the applicability of the existing electronic structure methods to larger molecules than could previously be treated. One of the most successful examples is the development of crystal orbital theory [31–33], which provides an

ab initio method of calculating the electronic and structural properties of infinite lattices. The underlying ideas of crystal orbital theory are to fully utilize the periodicity of lattices and to pre-screen long-range integrals which we can safely expect to give insignificant contributions to Fock matrix elements and to total energies.

General linear-combination-of-atomic-orbital (LCAO) self-consistent-field formalisms for infinite lattices have been derived independently by Del Re *et al.* [34] and by André *et al.* [35]. These formalisms correspond essentially to the spin-restricted Roothaan–Hall formalism [36,37] for closed-shell molecules. These authors have shown that Fock and overlap matrices of infinite lattices could be brought to a block-diagonal form by transforming the basis sets from localized atomic basis functions to delocalized Bloch basis functions. Therefore, instead of solving a matrix equation of an infinite dimension, we have only to deal with wavevector-dependent matrix equations of finite dimensions. A crystal orbital program based on these formalisms has been developed by André [38].

Crystal orbital calculations involve infinite summations of Coulomb and exchange matrix elements, which pose a considerably difficult problem [31,33]. In practical calculations, these summations are truncated after several neighboring unit cells, and the long-range contributions are usually neglected. Convergence behavior of these summations with respect to the number of included neighbors is dependent on the system and on the method of truncating the infinite summations [39–41]. Considerable progress has been achieved by Delhalle *et al.* [42] in treating the Coulomb lattice summations, which converge in the same manner as do usual Madelung summations. These authors have approximated the long-range electrostatic contributions to these summations using multipole expansion technique. They have also proposed a new method of truncating the lattice summations, which was not only ideally fit for the multipole expansion technique but also gave the fastest convergence for the Coulomb and exchange lattice summations among the truncation methods proposed so far [41]. Convergence of the exchange lattice summations is strongly influenced by the asymptotics of density matrix elements [31]. For the systems with nonzero band gaps, the density matrix elements decay exponentially [43,44], and hence we can expect to obtain converged exchange lattice summations within several neighbors. A significant amount of numerical data on different systems at the HF level has been accumulated [39–41], and the convergence behavior of the energetic and structural properties is now relatively well understood for one-dimensional lattices.

In the molecular orbital formalisms, various approximation methods have been ad-

vocated to account for electron correlation. Among them only the size-extensive [15,16] methods can be applied to infinite lattices. Configuration interaction, which is one of the most frequently used correlated theories for molecules, is not size-extensive. This means that a given level of approximation, e.g., configuration interaction doubles, yields less and less correlation energy per electron if the number of electrons increases. In the limit of infinite lattices, the electron correlation energy obtained with any truncated configuration interaction method will vanish. Size-extensive methods include Møller–Plesset perturbation theory, coupled cluster theory, and density functional theory.

The use of MP2 theory for describing dynamical electron correlation in infinite lattices was pioneered by Suhai [45]. Correlation energy was obtained by considering localized excitation between the Wannier functions constructed from different energy bands. An alternative approach to obtain the MP2 energy for infinite lattices, which used the canonical Bloch functions as zeroth-order wave functions, has also been proposed [45]. Suhai has further developed a method to obtain one-electron energy bands which incorporated the electron-correlation effects on the basis of the "electronic polaron" model of Toyozawa [46] (see also Refs. [47–50]). It has been shown that these correlation-corrected energy bands yield significantly better results for the band gaps and photoelectron spectra of polymers than those obtained from HF theory. So far Møller–Plesset perturbation theory for infinite lattices up to the fourth order has been implemented [51–53]. Coupled cluster theory has also been applied to infinite lattices using the localized Wannier functions or the delocalized Bloch functions [54–56].

Density functional theory using planewave basis sets and approximate core potentials has been widely used by solid-state physicists [57]. The method has been used mostly for metals and only rarely for organic and inorganic polymers and crystals. The crystal orbitals of these latter systems are more suitably described by linear combination of atomic orbitals rather than by planewaves. Mintmire *et al.* [58–61] have extensively applied the LCAO density functional theory to various hydrocarbon polymers using local exchange-correlation functionals. Very recently Suhai has implemented gradient-corrected and hybrid exchange-correlation functionals in LCAO density functional crystal orbital theory for infinite one-dimensional lattices [63,64].

So far the crystal orbital calculations have been carried out mostly for the purpose of investigating the electronic structures of infinite lattices at the experimental geometries. Only a limited number of studies have reported the vibrational frequencies of infinite

lattices on the basis of crystal orbital theory [41,65–71]. This situation is obviously due to the fact that analytical-derivative methods have not been developed for crystal orbital theory except for the gradients of HF energy. The analytical gradients for HF crystal orbital theory have been first implemented by Teramae *et al.* [68,69]. These authors have extended the gradient formulas originally derived for molecules by Pulay [7] to infinite one-dimensional lattices. They have derived compact formulas for the analytical energy gradients with respect to in-phase ($k = 0$) nuclear coordinates. Using the analytical-gradient method at the HF level, Teramae *et al.* have optimized the geometries and calculated the frequencies of $k = 0$ vibrations for several fundamental polymers such as polyethylene [68] and polyacetylene [69]. Teramae [40,41] has also studied intensively the convergence of the calculated structural parameters and vibrational frequencies with the number of neighbors included in the Coulomb and exchange lattice summations. Karpfen *et al.* [65–67,70,71] have also reported the structures and vibrations of polymers calculated at the HF level. Karpfen *et al.* have employed the pointwise method in which derivatives have been evaluated by calculating the potential energy surface at a number of points and fitting an analytical function to the points.

Since no analytical-derivative method has been developed for any correlated level of crystal orbital theory, the number of vibrational analyses of infinite lattices at correlated levels is very few. Recently Sun and Bartlett [72] have calculated the frequencies of $k = 0$ vibrations of *anti*-polymethineimine, taking into account the effects of electron correlation at the MP2 level. These authors have evaluated the force constants by numerically differentiating the total energy twice. Such an approach is apparently inefficient and may lead to numerically inaccurate results [73,74].

The purpose of the present study is two-fold; one is to develop efficient analytical-derivative methods for crystal orbital theory of one-dimensional lattices (polymers), and the other is to apply these methods to the calculations of structural and vibrational properties of polymers which are of interest from the physical chemistry point of view.

From the side of development of analytical-derivative methods, we have implemented analytical-gradient methods for hybrid HF/density functional and MP2 crystal orbital theories and an analytical-second-derivative method for HF crystal orbital theory. Hybrid HF/density functional crystal orbital theory encompasses pure HF crystal orbital theory and pure LCAO density functional crystal orbital theory as particular cases. In

the last decade, extensive investigations have been carried out on the energetic [28,75–83], structural [28,75,80,83,84], and vibrational [28,75,80,83,85,86] properties of molecules using various ab initio molecular orbital and density functional models. These studies have concluded that the hybrid HF/density functional models provide comparable or even better results for these properties than correlated ab initio molecular orbital models, which generally require much larger computational resources than density functional models. This conclusion suggests that hybrid HF/density functional theory can predict energetic, structural, and vibrational properties of polymers with considerable accuracy, and strongly encourages us to develop the analytical-derivative methods for hybrid HF/density functional crystal orbital theory.

In spite of excellent performance of modern hybrid exchange-correlation functionals, there are some important effects, e.g., dispersion energy, which density functional theory cannot yet treat. There is no technique to systematically improve the exchange-correlation functionals used in density functional theory. Therefore, if we aim at higher accuracy than density functional theory, we have to use an alternative method which will lead to converged correlated results. Such an alternative method is offered by Møller–Plesset perturbation theory. An analytical-gradient method for MP2 crystal orbital theory provides the basic theory common to analytical-derivative methods for all higher-order Møller–Plesset perturbation crystal orbital theories.

We have also implemented analytical second derivatives for HF crystal orbital theory. The analytical-second-derivative method provides a route to obtain the frequencies of the infrared- and Raman-active vibrations of polymers with increased efficiency and accuracy. In order to evaluate analytically the second derivatives of HF energy (and first derivatives of MP2 energy also), we have to know the first derivatives of crystal orbital coefficients. These latter quantities are obtained as solution to "polymer" CPHF equation, which is a generalization of the molecular CPHF equation [9]. It is essential to elucidate the fundamental features of the polymer CPHF equation, because the derivative formulas for a number of correlated crystal orbital theories are expected to share the same equation.

From the side of application of crystal orbital theory, we have chosen polyacetylene and polyethylene as one of the most fundamental conjugated and non-conjugated hydrocarbon polymers. We have evaluated the performance of the crystal orbital models on the basis of the comparison between the calculated and observed structural parameters and vibrational frequencies. Polyacetylene and polyethylene are ideal systems for this purpose,

because the size of the translational repeat unit is relatively small, and their structures and normal vibrations have thoroughly been investigated experimentally and are relatively well understood [87–89].

We have also applied crystal orbital theory to polymethineimine, whose structural and vibrational properties had hardly been elucidated experimentally or theoretically. Polymethineimine was first synthesized by Wöhlre [90,91], who also reported the frequencies of the characteristic infrared bands of this compound. However, the isomeric form of polymethineimine in the actual samples has not been established experimentally. It is important, therefore, to clarify this point on the basis of crystal orbital calculations. It is also of interest to compare the energetic, structural, and vibrational properties of polymethineimine with those of the isoelectronic analog, i.e., polyacetylene.

Another important target system for crystal orbital theory is consecutively hydrogen-bonded chains. Cooperativity of the hydrogen bonds renders the binding energies of the hydrogen-bonded systems in the condensed phase much larger than those in the small clusters in the gas phase [92–99]. Cooperativity of hydrogen bonds is expected to play essential roles in many important problems from the biochemistry and physical chemistry viewpoints, e.g., the folding of polypeptides and proteins, and structures and dynamics of water molecules in liquid water and ice. We have chosen crystalline hydrogen fluoride as one of the experimentally best-characterized hydrogen-bonded systems in the condensed phase and have studied the cooperativity of this consecutively hydrogen-bonded system quantitatively. Since crystalline hydrogen fluoride consists of planar zigzag hydrogen-bonded chains of hydrogen fluoride molecules, which have only weak interchain interactions [100–102], we have employed a single chain approximation and have performed crystal orbital calculations on isolated hydrogen fluoride polymers. The emphasis will be on the effects of electron correlation on the cooperative binding behavior.

The thesis is organized as follows: in Chapter 2, the formulas and computer implementation of self-consistent-field procedure of hybrid HF/density functional crystal orbital theory are described. The structures and energetics of the geometric isomers of polyacetylene are studied using local, gradient-corrected, and hybrid exchange-correlation functionals. In Chapter 3, the formulas and computer implementation of an analytical-gradient method for hybrid HF/density functional crystal orbital theory are presented. The structures and frequencies of the infrared- and Raman-active vibrations are calcu-

lated for the geometric isomers of polyacetylene and polymethineimine and are compared with the experimental results. In Chapter 4, the structures, frequencies of the infrared- and Raman-active vibrations, phonon dispersion curves, and inelastic neutron scattering spectra of all-*trans* polyethylene are calculated and are compared with the experimental results. Local, gradient-corrected, and hybrid exchange-correlation functionals are used. In Chapter 5, the structures, binding energies, and frequencies of the infrared- and Raman-active vibrations are calculated for an infinite hydrogen fluoride polymer and are compared with the experimental data obtained from crystalline hydrogen fluoride. Gradient-corrected and hybrid density functional theory as well as HF theory is used in conjunction with an extended basis set. In Chapter 6, an analytical-second-derivative method for HF crystal orbital theory is developed. Polymer version of the CPHF equation is formulated and an efficient algorithm for solving the equation is described. Dependence of the vibrational frequencies calculated with the analytical-second-derivative method on several parameters of calculations is investigated. Illustrative calculations are carried out on all-*trans* polyethylene. In Chapter 7, the formulas and computer implementation of an analytical-gradient method for MP2 crystal orbital theory are presented. Efficiency of the analytical-gradient and finite-difference methods is examined on the basis of the execution times. The effects of electron correlation, as taken into account at the MP2 level, on the vibrational frequencies of all-*trans* polyacetylene are investigated. Summary of the thesis and general conclusion drawn from the present research are given in Chapter 8.

References

[1] P. Pulay, in *Applications of Electronic Structure Theory,* edited by H. F. Schaefer III (Plenum, New York, 1977), p. 153.

[2] G. Fogarasi and P. Pulay, Ann. Rev. Phys. Chem., **35,** 191 (1984).

[3] P. Jørgensen and J. Simons, *Geometrical Derivatives of Energy Surfaces and Molecular Properties,* (D. Reidel Publishing, Dordrecht, 1985).

[4] R. D. Amos, in *Ab Initio Methods in Quantum Chemistry I,* edited by K. P. Lawley (Wiley, New York, 1987), p. 99.

[5] P. Pulay, in *Ab Initio Methods in Quantum Chemistry II,* edited by K. P. Lawley (Wiley, New York, 1987), p. 241.

[6] Y. Yamaguchi, Y. Osamura, J. D. Goddard, and H. F. Schaefer III, *A New Dimension to Quantum Chemistry: Analytic Derivative Methods in Ab Initio Molecular Electronic*

Structure Theory, (Oxford University Press, New York, 1994).

[7] P. Pulay, Mol. Phys., **17,** 197 (1969); **18,** 473 (1970).

[8] J. A. Pople, R. Krishnan, H. B. Schlegel, and J. S. Binkley, Int. J. Quantum Chem. Quantum Chem. Symp., **13,** 225 (1979).

[9] J. Gerratt and I. M. Mills, J. Chem. Phys., **49,** 1719 (1968); **49,** 1730 (1968).

[10] J. F. Gaw, Y. Yamaguchi, and H. F. Schaefer III, J. Chem. Phys., **81,** 6395 (1984).

[11] C. Møller and M. S. Plesset, Phys. Rev., **46,** 618 (1934).

[12] K. F. Freed, Ann. Rev. Phys. Chem., **22,** 313 (1971).

[13] J. Paldus and J. Čížek, Adv. Quantum Chem., **9,** 105 (1975).

[14] W. Kutzelnigg, in *Methods of Electronic Structure Theory,* edited by H. F. Schaefer III (Plenum, New York, 1977), p. 129.

[15] R. J. Bartlett, Ann. Rev. Phys. Chem., **32,** 359 (1981).

[16] R. J. Bartlett and G. D. Purvis, Int. J. Quantum Chem., **14,** 561 (1978).

[17] N. C. Handy, R. D. Amos, J. F. Gaw, J. E. Rice, and E. D. Simandiras, Chem. Phys. Lett., **120,** 151 (1985).

[18] G. W. Trucks, E. A. Salter, C. Sosa, and R. J. Bartlett, Chem. Phys. Lett., **147,** 359 (1988).

[19] G. W. Trucks, J. D. Watts, E. A. Salter, and R. J. Bartlett, Chem. Phys. Lett., **153,** 490 (1988).

[20] B. R. Brooks, W. D. Laidig, P. Saxe, J. D. Goddard, Y. Yamaguchi, and H. F. Schaefer III, J. Chem. Phys., **72,** 4652 (1980).

[21] R. Krishnan, H. B. Schlegel, and J. A. Pople, J. Chem. Phys., **72,** 4654 (1980).

[22] L. Adamowicz, W. D. Laidig, and R. J. Bartlett, Int. J. Quantum. Chem. Quantum Chem. Symp., **18,** 245 (1984).

[23] R. G. Parr and W. Yang, *Density-Functional Theory of Atoms and Molecules* (Oxford University Press, NewYork, 1989).

[24] T. Ziegler, Chem. Rev., **91,** 651 (1991).

[25] N. C. Handy, in *Lecture Notes in Quantum Chemistry II,* edited by B. O. Roos (Springer–Verlag, Berlin, 1994), p. 91.

[26] C. Satoko, Chem. Phys. Lett., **83,** 111 (1981).

[27] J. A. Pople, P. M. W. Gill, and B. G. Johnson, Chem. Phys. Lett., **199,** 557 (1992).

[28] B. G. Johnson, P. M. W. Gill, and J. A. Pople, J. Chem. Phys., **98,** 5612 (1993).

[29] B. G. Johnson and M. J. Frisch, Chem. Phys. Lett., **216,** 133 (1993).

[30] B. G. Johnson and M. J. Frisch, J. Chem. Phys., **100,** 7429 (1994).

[31] M. Kertész, Adv. Quantum Chem., **15**, 161 (1982).

[32] J. Ladik, J.-M. André, and M. Seel, *Quantum Chemistry of Polymers—Solid State Aspects,* (D. Reidel Publishing, Dordrecht, 1983).

[33] J. J. Ladik, *Quantum Theory of Polymers as Solids* (Plenum Press, New York, 1988).

[34] G. Del Re, J. Ladik, and G. Biczó, Phys. Rev, **155,** 997 (1967).

[35] J.-M. André, L. Gouverneur, and G. Leroy, Int. J. Quantum Chem., **1,** 427 (1967); **1,** 451 (1967).

[36] C. C. J. Roothaan, Rev. Mod. Phys., **23,** 69 (1951).

[37] G. G. Hall, Proc. Roy. Soc. (London) A, **205,** 541 (1951).

[38] J. M. André, J. Chem. Phys., **50,** 1536 (1969).

[39] S. Suhai, J. Chem. Phys., **73,** 3843 (1980).

[40] H. Teramae, J. Chem. Phys., **85,** 990 (1986).

[41] H. Teramae, Theor. Chim. Acta, **94,** 311 (1996).

[42] J. Delhalle, L. Piela, J.-L. Brédas, and J.-M. André, Phys. Rev. B, **22,** 6254 (1980).

[43] L. Piela, J.-M. André, J. G. Fripiat, and J. Delhalle, Chem. Phys. Lett., **77,** 143 (1981).

[44] H. J. Monkhorst and M. Kertesz, Phys. Rev. B, **24,** 3015 (1981).

[45] S. Suhai, Chem. Phys. Lett., **96,** 619 (1983); Phys. Rev. B, **27,** 3506 (1983).

[46] Y. Toyozawa, Prog. Theor. Phys. (Kyoto), **12,** 421 (1954).

[47] A. B. Kunz, Phys. Rev. B, **6,** 606 (1972).

[48] J. T. Devereese, A. B. Kunz, and T. C. Collins, Solid State Commun., **11,** 673 (1972).

[49] D. J. Mickish, A. B. Kunz, and T. C. Collins, Phys. Rev. B, **9,** 4461 (1974).

[50] S. T. Pantelides, D. J. Mickish, and A. B. Kunz, Phys. Rev. B, **10,** 2602 (1974).

[51] C.-M. Liegener, J. Phys. C, **18,** 6011 (1985); J. Chem. Phys., **88,** 6999 (1988).

[52] S. Suhai, Int. J. Quantum Chem. Quantum Chem. Symp., **27,** 131 (1993).

[53] S. Suhai, Phys. Rev. B, **50,** 14791 (1994).

[54] W. Förner, Int. J. Quantum Chem., **43,** 221 (1992).

[55] Y.-J. Ye, W. Förner, and J. Ladik, Chem. Phys., **178,** 1 (1993).

[56] W. Förner, R. Knab, J. Čížek, and J. Ladik, J. Chem. Phys., **106,** 10248 (1997).

[57] J. C. Slater, *Quantum Theory of Molecules and Solids, Vol. 4: The Self-Consistent Field for Molecules and Solids* (McGraw–Hill, NewYork, 1974).

[58] J. W. Mintmire and C. T. White, Phys. Rev. Lett., **50,** 101 (1983).

[59] J. W. Mintmire and C. T. White. Phys. Rev. B, **27,** 1447 (1983).

[60] J. W. Mintmire and C. T. White, Phys. Rev. B, **35,** 4180 (1987).

[61] J. W. Mintmire, F. W. Kutzler, and C. T. White, Phys. Rev. B, **36,** 3312 (1987).

[62] M. S. Miao, P. E. Van Camp, V. E. Van Doren, J. J. Ladik, and J. W. Mintmire, Phys. Rev. B, **54,** 10430 (1996).

[63] S. Suhai, Phys. Rev. B, **51,** 16553 (1995).

[64] S. Suhai, Phys. Rev. B, **52,** 1674 (1995).

[65] A. Karpfen, J. Phys. C, **12,** 3227 (1979).

[66] A. Beyer and A. Karpfen, Chem. Phys., **64,** 343 (1982).

[67] A. Karpfen, Chem. Phys., **79,** 211 (1983).

[68] H. Teramae, T. Yamabe, C. Satoko, and A. Imamura, Chem. Phys. Lett., **101,** 149 (1983).

[69] H. Teramae, T. Yamabe, and A. Imamura, J. Chem. Phys., **81,** 3564 (1984).

[70] A. Karpfen, Chem. Phys., **88,** 415 (1984).

[71] M. Kofranek, H. Lischka, and A. Karpfen, J. Chem. Phys., **96,** 982 (1992).

[72] J.-Q. Sun and R. J. Bartlett, J. Chem. Phys., **108,** 301 (1998).

[73] R. F. Hout, Jr., B. A. Levi, and W. J. Hehre, J. Comput. Chem., **3,** 234 (1982).

[74] W. J. Hehre, L. Radom, P. v. R. Schleyer, and J. A. Pople, *Ab Initio Molecular Orbital Theory* (Wiley, New York, 1986).

[75] J. Andzelm and E. Wimmer, J. Chem. Phys., **96,** 1280 (1992).

[76] A. D. Becke, J. Chem. Phys., **96,** 2155 (1992).

[77] A. D. Becke, J. Chem. Phys., **97,** 9173 (1992).

[78] P. M. W. Gill, B. G. Johnson, J. A. Pople, and M. J. Frisch, Chem. Phys. Lett., **197,** 499 (1992).

[79] A. D. Becke, J. Chem. Phys., **98,** 5648 (1993).

[80] H. Chen, M. Krasowski, and G. Fitzgerald, J. Chem. Phys., **98,** 8710 (1993).

[81] J. M. Seminario, Chem. Phys. Lett., **206,** 547 (1993).

[82] J. B. Foresman and Æ. Frisch, *Exploring Chemistry with Electronic Structure Methods,* 2nd ed. (Gaussian Inc., Pittsburgh, 1996).

[83] M. J. Frisch, G. W. Trucks, and J. R. Cheeseman, in *Recent Developments and Applications of Modern Density Functional Theory,* edited by J. M. Seminario (Elsevier, Amsterdam, 1996).

[84] R. M. Dickson and A. D. Becke, J. Chem. Phys., **99,** 3898 (1993).

[85] M. W. Wong, Chem. Phys. Lett., **256,** 391 (1996).

[86] A. P. Scott and L. Radom, J. Phys. Chem., **100,** 16502 (1996).

[87] J. C. W. Chien, *Polyacetylene: Chemistry, Physics, and Material Science* (Academic Press, Orlando, 1984).

[88] J. Barnes and B. Fanconi, J. Phys. Chem. Ref. Data, **7,** 1309 (1978).

[89] D. I. Bower and W. F. Maddams, *The Vibrational Spectroscopy of Polymers,* (Cambridge University Press, Cambridge, 1989).

[90] D. Wöhrle, Tetrahedron Lett., **22,** 1969 (1971).

[91] D. Wöhrle, Makromol. Chem., **175,** 1751 (1974).

[92] H. S. Frank, Proc. Roy. Soc. (London) A, **247,** 481 (1958).

[93] J. Del Bene and J. A. Pople, J. Chem. Phys., **52,** 4858 (1970).

[94] J. E. Del Bene and J. A. Pople, J. Chem. Phys., **55,** 2296 (1971).

[95] J. E. Del Bene and J. A. Pople, J. Chem. Phys., **58,** 3605 (1973).

[96] P. Schuster, G. Zundel, and C. Sandorfy, *The Hydrogen Bond, Vol. 1–3* (North-Holland, Amsterdam, 1976).

[97] G. A. Jeffrey, M. E. Gress, and S. Takagi, J. Am. Chem. Soc., **99,** 609 (1977).

[98] Y.-C. Tse and M. D. Newton, J. Am. Chem. Soc., **99,** 611 (1977).

[99] G. A. Jeffrey and W. Saenger, *Hydrogen Bonding in Biological Structures* (Springer-Verlag, Berlin, 1991).

[100] M. Atoji and W. N. Lipscomb, Acta Cryst., **7,** 173 (1954).

[101] M. W. Johnson, E. Sándor, and E. Arzi, Acta Cryst. B, **31,** 1998 (1975).

[102] M. L. N. Sastri and D. F. Hornig, J. Chem. Phys., **39,** 3497 (1963).

Chapter 2

Structures and energetics of polyacetylene isomers

So Hirata, Hajime Torii, and Mitsuo Tasumi, "Density-functional crystal orbital study on the structures and energetics of polyacetylene isomers," Phys. Rev. B, **57**(19), 11994–12001 (1998).

Abstract

Total energies and optimized molecular structures of the *trans*-transoid (Tt) and *cis*-transoid (Ct) forms of polyacetylene are calculated by the density functional crystal orbital method. The Slater–Vosko–Wilk–Nusair (SVWN), the Becke–Lee–Yang–Parr (BLYP), and the Becke3–Lee–Yang–Parr (B3LYP) functionals are used with the 3-21G and 6-31G(d) basis sets. Potential energy curves of the Ct form along the bond-alternation coordinate [which represents the transition from the Ct form to the *trans*-cisoid (Tc) form] are calculated with the SVWN, BLYP, and B3LYP functionals. The SVWN and BLYP functionals seriously underestimate the double-minimum character of the potential energy curves, so that the calculated potential energy curves have no local minimum at the Tc structure. The potential energy curves calculated with the B3LYP functional have distinct shoulders at the Tc structure, and the structural parameters of the Tc form are optimized with this functional. The structural parameters and ultraviolet photoelectron spectra of the Tt and Ct forms calculated by using the B3LYP functional are in reasonable agreement with the experimental results. Potential energy curves along the CC–CC dihedral angle coordinate are calculated with the B3LYP functional. It is found that the calculated potential energy curve has a shallow local minimum at the *cis*-gauche (Cg) form. The B3LYP functional predicts the total energies of the polyacetylene isomers increase in the order Tt < Ct < Tc < Cg.

2.1 Introduction

Density functional theory has been extensively used for the calculations of energetics, structures, and vibrations of molecular systems [1,2]. This is because density functional calculations can include electron correlation with relatively small computational costs, which are in the same order of magnitude as the costs needed for Hartree–Fock (HF) calculations. Density functional theory is applicable to relatively large systems for which HF-based correlated calculations are not feasible.

It is therefore natural to adopt density functional theory for the description of the electronic and structural properties of conjugated π-electron polymers, for which the effect of electron correlation is essential. Among these conjugated π-electron polymers, polyacetylene [3] is the most frequently studied material because of its intriguing electrical and spectroscopic behavior. There have been a number of density functional studies

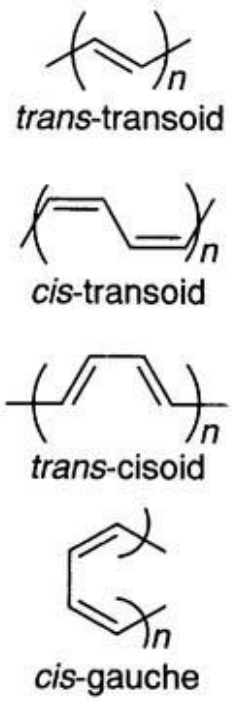

Figure 2.1 Isomers of polyacetylene.

on polyacetylene [4–15]. Suhai [15] has recently published a paper in which the bond alternation in the *trans*-transoid (Tt) form of polyacetylene is thoroughly investigated with various exchange-correlation functionals. Suhai has found that the magnitude of the bond alternation in the Tt form is reasonably predicted when functionals mixed with exact exchange are used.

Although the electronic and structural properties of Tt polyacetylene have been repeatedly investigated, studies on the other geometric isomers, namely, the *cis*-transoid (Ct), *trans*-cisoid (Tc), and *cis*-gauche (Cg) [16] forms, are not abundant. The structures of these four isomers are shown in Fig. 2.1. It is not only of interest but also of importance to study the structures and energetics of these isomers at an equal theoretical level which takes the effect of electron correlation into account.

In this chapter, we present the total energies and optimized molecular structures of the Tt and Ct forms of polyacetylene obtained from density functional crystal orbital calculations. The local Slater–Vosko–Wilk–Nusair (SVWN), the gradient-corrected Becke–Lee–Yang–Parr (BLYP), and the hybrid Becke3–Lee–Yang–Parr (B3LYP) functionals are used in combination with the standard 3-21G and 6-31G(d) basis sets. The role of the exact-exchange mixing in determining the shape of the potential energy curves along the

bond-alternation coordinate is discussed. The ultraviolet photoelectron spectra calculated with the B3LYP functional are compared with the experimental results for the Tt and Ct forms. Structures and energetics of the Tc and Cg forms are also examined with the B3LYP functional. The relative energies of the four forms of polyacetylene are discussed.

2.2 Formulas for the self-consistent-field procedure

The density functional crystal orbital method for infinite one-dimensional lattices (polymers) is a combination of the HF crystal orbital method [17–21] and the molecular density functional method [22,23]. The basic formulas for the self-consistent-field procedure is described in this section for hybrid HF/density functional crystal orbital theory. The formulas for pure HF and pure density functional theory are encompassed as particular cases.

In the framework of spin-restricted hybrid HF/density functional crystal orbital theory of polymers [15], Kohn–Sham crystal (Bloch) orbitals are expressed as linear combinations of atomic orbitals $\chi_\mu^{(q)}(\mathbf{r})$ in the form

$$\psi_n^{[k]}(\mathbf{r}) = \frac{1}{\sqrt{K}} \sum_\mu \sum_q C_{\mu n}^{[k]} \exp(ikqa) \chi_\mu^{(q)}(\mathbf{r}), \tag{2.1}$$

where a is the translational period, and K is the number of unit cells in the system. The crystal orbital $\psi_n^{[k]}(\mathbf{r})$ and crystal orbital coefficient $C_{\mu n}^{[k]}$ are characterized by energy band n and quasi-momentum k, which are indicated by subscripts and square-bracketed superscripts, respectively. The atomic orbital $\chi_\mu^{(q)}(\mathbf{r})$ is located in unit cell q and bears the following relation:

$$\chi_\mu^{(q)}(\mathbf{r}) = \chi_\mu^{(0)}(\mathbf{r} - qa). \tag{2.2}$$

By using the above-mentioned symmetry-adapted basis functions and applying Ritz variation principle to the total energy expectation value, the following k-dependent Hartree–Fock–Roothaan equation [17–21] is obtained:

$$\mathbf{F}^{[k]}\mathbf{C}^{[k]} = \mathbf{S}^{[k]}\mathbf{C}^{[k]}\epsilon^{[k]}, \tag{2.3}$$

where $\epsilon^{[k]}$ is a diagonal matrix of one-electron energies. The elements of the k-dependent Fock matrix are defined as

$$F_{\mu\nu}^{[k]} = \sum_q F_{\mu\nu}^{(q)} \exp(ikqa), \tag{2.4}$$

and

$$S_{\mu\nu}^{[k]} = \sum_{q} S_{\mu\nu}^{(q)} \exp(ikqa), \tag{2.5}$$

where

$$\begin{aligned} F_{\mu\nu}^{(q)} &= H_{\mu\nu}^{(q)} + \sum_{\lambda,\sigma}\sum_{\gamma} D_{\gamma}\left(\mu^{(0)}\nu^{(q)}|\gamma\right) + m_1 X_{\mu\nu}^{(q)} \\ &\quad -\frac{m_2}{2}\sum_{\lambda,\sigma}\sum_{r,s} P_{\lambda\sigma}^{(s-r)}\left(\mu^{(0)}\lambda^{(r)}|\nu^{(q)}\sigma^{(s)}\right), \end{aligned} \tag{2.6}$$

and

$$S_{\mu\nu}^{(q)} = \int \chi_{\mu}^{(0)}(\mathbf{r})\chi_{\nu}^{(q)}(\mathbf{r})d\mathbf{r}. \tag{2.7}$$

The matrix H in Eq. (2.6) is the one-electron part of the Fock matrix, whose elements are given by

$$\begin{aligned} H_{\mu\nu}^{(q)} &= \int \chi_{\mu}^{(0)}(\mathbf{r})\left(-\frac{1}{2}\nabla^2\right)\chi_{\nu}^{(q)}(\mathbf{r})d\mathbf{r} \\ &\quad -\sum_{A}\sum_{r}\int \chi_{\mu}^{(0)}(\mathbf{r})\frac{Z_A}{|\mathbf{r}-\mathbf{R}_A^{(r)}|}\chi_{\nu}^{(q)}(\mathbf{r})d\mathbf{r}, \end{aligned} \tag{2.8}$$

where Z_A is the charge of nucleus A at position $\mathbf{R}_A^{(r)}$. The elements of the density matrix $P_{\mu\nu}^{(q)}$ are defined as

$$P_{\mu\nu}^{(q)} = \frac{2}{K}\sum_{j}^{\text{occ.}}\sum_{k}^{\text{BZ}} C_{\mu j}^{[k]*} C_{\nu j}^{[k]} \exp(ikqa), \tag{2.9}$$

where the summations are over all the occupied states in the first Brillouin zone. In order to minimize the computational tasks concerning the accumulation of the long-range electron repulsion integrals, we expanded the electron density by auxiliary basis functions according to the method of Dunlap *et al.* [24] in Eq. (2.6). The procedure of obtaining the expansion coefficients D_{γ} is given in Appendix. Two-electron integrals are defined as

$$\left(\mu^{(0)}\nu^{(q)}|\lambda^{(r)}\sigma^{(s)}\right) = \int\int \chi_{\mu}^{(0)}(\mathbf{r}_1)\chi_{\nu}^{(q)}(\mathbf{r}_1)\frac{1}{r_{12}}\chi_{\lambda}^{(r)}(\mathbf{r}_2)\chi_{\sigma}^{(s)}(\mathbf{r}_2)d\mathbf{r}_1 d\mathbf{r}_2, \tag{2.10}$$

and

$$\left(\mu^{(0)}\nu^{(q)}|\gamma\right) = \sum_{r}\int\int \chi_{\mu}^{(0)}(\mathbf{r}_1)\chi_{\nu}^{(q)}(\mathbf{r}_1)\frac{1}{r_{12}}\theta_{\gamma}^{(r)}(\mathbf{r}_2)d\mathbf{r}_1 d\mathbf{r}_2. \tag{2.11}$$

where $\theta_{\gamma}^{(r)}(\mathbf{r})$ is the auxiliary basis function centered in unit cell r. Parameters m_1 and m_2 in Eq. (2.6) denote the mixing ratios of exchange-correlation energy and exact-exchange energy, respectively. For pure density functional calculations, i.e., $m_2 = 0$, we can avoid

the evaluation of four-index electron repulsion integrals completely. We assume that the exchange-correlation functional has the form

$$f = f\left[\rho, \nabla\rho\right], \tag{2.12}$$

where ρ and $\nabla\rho$ are electron density and its gradient. The elements of the exchange-correlation part $X_{\mu\nu}^{(q)}$ of the Fock matrix are given by (see Refs. [22,23])

$$X_{\mu\nu}^{(q)} = \int \left\{ \chi_\mu^{(0)} v_{\rm XC} \chi_\nu^{(q)} + \nabla\chi_\mu^{(0)} \cdot \mathbf{g}_{\rm XC} \chi_\nu^{(q)} + \chi_\mu^{(0)} \mathbf{g}_{\rm XC} \cdot \nabla\chi_\nu^{(q)} \right\} d\mathbf{r}, \tag{2.13}$$

with

$$v_{\rm XC} = \frac{\partial f}{\partial \rho}, \tag{2.14}$$

$$\mathbf{g}_{\rm XC} = \left\{ \frac{\partial f}{\partial \gamma_{\alpha\alpha}} + \frac{1}{2} \frac{\partial f}{\partial \gamma_{\alpha\beta}} \right\} \nabla\rho, \tag{2.15}$$

$$\gamma_{\alpha\alpha} = \nabla\rho_\alpha \cdot \nabla\rho_\alpha, \tag{2.16}$$

$$\gamma_{\alpha\beta} = \nabla\rho_\alpha \cdot \nabla\rho_\beta, \tag{2.17}$$

where α and β denote spins.

The total energy per unit cell is then expressed as

$$\begin{aligned} E = & \sum_{\mu,\nu} \sum_{q} P_{\mu\nu}^{(q)} H_{\mu\nu}^{(q)} + \sum_{\mu,\nu} \sum_{\gamma} \sum_{q,r,s} P_{\mu\nu}^{(q)} D_\gamma \left(\mu^{(0)} \nu^{(q)} | \gamma \right) \\ & - \frac{1}{2} \sum_{\gamma,\delta} D_\gamma D_\delta \left(\gamma | \delta \right) + m_1 \int_{\rm cell} f\left[\rho, \nabla\rho\right] d\mathbf{r} \\ & - \frac{m_2}{4} \sum_{\mu,\nu} \sum_{\lambda,\sigma} \sum_{q,r,s} P_{\mu\nu}^{(q)} P_{\lambda\sigma}^{(s-r)} \left(\mu^{(0)} \lambda^{(r)} | \nu^{(q)} \sigma^{(s)} \right) + E_{\rm NR}, \end{aligned} \tag{2.18}$$

where $E_{\rm NR}$ is the nuclear repulsion energy per unit cell. Two-index electron repulsion are defined as

$$\left(\gamma | \delta \right) = \sum_{q} \int \int \theta_\gamma^{(0)}(\mathbf{r}_1) \frac{1}{r_{12}} \theta_\delta^{(q)}(\mathbf{r}_2) d\mathbf{r}_1 d\mathbf{r}_2. \tag{2.19}$$

2.3 Computer implementation

We employed the Gaussian basis sets for the expansion of Kohn–Sham orbitals, and hence the overlap integrals, kinetic energy integrals, and nuclear attraction integrals were analytically evaluated by the Obara–Saika recursion formula [25]. Electron density was also expanded by sets of auxiliary Gaussian functions, so that the Coulomb matrix elements were calculated by the two- and three-index electron repulsion integrals. These integrals

were analytically evaluated by the Obara–Saika recursion scheme reformulated by Andzelm and Wimmer [26] for the computation of the two- and three-index electron repulsion integrals. The expansion of electron density was based on the method of Dunlap *et al.* [24], which was previously adopted by Mintmire and White [6,8] for the $X\alpha$ calculations of the Tt form of polyacetylene. It should be emphasized that the approximate total Coulomb energy calculated by this method is a variational extremum with respect to the expansion coefficients (see Appendix), and that the errors in the calculated energies introduced in this treatment will almost cancel each other as far as the total energy difference is concerned. The lattice sums used in evaluating the Coulomb matrix elements exhibit slow convergence due to the long-range nature of Coulomb interactions [27,28]. We calculated these lattice sums by evaluating explicitly the relevant two- and three-index electron repulsion integrals extending to the twentieth neighboring C_2H_2 unit cells within the Namur cutoff procedure [29,30]. For the other molecular integrals, we took into account the interactions up to the fourth to eighth neighboring C_2H_2 unit cells depending upon the basis set used and upon the translational period of the system.

The exchange-correlation integrals were computed numerically by the method developed by Becke [31] applying a second-kind Gauss–Chebyshev quadrature for the radial integration and a Lebedev quadrature [32–34] for the angular integration. The numerical grid consisted of 50 radial points and 302 angular points. Smaller angular grids were used for radial shells close to the nuclei (38-point angular grid for radial shells 1–12 and 50-point angular grid for radial shells 13–25) and the M4 mapping of radial grid points was adopted according to the recommendation of Treutler and Ahlrichs [35]. The resulting 8656-point grid was used for carbon and hydrogen, and an error in the integrated electron density of polyacetylene was typically 1×10^{-5} per atom.

We employed the standard 3-21G [36] and 6-31G(d) [37,38] basis sets for the expansion of Kohn–Sham orbitals and 200 evenly spaced wavevectors to describe the first Brillouin zone (only one of the two points at the zone boundaries was counted). It has been pointed out [8,11,14] that a sufficiently large number of wavevectors are necessary to accurately evaluate the magnitude of bond alternation in the Tt form of polyacetylene. Two sets of auxiliary basis functions were employed: auxiliary basis set I for the 3-21G calculations and auxiliary basis set II for the 6-31G(d) calculations. Auxiliary basis set I consisted of uncontracted s-type Gaussian functions and blocks of uncontracted s-type, p-type, and d-type Gaussian functions with shared exponents. Auxiliary basis set II consisted of

Table 2.1 Exponents of the auxiliary Gaussian functions for hydrogen and carbon.

Auxiliary basis set I		Auxiliary basis set II	
Hydrogen	Carbon	Hydrogen	Carbon
s		s	
10.89	344.5	37.46	512.6
3.298	99.63	21.56	170.9
	33.21	19.37	56.95
	11.07	18.89	18.98
		5.651	15.74
		3.466	10.80
		2.987	6.328
			5.399
spd		spd	
1.099	7.330	1.280	2.699
0.3664	3.525	0.8014	
	1.175	spdf	
	0.3917	0.3226	1.350
			0.6749
			0.3374

uncontracted s-type, p-type, d-type, and f-type Gaussian functions, some of which have shared exponents. The exponents of the auxiliary basis functions are given in Table 2.1.

Since the convergence of the lattice sums for the exact-exchange matrix elements is generally much faster than that for the Coulomb matrix elements [21], the four-index electron repulsion integrals, which were necessary to compute the exact-exchange matrix elements, were explicitly evaluated by using the Obara–Saika recursion formula. In the present study, the Slater local exchange [39], the Vosko–Wilk–Nusair local correlation [40], the Becke gradient-corrected exchange [41], and the Lee–Yang–Parr gradient-corrected correlation [42,43] functionals were used. The effect of the exact-exchange mixing was examined with the B3LYP functional [44]. These three exchange-correlation functionals are widely used in molecular applications, and the performance of these functionals for predicting thermochemical quantities [23,26,44–51], equilibrium structures [23,26,49,51,52], and harmonic vibrational frequencies [23,26,49,51,53,54] has been investigated.

The DIIS (direct inversion in the iterative subspace) extrapolation [55] was employed for the convergence acceleration of the self-consistent-field iteration. The criterion for the convergence of the density matrix elements was set to 10^{-6}. The geometry optimization was performed by Powell's conjugate direction method [56], in which the minimization along each conjugate direction was based on the three-point parabolic interpolation. As far as the numerical accuracy in the present optimization method is concerned, the bond

Table 2.2 Optimized structural parameters of polyacetylene in units of Å (bond length) and degrees (bond angle).

	SVWN		BLYP		B3LYP	
Structural parameter	3-21G	6-31G(d)	3-21G	6-31G(d)	3-21G	6-31G(d)
			Trans-transoid			
C=C bond length	1.383	1.384	1.404	1.398	1.366	1.369
C–C bond length	1.395	1.392	1.410	1.413	1.428	1.426
C–H bond length	1.101	1.102	1.097	1.099	1.090	1.091
CCC angle	124.2	124.3	124.3	124.6	124.3	124.5
C=CH angle	118.0	117.9	117.9	117.9	118.5	118.3
			Cis-transoid			
C=C bond length	1.372	1.375	1.388	1.390	1.366	1.369
C–C bond length	1.414	1.412	1.435	1.433	1.438	1.435
C–H bond length	1.098	1.099	1.093	1.095	1.086	1.087
CCC angle	125.9	126.0	126.6	127.0	126.5	126.7
C=CH angle	117.0	116.9	116.3	116.1	116.7	116.4
			Trans-cisoid			
C=C bond length	*a*	*a*	*a*	*a*	1.373	*b*
C–C bond length					1.429	
C–H bond length					1.087	
CCC angle					126.9	
C=CH angle					117.9	

[a] No local minimum corresponding to the *trans*-cisoid form was found with the SVWN and BLYP functionals. [b] See text.

lengths (in Å) are accurate to three decimal places and bond angles (in degrees) are accurate to one decimal place.

2.4 Results and discussion

Optimized structural parameters for the Tt and Ct forms of polyacetylene obtained with the SVWN, BLYP, and B3LYP functionals are shown in Table 2.2. Structure is optimized also for the Tc form at the B3LYP/3-21G level. In the present geometry optimization, the planarity of the polyacetylene molecule was assumed, and all the remaining structural parameters were optimized. The assumption of planarity of the molecule is partially supported by the results of the present study, where the potential energies are plotted along the CC–CC dihedral angle (see below), and by the results of the vibrational analyses of the polyacetylene isomers [57–59].

The magnitude of the bond alternation (hereafter designated as Δr) in the Tt form calculated at the SVWN/3-21G and SVWN/6-31G(d) levels are 0.012 and 0.008 Å, respectively, and are much smaller than the experimental value (0.08 Å) [60]. It has already been reported [8,10–12,14] that the calculated values of Δr tend to be too small in the framework of the local density approximation. Suhai [15] has analyzed the effects of the

gradient correction and the exact-exchange mixing on the calculated value of Δr. He has found that the situation is hardly improved by the gradient correction, but the mixing of exact exchange at the Becke-half-and-half–Lee–Yang–Parr (BHandHLYP) level yields a reasonable value for Δr. In the present study also, the values of Δr calculated at the BLYP/3-21G and BLYP/6-31G(d) levels (0.006 and 0.015 Å, respectively) are too small, but the values obtained with the B3LYP functional seems to be reasonable. The C=C and C–C bond lengths calculated at the B3LYP/3-21G level (1.366 and 1.428 Å, respectively) and at the B3LYP/6-31G(d) level (1.369 and 1.426 Å, respectively) are consistent with the values obtained experimentally (1.36±0.01, and 1.44±0.01 Å, respectively) [60]. The structural parameters calculated at the B3LYP/6-31G(d) level are close to those obtained at the B3LYP/3-21G level and hence the basis-set dependence of the structural parameters is not prominent for this system.

For the Ct form, the calculated C=C and C–C bond lengths are significantly different from each other with all the functionals used. This result is reasonable in view of the geometrical non-equivalence of the adjacent CC bonds in the Ct form. However, the shape of the potential energy curve along the bond-alternation coordinate is strongly affected by the mixing of exact exchange not only for the Tt form but also for the Ct form. The potential energy curves of the Ct form along the bond-alternation coordinate Δr (which represents the transition from the Ct form to the Tc form) are shown in Fig. 2.2, with the sign of Δr being taken to be positive for the Ct structure. The curves obtained with the 6-31G(d) basis set overlap with those obtained with the 3-21G basis set, indicating that the basis-set dependence on the potential energy curves along Δr is again small regardless of the exchange-correlation functionals used. The small basis-set dependence is expected since the total energies of the structures with different values of Δr are lowered by a similar amount by augmenting the basis set. With the SVWN and BLYP functionals, the potential energy curves deviate only slightly from the harmonic shape around the region $\Delta r \approx -0.05$ Å where the local minimum corresponding to the Tc form is expected to appear. When the B3LYP functional is used, a distinct shoulder appears at $\Delta r \approx -0.05$ Å. The curve obtained at the B3LYP/3-21G level has a shallow local minimum at $\Delta r \approx -0.05$ Å, which corresponds to the Tc form. The potential energy curve calculated at the B3LYP/6-31G(d) level, on the other hand, does not have a local minimum at the Tc structure. Since the structural parameters are not optimized at each value of Δr, the present result does not necessarily rule out the existence of the

local minimum of the Tc form at the B3LYP/6-31G(d) level. However, no attempt was made to locate the local minimum of the Tc form at the B3LYP/6-31G(d) level, because the convergence of the self-consistent field procedure is much slower in this Δr region, probably due to the small HOMO–LUMO band gap, than in the other region. Figure 2.2(c) suggests that the energy barrier for the Tc→Ct isomerization is very low and the Tc isomer can easily isomerize to the Ct isomer by interchanging the C=C and C–C bond lengths even if a local minimum exists for the Tc form. It should be remembered that Tc polyacetylene has not been experimentally detected as a stable isomer.

The magnitude of the bond alternation in the Ct form calculated with the SVWN and BLYP functionals are in the range of 0.03–0.05 Å, and are smaller than the value obtained with the B3LYP functional (about 0.07 Å). It is considered that the potential energy curves calculated with the SVWN and BLYP functionals tend to have too weak double-minimum character. The too small degree of bond alternation calculated with the SVWN and BLYP functionals for the Tt form suggests that the potential energy curves calculated with these functionals are not satisfactory also for the Ct form. It should also be added that the B3LYP calculations reproduced the frequencies of the infrared- and Raman-active vibrations of the Tt and Ct forms with considerable accuracy [59]. It is, therefore, considered that the potential energy curves calculated with the B3LYP functional are reasonable.

In our previous study [58], the structural parameters of the Ct and Tc forms were extrapolated from those of the Ct and Tc oligoenes calculated at the B3LYP/6-31G(d) level. Although the structural parameters of the Ct form obtained by extrapolation are not far from the result of the present study, the C=C and C–C bond lengths obtained by extrapolation (1.374 and 1.429 Å, respectively) differ from the values obtained in the present study (1.369 and 1.435 Å, respectively). These differences are due to the overestimation of the chain-length dependence of the C=C and C–C bond lengths in the extrapolation in our previous study [58]. Nevertheless, the C=C bond lengths calculated by either of the above two methods are within the error of the experimental value (1.37±0.01 Å) [60].

There have been a number of density functional studies which analyzed the conformation and internal rotation potential about the C–C bonds in conjugated and non-conjugated molecules [61–67]. These studies have demonstrated that the relative energies of conformers predicted by density functional theory are generally in good agreement with the experimental results and with the results obtained by high-level ab initio molecular

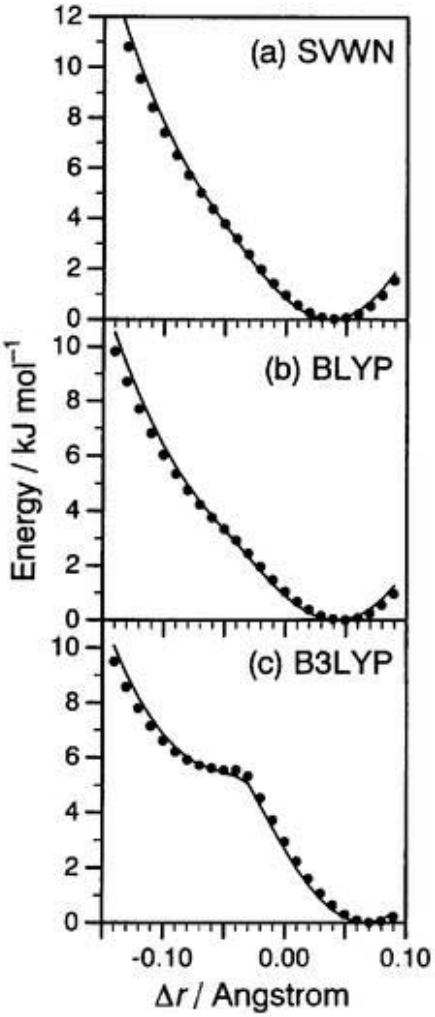

Figure 2.2 Energy per C_2H_2 unit of the *cis*-transoid (*trans*-cisoid) form of polyacetylene calculated with the (a) SVWN, (b) BLYP, and (c) B3LYP functionals as a function of the degree of bond alternation (Δr). The results obtained with the 3-21G basis set are represented by filled circles, and those obtained with the 6-31G(d) basis set by solid curves. Energy is zero for the *cis*-transoid form. The C–H bond length, CCC angle, C=CH angle, and the sum of the C=C and C–C bond lengths are fixed at the optimized values for the *cis*-transoid form.

Table 2.3 Calculated total and relative energies of polyacetylene. Total energies (E) in hartrees per C_2H_2 unit, and energies relative to the *trans*-transoid form (ΔE) in kJ mol^{-1} per C_2H_2 unit.

Functional /	*Trans*-transoid		*Cis*-transoid		*Trans*-cisoid	
Basis set	E	ΔE	E	ΔE	E	ΔE
SVWN/3-21G	−76.54305	0.0	−76.54010	7.7	*a*	
SVWN/6-31G(d)	−76.96314	0.0	−76.95957	9.4	*a*	
BLYP/3-21G	−76.94659	0.0	−76.94296	9.5	*a*	
BLYP/6-31G(d)	−77.37123	0.0	−77.36708	10.9	*a*	
B3LYP/3-21G	−76.98339	0.0	−76.98017	8.5	−76.97824	13.5
B3LYP/6-31G(d)	−77.40782	0.0	−77.40408	9.8	*b*	

[a] No local minimum corresponding to the *trans*-cisoid form was found with the SVWN and BLYP functionals. [b] See text.

orbital calculations, except for the recent study of Choi *et al.* [67] (see below). In what follows, the relative stability and internal rotation potentials of the polyacetylene isomers are examined by making use of the B3LYP functional.

The total and relative energies of the three forms of polyacetylene at their optimized structures are shown in Table 2.3. With all the functionals used, the relative stability of the Tt and Ct forms is predicted in the order expected from experiment. The relative energies of the Ct and Tc forms calculated at the B3LYP/3-21G level are 8.5 and 13.5 kJ mol^{-1}, respectively. These values are comparable to those obtained at the HF/4-31G level (8.7 and 15.0 kJ mol^{-1}, respectively) [28]. The relative energy of the Ct form calculated at the B3LYP/6-31G(d) level is 9.8 kJ mol^{-1} and is consistent with the result of our previous calculations on oligoenes at the B3LYP/6-31G(d) level (for example, the corresponding relative energies is 6.4 kJ mol^{-1} for 1,3,5,7,9,11,13-tetradecaheptaene, and is expected to increase with increasing chain length) [58]. The present result, on the other hand, disagrees with the result of a previous linear-muffin-tin-orbital local density functional study [7], which predicted that the Tc form was more stable than the Ct form.

The energies of the various forms of polyacetylene calculated with the B3LYP functional are plotted as a function of the CC–CC dihedral angle in Fig. 2.3. The plot in Fig. 2.3(a) was obtained by changing the dihedral angle alone with all the remaining structural parameters fixed at the optimized values of the Tt form. The filled circles represent the results obtained at the B3LYP/3-21G level and the solid curves represent those obtained at the B3LYP/6-31G(d) level. The filled circles and solid curves in Fig. 2.3(b) were likewise drawn by fixing all the structural parameters other than the CC–CC dihedral angle at the optimized values of the Ct form.

The potential energy curve in Fig. 2.3(a) has minima at the dihedral angles of 0° and

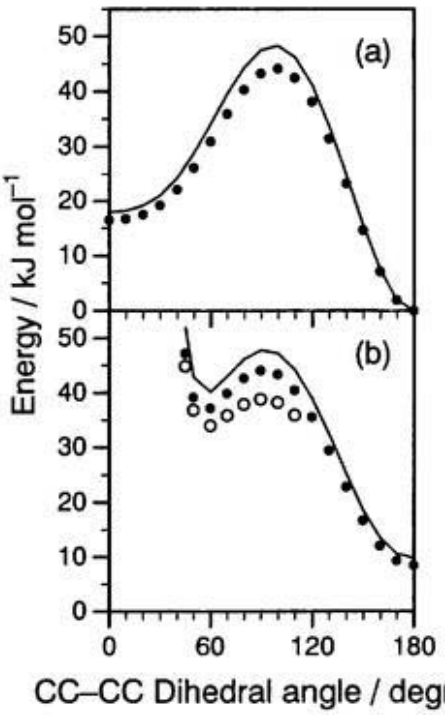

Figure 2.3 Energies per C_2H_2 unit of (a) the *trans*-transoid (*trans*-cisoid) and (b) the *cis*-transoid (*cis*-gauche) forms of polyacetylene calculated with the B3LYP functional as a function of the CC–CC dihedral angle. The results obtained with the 3-21G basis set are represented by filled circles, and those obtained with the 6-31G(d) basis set by solid curves. Energy is zero for the *trans*-transoid form. Filled circles and solid curves in (a) and (b) are obtained by changing the CC–CC angles with all the other structural parameters fixed at the optimized values of the *trans*-transoid and *cis*-transoid forms, respectively. Open circles in (b) are plotted by optimizing the C=C and C–C bond lengths for each CC–CC angle by using the 3-21G basis set.

180° corresponding to the Tc and Tt forms, respectively. The calculated potential energy curve suggests that the Tc form as well as the Tt form has a planar structure. The same conclusion has been drawn by Teramae *et al.* [68] on the basis of the vibrational analysis of the Tc form at the HF/STO-3G level. The potential energy curve calculated with the 6-31G(d) basis set has a slightly higher energy barrier at about 100° than that calculated with the 3-21G basis set.

The potential energy curves in Fig. 2.3(b) have a deep minimum at 180° (Ct form) and a shallow minimum at about 60°. At the latter minimum, the conformation about the C–C bonds is *gauche* rather than *s-cis*. It is therefore more appropriate to call this form *cis*-gauche (Cg) rather than *cis*-cisoid (Cc). The potential energy curve rises sharply at 45° and reaches infinity at 0° due to steric hindrance. The potential energy curve obtained with the 3-21G basis set is almost parallel to that obtained with the 6-31G(d) basis set, although the use of the 6-31G(d) basis set slightly raises the internal rotation barrier for Cg→Ct isomerization from 6.9 to 7.7 kJ mol^{-1}. Owing to π-electron conjugation, it is expected that the C=C and C–C bond lengths change significantly with the CC–CC dihedral angle. The potential energy curve calculated with the 3-21G basis set by optimizing the C=C and C–C bond lengths at each fixed dihedral angle is shown in Fig. 2.3(b) by open circles. For all the dihedral angles investigated, the C–C bond lengths are longer and the C=C bond lengths are shorter than the corresponding optimized values of the Ct form (1.438 and 1.366 Å, respectively). The C–C bond is longest (1.484 Å) at 100°, which is longer than that at 180° (Ct form) by as much as 0.046 Å. This contrasts with non-conjugated systems such as polyethylene, for which the variation in the C–C bond length is 0.02 Å at maximum [66]. The internal rotation barrier for the Cg→Ct isomerization is lowered from 6.9 to 4.8 kJ mol^{-1} by taking the structural relaxation into account, but the local minimum still exists at the Cg structure. (The present result does not necessarily mean that polyenes with finite chain lengths can also exist in the Cg structure. For example, geometry optimizations at the B3LYP/3-21G level suggest that 1,3,5,7,9,11-dodecahexaene in the Cg form is unstable along the internal rotation coordinate about the central C–C bond, and 1,3,5,7,9,11,13,15-hexadecaoctaene in the Cg form is unstable along the internal rotation about the C_4-C_5 and $C_{12}-C_{13}$ bonds.) As a helix, the Cg form has much higher energy than the other forms. The energy difference between the Cg and Tt forms is larger than 30 kJ mol^{-1}. This result is a consequence of the fact that the energy lowering due to the π-electron delocalization is much less in the helical Cg form than in the other planar

forms.

The present calculations, therefore, conclude that the total energies of the polyacetylene isomers increase in the order Tt < Ct < Tc < Cg, in accordance with the result of our previous oligomer calculations [58]. One should also keep in mind that the existence of the local minimum for the Tc form is not confirmed at the B3LYP/6-31G(d) level. Rather, the B3LYP/6-31G(d) calculations suggest that the Tc form is unstable toward the formation of the Ct form by interchanging the C=C and C–C bond lengths. This result as well as the predicted order of total energies is consistent with the experimental results that the most stable polyacetylene isomer is the Tt form and the second most stable isomer is the Ct form [69], and that the Tc and Cg forms have not been synthesized or detected with confidence. The present result, however, disagrees with the results of previous experimental [70] and theoretical studies [71,72], which suggested that the Cg form is more stable than the Ct form in solution.

Recently, Choi *et al.* [67] demonstrated that the internal rotation potential about the central C–C bond of 1,3-butadiene calculated by density functional theory was different from those calculated with the ab initio molecular orbital theory. Internal rotation barrier between the *s-trans* and *gauche* minima predicted by the density functional theory was higher than those obtained with the HF and second-order Møller–Plesset perturbation (MP2) methods as well as the experimental results. Although the internal rotation potential calculated with the B3LYP functional was found to be in the best agreement with the experimental results among various exchange-correlation functionals examined, there still existed noticeable differences between them [67]. Choi *et al.* suggested that density functional theory tended to overestimate the barriers for the internal rotation involving partial π-bond breaking. In light of these results, the internal rotation barriers between the Tt and Tc minima and between the Ct and Cg minima calculated with the B3LYP functional may be overestimated. Since the Cg form has a non-planar structure with the π-electron conjugation being partially broken, the energy differences between the Cg form and the other three planar forms (Tt, Ct, and Tc) may also be overestimated.

Notwithstanding the above-mentioned limitations, we consider that the order of the total energies of the polyacetylene isomers predicted with the B3LYP functional is reliable, because the B3LYP functional correctly reproduced the order of the total energies of the *s-trans*, *gauche*, and *s-cis* forms of 1,3-butadiene [67]. Oie *et al.* [64] have also found that the energy differences between the conformers of various conjugated molecules

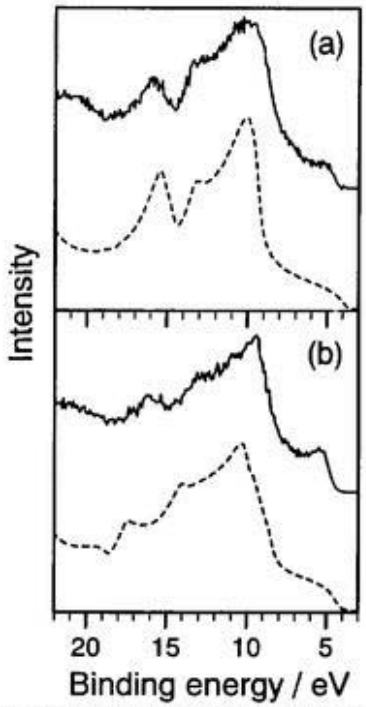

Figure 2.4 Calculated (broken curves) and observed (solid curves) ultraviolet photoelectron spectra of (a) the *trans*-transoid and (b) the *cis*-transoid forms of polyacetylene. The observed spectra are taken from Ref. [74].

obtained by gradient-corrected density functional theory are in reasonable agreement with the experimental results as well as the results obtained with the MP2 or MP4 calculations.

Crystal orbital calculations based on density functional theory are helpful in the interpretation of photoelectron spectra, as has been demonstrated by Springborg and Lev [73] and by Miao *et al.* [66] in the case of polyethylene. In Fig. 2.4, the calculated ultraviolet photoelectron spectra of the Tt and Ct forms are compared with the observed spectra [74]. The calculated spectra were obtained by convoluting a band shape function with the density of states for one-particle orbitals derived from the B3LYP/6-31G(d) calculations. As the band shape function, an 'asymmetric' Lorentzian function, whose HFHM (half width at half maximum) was 0.25 eV for the low-energy side and 1.35 eV for the high-energy side, was used. The use of the asymmetric function will be justified by the presence of vibronic levels, which is expected to make the band profiles broader in the high energy side than in the low energy side. The overall profiles of the calculated spectra are in reasonable agreement with the observed, although the calculated peak positions are slightly higher than those observed for Ct polyacetylene. The agreement is better in the present study than in the previous one [74], in which the calculated spectra were obtained

by convoluting a symmetric band shape function with the energy levels of oligoenes. The observed spectra of Tt and Ct polyacetylene are similar to each other, but the observed spectrum of Tt polyacetylene is slightly more structured in the 10–20-eV region than that of Ct polyacetylene. The present calculations reproduce this difference in the spectra. This result indicates that the energy band structures obtained from the B3LYP/6-31G(d) calculations are sufficiently reliable for the analysis of experimental results, although some ambiguity remains in their physical meaning. The spectra calculated at the B3LYP/3-21G level (not shown) are practically the same as those calculated at the B3LYP/6-31G(d) level. Thus, the energy band structures are relatively insensitive to the basis set employed. The use of the SVWN and BLYP functionals also leads to similar spectra for the Tt and Ct forms, except that the peak positions calculated with the SVWN and BLYP functionals are lower than those calculated with the B3LYP functional by about 1 and 2 eV, respectively. However, it does not seem to be appropriate to use the energy band structures calculated with the SVWN and BLYP functionals in analyzing the experimental data at least for the Tt form, because these two functionals predict too small a band gap for the Tt form. The underestimation of the band gap is closely related to the underestimation of the bond alternation [8].

2.5 Conclusion

The results of the present study are summarized as follows. (1) The effect of the exact-exchange mixing is substantial on the shape of the potential energy curves along the bond-alternation coordinate. The SVWN and BLYP functionals tend to underestimate the double-minimum character of the potential energy curves not only for the Tt form but also for the Ct form of polyacetylene. (2) The optimized structural parameters of the Tt and Ct forms obtained from the B3LYP calculations are reasonable in comparison with the experimental results. (3) The potential energy curve of the Ct form along the bond-alternation coordinate suggests that the energy barrier for the Tc→Ct isomerization is very low. (4) The B3LYP calculations indicate that the total energies of the Tt, Ct, Tc, and Cg forms increase in this order. (5) The B3LYP calculations satisfactorily reproduce the observed ultraviolet photoelectron spectra of the Tt and Ct forms.

Appendix: Auxiliary fitting of electron density

Electron density of the whole polymer chain is first partitioned into electron density associated with each unit cell:

$$\rho^{(p)}(\mathbf{r}) = \sum_{\mu,\nu}\sum_{q} P_{\mu\nu}^{(q)}\chi_{\mu}^{(p)}(\mathbf{r})\chi_{\nu}^{(p+q)}(\mathbf{r}). \tag{2.20}$$

The unit cell density is approximated by a linear combination of auxiliary basis functions

$$\tilde{\rho}^{(p)}(\mathbf{r}) = \sum_{\gamma} D_{\gamma}\theta_{\gamma}^{(p)}(\mathbf{r}), \tag{2.21}$$

where $\theta_{\gamma}^{(p)}(\mathbf{r})$ is the auxiliary basis function centered in unit cell p with associated expansion coefficient D_{γ}. Here a tilde indicates an approximated quantity. The most accurate approximation to the Coulomb repulsion energy results from minimizing

$$\Delta = \sum_{q}\int \left[\rho^{(0)}(\mathbf{r}_1) - \tilde{\rho}^{(0)}(\mathbf{r}_1)\right]\frac{1}{r_{12}}\left[\rho^{(q)}(\mathbf{r}_2) - \tilde{\rho}^{(q)}(\mathbf{r}_2)\right]d\mathbf{r}_1 d\mathbf{r}_2, \tag{2.22}$$

which corresponds to the electron repulsion energy due to residual electron density and is a positive-definite quantity. Using simplified notation for integrals, we can rewrite Eq. (2.22) as

$$\Delta = \sum_{q}\left\{(\rho^{(0)}|\rho^{(q)}) - (\rho^{(0)}|\tilde{\rho}^{(q)}) - (\tilde{\rho}^{(0)}|\rho^{(q)}) + (\tilde{\rho}^{(0)}|\tilde{\rho}^{(q)})\right\} \tag{2.23}$$

$$= \sum_{q}\left\{(\rho^{(0)}|\rho^{(q)}) - \sum_{\gamma} D_{\gamma}(\rho^{(0)}|\gamma^{(q)}) - \sum_{\gamma} D_{\gamma}(\gamma^{(0)}|\rho^{(q)}) + \sum_{\gamma,\delta} D_{\gamma}D_{\delta}(\gamma^{(0)}|\delta^{(q)})\right\}. \tag{2.24}$$

We require that this to be stationary together with the normalization constraint

$$\int \tilde{\rho}(\mathbf{r})d\mathbf{r} = \sum_{\gamma} D_{\gamma}\int \theta_{\gamma}(\mathbf{r})d\mathbf{r} = N_e, \tag{2.25}$$

where N_e is the number of electrons per unit cell. This is equivalent to writing

$$\frac{\partial}{\partial D_{\gamma}}\left\{\Delta - \Lambda\left(\sum_{\delta} D_{\delta}\int \theta_{\delta}(\mathbf{r})d\mathbf{r} - N_e\right)\right\} = 0, \tag{2.26}$$

where Λ is a Lagrange multiplier. The differentiation results in

$$2\sum_{q}\sum_{\delta} D_{\delta}(\gamma^{(0)}|\delta^{(q)}) - 2\sum_{q}(\rho^{(0)}|\gamma^{(q)}) - \Lambda\int \theta_{\gamma}(\mathbf{r})d\mathbf{r} = 0, \tag{2.27}$$

or in matrix notation

$$\mathbf{S} \cdot \mathbf{d} = \mathbf{t} + \Lambda \mathbf{n}. \tag{2.28}$$

with

$$S_{\gamma\delta} = \sum_q (\gamma^{(0)}|\delta^{(q)}), \tag{2.29}$$

$$d_\gamma = D_\gamma, \tag{2.30}$$

$$t_\gamma = \sum_{q,r} \sum_{\mu,\nu} P^{(r)}_{\mu\nu} (\mu^{(0)}\nu^{(r)}|\gamma^{(q)}), \tag{2.31}$$

$$n_\gamma = \int \theta_\gamma(\mathbf{r}) d\mathbf{r}. \tag{2.32}$$

In Eq. (2.28), the factor of 2 has been folded into the Lagrange multiplier. Substitution of Eq. (2.28) into the constraint Eq. (2.25) leads to

$$N_e = \bar{\mathbf{n}} \cdot \mathbf{d} = \bar{\mathbf{n}} \cdot \mathbf{S}^{-1} \cdot \mathbf{t} + \Lambda \bar{\mathbf{n}} \cdot \mathbf{S}^{-1} \cdot \mathbf{n}, \tag{2.33}$$

where $\bar{\mathbf{n}}$ denotes the transposed matrix of $\mathbf{n}$. By combining this equation and Eq. (2.28), we obtain the explicit formula for expansion coefficients

$$\mathbf{d} = \mathbf{S}^{-1} \left(\mathbf{t} + \frac{N_e - \bar{\mathbf{n}} \cdot \mathbf{S}^{-1} \cdot \mathbf{t}}{\bar{\mathbf{n}} \cdot \mathbf{S}^{-1} \cdot \mathbf{n}} \mathbf{n} \right). \tag{2.34}$$

Since we have minimized Δ, which has been defined by Eq. (2.23), it is most reasonable to approximate Coulomb repulsion energy $\frac{1}{2}\sum_q (\rho^{(0)}|\rho^{(q)})$ as

$$\frac{1}{2} \sum_q (\rho^{(0)}|\rho^{(q)}) = \sum_q (\rho^{(0)}|\tilde{\rho}^{(q)}) - \frac{1}{2} \sum_q (\tilde{\rho}^{(0)}|\tilde{\rho}^{(q)}). \tag{2.35}$$

This expression is equivalent to the sum of the second and third terms of the right-hand side of Eq. (2.18).

References

[1] R. G. Parr and W. Yang, *Density-Functional Theory of Atoms and Molecules* (Oxford University Press, NewYork, 1989).

[2] T. Ziegler, Chem. Rev., **91,** 651 (1991).

[3] J. C. W. Chien, *Polyacetylene: Chemistry, Physics, and Material Science* (Academic Press, Orlando, 1984).

[4] P. M. Grant and I. P. Batra, Solid State Commun., **29,** 225 (1979).

[5] R. V. Kasowski, W. Y. Hsu, and E. B. Caruthers, J. Chem. Phys., **72,** 4896 (1980).

[6] J. W. Mintmire and C. T. White, Phys. Rev. Lett., **50,** 101 (1983).

[7] M. Springborg, Phys. Rev. B, **33,** 8475 (1986).

[8] J. W. Mintmire and C. T. White, Phys. Rev. B, **35,** 4180 (1987).

[9] J. von Boehm, P. Kuivalainen, and J.-L. Calais, Phys. Rev. B, **35,** 8177 (1987).

[10] P. Vogl and D. K. Campbell, Phys. Rev. Lett., **62,** 2012 (1989).

[11] J. Ashkenazi, W. E. Pickett, H. Krakauer, C. S. Wang, B. M. Klein, and S. R. Chubb, Phys. Rev. Lett., **62,** 2016 (1989).

[12] P. Vogl and D. K. Campbell, Phys. Rev. B, **41,** 12797 (1990).

[13] M. Springborg, J.-L. Calais, O. Goscinski, and L. A. Eriksson, Phys. Rev. B, **44,** 12713 (1991).

[14] J. Paloheimo and J. von Boehm, Phys. Rev. B, **46,** 4304 (1992).

[15] S. Suhai, Phys. Rev. B, **51,** 16553 (1995).

[16] This form has alternatively been referred to as the *cis*-cisoid (Cc) form. However, it has a helical structure with the conformation about the C–C bonds being *gauche* rather than *s-cis*, and therefore, it is more appropriate to call it the *cis*-gauche (Cg) form.

[17] G. Del Re, J. Ladik, and G. Biczo, Phys. Rev, **155,** 997 (1967).

[18] J. M. Andre, J. Chem. Phys., **50,** 1536 (1969).

[19] H. Fujita and A. Imamura, J. Chem. Phys., **53,** 4555 (1970).

[20] A. Imamura and H. Fujita, J. Chem. Phys., **61,** 115 (1974).

[21] M. Kertesz, Adv. Quantum Chem., **15,** 161 (1982).

[22] J. A. Pople, P. M. W. Gill, and B. G. Johnson, Chem. Phys. Lett., **199,** 557 (1992).

[23] B. G. Johnson, P. M. W. Gill, and J. A. Pople, J. Chem. Phys., **98,** 5612 (1993).

[24] B. I. Dunlap, J. W. D. Connolly, and J. R. Sabin, J. Chem. Phys., **71,** 3396 (1979).

[25] S. Obara and A. Saika, J. Chem. Phys., **84,** 3963 (1986).

[26] J. Andzelm and E. Wimmer, J. Chem. Phys., **96,** 1280 (1992).

[27] S. Suhai, J. Chem. Phys., **73,** 3843 (1980).

[28] H. Teramae, J. Chem. Phys., **85,** 990 (1986).

[29] J. Delhalle, L. Piela, J.-L. Bredas, and J.-M. Andre, Phys. Rev. B, **22,** 6254 (1980).

[30] J. M. Andre, D. P. Vercauteren, V. P. Bodart, and J. G. Fripiat, J. Comp. Chem., **5,** 535 (1984).

[31] A. D. Becke, J. Chem. Phys., **88,** 2547 (1988).

[32] V. I. Lebedev, Zh. Vychisl. Mat. Mat. Fiz., **15,** 48 (1975).

[33] V. I. Lebedev, Zh. Vychisl. Mat. Mat. Fiz., **16,** 293 (1976).

[34] V. I. Lebedev, Sibirsk. Mat. Zh., **18,** 132 (1977).

[35] O. Treutler and R. Ahlrichs, J. Chem. Phys., **102,** 346 (1995).

[36] J. S. Binkley, J. A. Pople, and W. J. Hehre, J. Am. Chem. Soc., **102,** 939 (1980).

[37] W. J. Hehre, R. Ditchfield, and J. A. Pople, J. Chem. Phys., **56,** 2257 (1972).

[38] P. C. Hariharan and J. A. Pople, Theor. Chim. Acta, **28,** 213 (1973).

[39] J. C. Slater, *Quantum Theory of Molecules and Solids, Vol. 4: The Self-Consistent Field for Molecules and Solids* (McGraw–Hill, NewYork, 1974).

[40] S. H. Vosko, L. Wilk, and M. Nusair, Can. J. Phys., **58,** 1200 (1980).

[41] A. D. Becke, Phys. Rev. A, **38,** 3098 (1988).

[42] C. Lee, W. Yang, and R. G. Parr, Phys. Rev. B, **37,** 785 (1988).

[43] B. Miehlich, A. Savin, H. Stoll, and H. Preuss, Chem. Phys. Lett., **157,** 200 (1989).

[44] A. D. Becke, J. Chem. Phys., **98,** 5648 (1993).

[45] A. D. Becke, J. Chem. Phys., **96,** 2155 (1992).

[46] P. M. W. Gill, B. G. Johnson, J, A, Pople, and M. J. Frisch, Chem. Phys. Lett., **197,** 499 (1992).

[47] A. D. Becke, J. Chem. Phys., **97,** 9173 (1992).

[48] J. M. Seminario, Chem. Phys. Lett., **206,** 547 (1993).

[49] H. Chen, M. Krasowski, and G. Fitzgerald, J. Chem. Phys., **98,** 8710 (1993).

[50] J. B. Foresman and Æ. Frisch, *Exploring Chemistry with Electronic Structure Methods,* 2nd ed. (Gaussian Inc., Pittsburgh, 1996).

[51] M. J. Frisch, G. W. Trucks, and J. R. Cheeseman, in *Recent Developments and Applications of Modern Density Functional Theory,* edited by J. M. Seminario (Elsevier, Amsterdam, 1996).

[52] R. M. Dickson and A. D. Becke, J. Chem. Phys., **99,** 3898 (1993).

[53] M. W. Wong, Chem. Phys. Lett., **256,** 391 (1996).

[54] A. P. Scott and L. Radom, J. Phys. Chem., **100,** 16502 (1996).

[55] P. Pulay, Chem. Phys. Lett., **73,** 393 (1980).

[56] W. H. Press, S. A. Teukolsky, W. T. Vetterling, and B. P. Flannery, *Numerical Recipes in FORTRAN: The Art of Scientific Computing,* 2nd ed. (Cambridge University Press, Cambridge, 1992).

[57] S. Hirata, H. Torii, and M. Tasumi, J. Chem. Phys., **103,** 8964 (1995).

[58] S. Hirata, H. Torii, and M. Tasumi, Bull. Chem. Soc. Jpn., **69,** 3089 (1996).

[59] Chapter 3 of the present thesis.

[60] C. S. Yannoni and T. C. Clarke, Phys. Rev. Lett., **51,** 1191 (1983).

[61] D. A. Dixon, N. Matsuzawa, and S. C. Walker, J. Phys. Chem., **96,** 10740 (1992).

[62] I. A. Topol and S. K. Burt, Chem. Phys. Lett., **204,** 611 (1993).

[63] G. I. Csonka and I. G. Csizmadia, Chem. Phys. Lett., **243,** 419 (1995).

[64] T. Oie, I. A. Topol, and S. K. Burt, J. Phys. Chem., **99,** 905 (1995).

[65] S. Tsuzuki, T. Uchimaru, and K. Tanabe, Chem. Phys. Lett., **246,** 9 (1995).

[66] M. S. Miao, P. E. Van Camp, V. E. Van Doren, J. J. Ladik, and J. W. Mintmire, Phys. Rev. B, **54,** 10430 (1996).

[67] C. H. Choi, M. Kertesz, and A. Karpfen, Chem. Phys. Lett., **276,** 266 (1997).

[68] H. Teramae, T. Yamabe, and A. Imamura, J. Chem. Phys., **81,** 3564 (1984).

[69] H. Shirakawa, T. Ito, and S. Ikeda, Polym. J., **4,** 460 (1973).

[70] F. S. Bates and G. L. Baker, Macromolecules, **16,** 1013 (1983).

[71] M. L. Elert and C. T. White, Phys. Rev B, **28,** 7387 (1983).

[72] B. K. Rao, J. A. Darsey, and N. R. Kestner, Phys. Rev. B, **31,** 1187 (1985).

[73] M. Springborg and M. Lev, Phys. Rev. B, **40,** 3333 (1989).

[74] K. Kamiya, T. Miyamae, M. Oku, K. Seki, H. Inokuchi, C. Tanaka, and J. Tanaka, J. Phys. Chem., **100,** 16213 (1996).

Chapter 3

Analytical energy gradients for density functional crystal orbital theory: application to normal vibrations of polyacetylene and polymethineimine

So Hirata and Suehiro Iwata, "Density functional crystal orbital study on the normal vibrations of polyacetylene and polymethineimine," J. Chem. Phys., **107**(23), 10075–10084 (1997).

Abstract

Optimized molecular structures and $k = 0$ (Brillouin zone center) vibrational frequencies are obtained for *trans*-transoid and *cis*-transoid polyacetylene and for *anti*-transoid and *syn*-transoid polymethineimine by the density functional crystal orbital method with the Becke3–Lee–Yang–Parr (B3LYP) functional. An analytical-energy-gradient scheme is implemented in the density functional crystal orbital method, and the force constants of the infinite polymers are evaluated by numerical differentiation of the analytical energy gradients. For the *trans*-transoid and *cis*-transoid isomers of polyacetylene, the vibrational frequencies calculated and then uniformly scaled by a single scale factor are in reasonable agreement with the observed frequencies. For polymethineimine, it is found that the calculated frequencies of the *anti*-transoid isomer completely disagree with the observed frequencies. In contrast, the calculated frequencies of *syn*-transoid polymethineimine are in agreement with the observed, although there are only three observed frequencies available. The total energy of *syn*-transoid polymethineimine is found to be lower than that of the *anti*-transoid isomer by 15.6 kJ mol^{-1}.

3.1 Introduction

Computational methods that are currently used to derive the vibrational force fields of polymers can be classified mainly into two categories—the oligomer approach and the polymer approach. In the oligomer approach, the force constants of oligomers, which are usually calculated by the ab initio molecular orbital or density functional methods, are transferred to polymers. Cui and Kertesz [1] demonstrated that this approach led to reasonable force fields for all-*trans* polyethylene by making use of the force constants of their oligomers calculated by the ab initio Hartree–Fock (HF) method and then scaled by the standard method proposed by Pulay *et al.* [2]. We [3,4] also examined the force constants of short oligoenes calculated at the second-order Møller–Plesset perturbation (MP2) level and at the Becke3–Lee–Yang–Parr (B3LYP) level for the purpose of obtaining reliable force fields of polyacetylene. In this case, however, the force constants of oligoenes could not be transferred to polyacetylene directly, because the force constants of oligoenes were strongly dependent on their chain lengths. The convergence of the force constants as a function of chain length was so slow that we had to extrapolate the force constants of the infinite chains by approximating the chain-length dependence of the force constants by

some phenomenological functions. This means that the effects of π-electron conjugation and electron correlation are slowly convergent with conjugation length. Although the phenomenological functions introduced in our previous study may possess information about the force constants of oligoenes with intermediate chain lengths, the arbitrariness of these functions cannot be completely removed.

Alternatively, one can adopt the polymer approach, in which the force constants of infinite polymers are directly evaluated by the crystal orbital method [5–9]. The polymer approach takes advantage of the periodicity (translational or screw-axis symmetry) of infinite polymer chains, and hence can be more efficient and accurate than the other approach. Teramae *et al.* [8] calculated the $k = 0$ (Brillouin zone center) vibrational frequencies of infinite polyacetylene and polymethineimine chains by using the analytical-energy-gradients scheme based on the ab initio HF crystal orbital method. The agreement between the calculated and observed frequencies of polyacetylene was, however, not satisfactory, primarily due to the neglect of electron correlation and to the lack of transferable scale factors. It is now recognized that electron correlation plays an essential role in determining some force constants of polyacetylene [3,9]. The effect of electron correlation is particularly large on the frequencies of the so-called "in-phase C=C stretching modes," which give rise to intense Raman bands. HF calculations tend to overestimate the frequencies of these modes, and this tendency cannot be eliminated by the standard scaling procedure [8,9]. It is expected that the situation be improved if we use a correlated theoretical level instead of the HF level. Density functional theory [10,11] is a strong candidate for such a purpose, because density functional calculations can include electron correlation with modest computational costs. The vibrational frequencies calculated with appropriate functionals are often in good agreement with the observed frequencies when the calculated frequencies are uniformly scaled with only one scale factor [12,13].

Density functional theory has been applied to polyacetylene mainly for the analysis of its electronic and molecular structures [14–26]. Suhai [25] thoroughly investigated the bond alternation in *trans*-transoid polyacetylene by using various exchange-correlation functionals. Suhai found that the magnitude of the bond alternation in *trans*-transoid polyacetylene could reasonably be predicted only when the exchange-correlation functionals mixed with exact exchange were used. We also examined the optimized structures of the geometric isomers of polyacetylene by using the Slater–Vosko–Wilk–Nusair (SVWN), Becke–Lee–Yang–Parr (BLYP), and B3LYP functionals [26]. In parallel with the results of

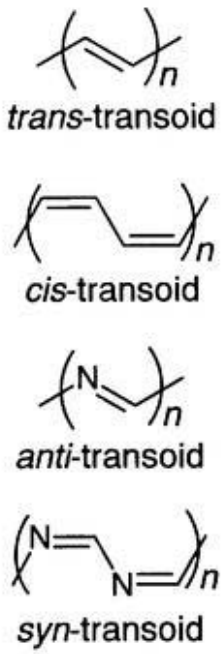

Figure 3.1 Isomers of polyacetylene and polymethineimine.

Suhai, we found that the optimized structures of *trans*-transoid polyacetylene were strongly dependent on the exchange-correlation functionals used. The results obtained with the SVWN and BLYP functionals were even qualitatively incorrect, while those obtained with the B3LYP functional seemed to be reasonable. Although the structural parameters of *cis*-transoid polyacetylene were found to be less sensitive to the exchange-correlation functionals, the differences in the optimized structures obtained with the SVWN, BLYP, and B3LYP functionals were not negligible. It is, therefore, less meaningful to calculate the vibrational frequencies of polyacetylene by using exchange-correlation functionals without exact-exchange mixing. Judging from the optimized structures, the B3LYP functional is expected to yield reasonable vibrational frequencies for polyacetylene.

In this chapter, we report the $k = 0$ vibrational frequencies of *trans*-transoid and *cis*-transoid polyacetylene and their isoelectronic polymers, *anti*-transoid and *syn*-transoid polymethineimine, calculated with the density functional crystal orbital method by using the B3LYP functional. We implemented an analytical-energy-gradient scheme in the density functional crystal orbital method, and the force constants of the infinite polymers were obtained by numerical differentiation of the analytical energy gradients. The structures of the polymers treated in the present study are depicted in Fig. 3.1. For *trans*-transoid and *cis*-transoid polyacetylene, the vibrational assignments were established for most of the

observed infrared and Raman bands [27–39], and hence the comparison between the calculated and observed frequencies serves as a test for the reliability of the present method. For polymethineimine, frequencies of only three observed infrared bands were reported [40], and the structure—the configuration and conformation—in the actual samples has not been established yet. On the basis of the calculated vibrational frequencies and the total energies of *anti*-transoid and *syn*-transoid polymethineimine, we discussed which isomer is more likely to constitute the actual polymethineimine samples.

3.2 Formulas for the analytical energy gradients

In this section, we will describe the analytical energy gradient formulas in the framework of density functional crystal orbital theory [41]. The formulas given below are based on the analytical energy gradient formulas for ab initio HF crystal orbital theory [7,8] and those for molecular density functional theory [42–44]. For the self-consistent-field procedures of the linear-combination-of-atomic-orbital crystal orbital method, the readers are referred to Refs. [26,45–50]. We start with the following expression for the total energy:

$$E = E_{\mathrm{T}} + E_{\mathrm{V}} + E_{\mathrm{J}} + m_1 E_{\mathrm{XC}} + m_2 E_{\mathrm{XX}} + E_{\mathrm{NR}}. \tag{3.1}$$

Here E_{T} is the kinetic energy, E_{V} and E_{J} are the electron-nuclear attraction and electron-electron repulsion energies, E_{XC} and E_{XX} are the electron-correlation and exact-exchange energies with the mixing ratios m_1 and m_2 [51], and E_{NR} is the nuclear-nuclear repulsion energy. E_{T} and E_{V} are given by

$$E_{\mathrm{T}} = \sum_{\mu,\nu}\sum_{q} P_{\mu\nu}^{(q)} T_{\mu\nu}^{(q)}, \tag{3.2}$$

$$E_{\mathrm{V}} = \sum_{\mu,\nu}\sum_{q} P_{\mu\nu}^{(q)} N_{\mu\nu}^{(q)}, \tag{3.3}$$

where $P_{\mu\nu}^{(q)}$ is the density matrix element between atomic orbitals μ and ν in unit cells 0 and q, whose definition is given in Chapter 2. T and N are the kinetic and electron-nuclear attraction integral matrices, respectively, and are defined as

$$T_{\mu\nu}^{(q)} = \int \chi_{\mu}^{(0)}(\mathbf{r}) \left(-\frac{1}{2}\nabla^2\right) \chi_{\nu}^{(q)}(\mathbf{r}) d\mathbf{r}, \tag{3.4}$$

$$N_{\mu\nu}^{(q)} = \sum_{A}\sum_{r} \int \chi_{\mu}^{(0)}(\mathbf{r}) \frac{-Z_A}{|\mathbf{r} - \mathbf{R}_A^{(r)}|} \chi_{\nu}^{(q)}(\mathbf{r}) d\mathbf{r}, \tag{3.5}$$

where $\chi_{\nu}^{(q)}(\mathbf{r})$ denotes the atomic basis function centered in unit cell q and Z_A the charge of nucleus A at position $\mathbf{R}_A^{(r)}$. In order to minimize the computational tasks concerning

the accumulation of the long-range electron repulsion integrals, we expanded the electron density by auxiliary basis functions according to the method of Dunlap *et al.* [52,53]. The expression for E_J is then given by

$$E_J = \sum_{\mu,\nu}\sum_{\gamma}\sum_{q} P_{\mu\nu}^{(q)} D_\gamma J_{\mu\nu\gamma}^{(q)} - \frac{1}{2}\sum_{\gamma,\delta} D_\gamma D_\delta A_{\gamma\delta}, \tag{3.6}$$

where the subscripts μ and ν specify the orbital basis functions, and the subscripts γ and δ the auxiliary basis functions. D_γ and D_δ are the expansion coefficients for the auxiliary basis functions θ_γ and θ_δ, respectively, and $J_{\mu\nu\gamma}^{(q)}$ and $A_{\gamma\delta}$ are the three-index and two-index electron repulsion integrals defined as follows:

$$J_{\mu\nu\gamma}^{(q)} = \sum_{r}\int \chi_\mu^{(0)}(\mathbf{r}_1)\chi_\nu^{(q)}(\mathbf{r}_1)\frac{1}{r_{12}}\theta_\gamma^{(r)}(\mathbf{r}_2)d\mathbf{r}_1 d\mathbf{r}_2, \tag{3.7}$$

$$A_{\gamma\delta} = \sum_{r}\int \theta_\gamma^{(0)}(\mathbf{r}_1)\frac{1}{r_{12}}\theta_\delta^{(r)}(\mathbf{r}_2)d\mathbf{r}_1 d\mathbf{r}_2. \tag{3.8}$$

The expansion coefficients D can be obtained with these integrals and the normalization coefficients of the auxiliary basis functions [52,53] (see also Appendix of Chapter 2). The choice of the auxiliary basis functions in the present study will be described in the next section. E_{XC} and E_{XX} are given by

$$E_{XC} = \int_{\text{cell}} f[\rho, \nabla\rho]d\mathbf{r}, \tag{3.9}$$

$$E_{XX} = -\frac{1}{4}\sum_{\mu,\nu}\sum_{\lambda,\sigma}\sum_{q,r,s} P_{\mu\nu}^{(r)} P_{\lambda\sigma}^{(s-q)} \left(\mu^{(0)}\lambda^{(q)}|\nu^{(r)}\sigma^{(s)}\right), \tag{3.10}$$

where $f[\rho, \nabla\rho]$ is an exchange-correlation functional of electron density ρ and of electron density gradients $\nabla\rho$ and $\left(\mu^{(0)}\lambda^{(q)}|\nu^{(r)}\sigma^{(s)}\right)$ is the four-index electron repulsion integrals

$$\left(\mu^{(0)}\nu^{(q)}|\lambda^{(r)}\sigma^{(s)}\right) = \int\int \chi_\mu^{(0)}(\mathbf{r}_1)\chi_\nu^{(q)}(\mathbf{r}_1)\frac{1}{r_{12}}\chi_\lambda^{(r)}(\mathbf{r}_2)\chi_\sigma^{(s)}(\mathbf{r}_2)d\mathbf{r}_1 d\mathbf{r}_2. \tag{3.11}$$

In the present implementation, the exchange-correlation energy and the associated exchange-correlation integrals were evaluated numerically. Accordingly, the formulation given below does not involve the auxiliary fitting of the exchange-correlation potential.

The energy gradient with respect to a nuclear coordinate Q is then given by the following expression with the aid of the energy-weighted density matrix W and the overlap integral matrix S.

$$\frac{\partial E}{\partial Q} = \sum_{\mu,\nu}\sum_{q} P_{\mu\nu}^{(q)}\left(\frac{\partial T_{\mu\nu}^{(q)}}{\partial Q} + \frac{\partial N_{\mu\nu}^{(q)}}{\partial Q}\right)$$

$$+\sum_{\mu,\nu}\sum_{\gamma}\sum_{q} P_{\mu\nu}^{(q)} D_\gamma \frac{\partial J_{\mu\nu\gamma}^{(q)}}{\partial Q} - \frac{1}{2}\sum_{\gamma,\delta} D_\gamma D_\delta \frac{\partial A_{\gamma\delta}}{\partial Q} + m_1 \left(\frac{\partial E_{\rm XC}}{\partial Q}\right)'$$
$$-\frac{m_2}{4}\sum_{\mu,\nu}\sum_{\lambda,\sigma}\sum_{q,r,s} P_{\mu\nu}^{(r)} P_{\lambda\sigma}^{(s-q)} \left(\frac{\partial}{\partial Q}\right)\left(\mu^{(0)}\lambda^{(q)}|\nu^{(r)}\sigma^{(s)}\right)$$
$$+\frac{\partial E_{\rm NR}}{\partial Q} - \sum_{\mu,\nu}\sum_{q} W_{\mu\nu}^{(q)} \frac{\partial S_{\mu\nu}^{(q)}}{\partial Q}. \tag{3.12}$$

The elements of the overlap integral matrix are defined as

$$S_{\mu\nu}^{(q)} = \int \chi_\mu^{(0)}(\mathbf{r})\chi_\nu^{(q)}(\mathbf{r})d\mathbf{r}. \tag{3.13}$$

The definition of the energy-weighted density matrix elements for crystal orbital theory is obtained by the straightforward generalization of that for molecular orbital theory. Equation (3.12) is obtained by assuming that all the nuclei that are equivalent by the translational (screw-axis) symmetry move in phase [7,8]. It should be noted that the terms which involve the differentiation of D_γ with respect to Q cancel with each other and do not appear in Eq. (3.12) [42]. The primed term $(\partial E_{\rm XC}/\partial Q)'$ is the first derivative of the exchange-correlation energy $E_{\rm XC}$, but it excludes the contribution involving the differentiation of the density matrix elements with respect to Q, which is already taken into account in the last term of Eq. (3.12). Thus, this term is given by

$$\left(\frac{\partial E_{\rm XC}}{\partial Q}\right)' = \sum_{\mu,\nu}\sum_{q} P_{\mu\nu}^{(q)} \int \left\{ \chi_\mu^{(0)} v_{\rm XC} \frac{\partial \chi_\nu^{(q)}}{\partial Q} + \frac{\partial \chi_\mu^{(0)}}{\partial Q} v_{\rm XC} \chi_\nu^{(q)} + \nabla\chi_\mu^{(0)} \cdot \mathbf{g}_{\rm XC} \frac{\partial \chi_\nu^{(q)}}{\partial Q} \right.$$
$$\left. + \frac{\partial \nabla\chi_\mu^{(0)}}{\partial Q} \cdot \mathbf{g}_{\rm XC}\chi_\nu^{(q)} + \chi_\mu^{(0)}\mathbf{g}_{\rm XC} \cdot \frac{\partial \nabla\chi_\nu^{(q)}}{\partial Q} + \frac{\partial \chi_\mu^{(0)}}{\partial Q}\mathbf{g}_{\rm XC} \cdot \nabla\chi_\nu^{(q)} \right\} d\mathbf{r} \tag{3.14}$$

with

$$\begin{aligned} v_{\rm XC} &= \frac{\partial f}{\partial \rho}, \\ \mathbf{g}_{\rm XC} &= \left(\frac{\partial f}{\partial \gamma_{\alpha\alpha}} + \frac{1}{2}\frac{\partial f}{\partial \gamma_{\alpha\beta}}\right)\nabla\rho, \\ \gamma_{\alpha\alpha} &= \nabla\rho_\alpha \cdot \nabla\rho_\alpha, \\ \gamma_{\alpha\beta} &= \nabla\rho_\alpha \cdot \nabla\rho_\beta. \end{aligned} \tag{3.15}$$

Here the subscripts α and β denote spins. In the expression of the exchange-correlation first derivatives, Johnson *et al.* [44] included the derivatives of the quadrature weights with respect to nuclear coordinates. Although the contributions of the quadrature weight derivatives to the total energy gradients are not negligible for small numerical integration grids, they can be made insignificant by taking a sufficiently large number of grid points

[44,54]. The grids employed in the present study, which are specified in the next section, are sufficiently large such that the contributions of the quadrature weight derivatives can safely be neglected.

Teramae *et al.* [7,8] derived a formula for the energy gradient with respect to the translational period a in the framework of the HF crystal orbital method. The corresponding formula for the density functional crystal orbital method is obtained analogously by using the following relation:

$$\frac{\partial}{\partial a} = \sum_q \sum_A \frac{\partial Q_z^{A(q)}}{\partial a} \frac{\partial}{\partial Q_z^{A(q)}} = \sum_q \sum_A q \frac{\partial}{\partial Q_z^{A(q)}}. \tag{3.16}$$

Here $Q_z^{A(q)}$ is the z coordinate of nucleus A in unit cell q, and we assumed that the chain axis is parallel to the z axis. However, attention must be paid to the fact that the region of numerical integration of exchange-correlation energy E_{XC} depends on the translational period. As a result, the exchange-correlation energy contribution to the energy gradient contains a two-dimensional integral whose region of integration is the boundary plane between two adjacent unit cells.

$$\begin{aligned}
\left(\frac{\partial E_{\mathrm{XC}}}{\partial a}\right)' &= \left(\frac{\partial}{\partial a}\right)' \int_{\mathrm{cell}} f[\rho, \nabla\rho] dxdydz \\
&= \int_{\mathrm{boundary}} f[\rho, \nabla\rho] dxdy \\
&\quad + \sum_{\mu,\nu} \sum_q \sum_A q P_{\mu\nu}^{(q)} \int \left\{ \chi_\mu^{(0)} v_{\mathrm{XC}} \frac{\partial \chi_\nu^{(q)}}{\partial Q_z^{A(q)}} \right. \\
&\quad \left. + \nabla\chi_\mu^{(0)} \cdot \mathbf{g}_{\mathrm{XC}} \frac{\partial \chi_\nu^{(q)}}{\partial Q_z^{A(q)}} + \chi_\mu^{(0)} \mathbf{g}_{\mathrm{XC}} \cdot \frac{\partial \nabla\chi_\nu^{(q)}}{\partial Q_z^{A(q)}} \right\} dxdydz.
\end{aligned} \tag{3.17}$$

The two-dimensional integral [the first term in the right-hand side of Eq. (3.17)] can be transformed to three-dimensional integrals by virtue of Gauss theorem:

$$\begin{aligned}
&\int_{\mathrm{boundary}} f[\rho, \nabla\rho] dxdy = \frac{E_{\mathrm{XC}}}{a} \\
&+ \sum_{\mu,\nu} \sum_q P_{\mu\nu}^{(q)} \int \frac{z}{a} \left\{ \chi_\mu^{(0)} v_{\mathrm{XC}} \frac{\partial \chi_\nu^{(q)}}{\partial z} + \frac{\partial \chi_\mu^{(0)}}{\partial Q} v_{\mathrm{XC}} \chi_\nu^{(q)} \right. \\
&+ \nabla\chi_\mu^{(0)} \cdot \mathbf{g}_{\mathrm{XC}} \frac{\partial \chi_\nu^{(q)}}{\partial z} + \frac{\partial \nabla\chi_\mu^{(0)}}{\partial z} \cdot \mathbf{g}_{\mathrm{XC}} \chi_\nu^{(q)} \\
&+ \left. \chi_\mu^{(0)} \mathbf{g}_{\mathrm{XC}} \cdot \frac{\partial \nabla\chi_\nu^{(q)}}{\partial z} + \frac{\partial \chi_\mu^{(0)}}{\partial z} \mathbf{g}_{\mathrm{XC}} \cdot \nabla\chi_\nu^{(q)} \right\} dxdydz.
\end{aligned} \tag{3.18}$$

The differentiation with respect to z can also be viewed as the differentiation with respect to a nuclear coordinate with the opposite sign [55]. The right-hand side of Eq. (3.18) can

Table 3.1 Exponents of the auxiliary Gaussian functions for hydrogen, carbon, and nitrogen.

Auxiliary basis set I		Auxiliary basis set II	
Hydrogen and nitrogen	Carbon	Hydrogen	Carbon
s		s	
37.46	512.6	37.46	512.6
21.56	170.9	21.56	170.9
19.37	56.95	19.37	56.95
18.89	18.98	18.89	18.98
5.651	6.328	5.651	15.74
3.466		3.466	10.80
		2.987	6.328
			5.399
spd		spd	
2.987	15.74	1.280	2.699
1.280	10.80	0.8014	
0.8014	5.399	spdf	
0.3226	2.699	0.3226	1.350
	1.350		0.6749
	0.6749		0.3374
	0.3374		

be evaluated by adding only a few statements to the programs for the evaluation of the right-hand side of Eq. (3.14).

3.3 Computer implementation

We employed the 3-21G [56] and the 6-31G(d) [57,58] basis sets for the expansion of the Kohn–Sham orbitals. We prepared two auxiliary basis sets—auxiliary basis set I for the 3-21G calculations and auxiliary basis set II for the 6-31G(d) calculations. Auxiliary basis set I consisted of uncontracted s-type Gaussian functions and blocks of uncontracted s-type, p-type, and d-type Gaussian functions with shared exponents. Auxiliary basis set II included f-type functions in addition to s-type, p-type, and d-type functions. We summarized in Table 3.1 the exponents of the auxiliary Gaussian functions, which were determined in a similar manner as proposed by Dunlap *et al.* [52,53] on the basis of the exponents of the 6-31G(d) basis set.

The long-range Coulomb interaction was taken into account by explicitly evaluating the relevant two- and three-index electron repulsion integrals extending to the twentieth neighboring C_2H_2 and CHN unit cells. The total energies of the polymethineimine isomers were also calculated by taking into account the two- and three-index electron repulsion integrals extending to the fiftieth and hundredth neighboring CHN unit cells. For the

other molecular integrals, we took into account interactions up to the fourth neighboring unit cells for the 3-21G calculations and interactions up to the fifth neighboring unit cells for the 6-31G(d) calculations.

The exchange-correlation energy and the associated exchange-correlation integrals were evaluated numerically by using the atomic partitioning scheme developed by Becke [59]. The single-center integrations were performed by applying a second-kind Gauss–Chebyshev quadrature for the radial integration and Lebedev quadratures [60–62] for the angular integration. Numerical grids (for each atom) consisted of 50 radial points and 302 angular points. For radial shells close to the nuclei, 38-point and 50-point angular grids were employed instead of the 302-point grid, and the total number of the grid points was 8656 per atom.

The geometry optimization was performed by the GDIIS (geometry direct inversion in the iterative subspace) extrapolation [63] in combination with the steepest-descent method. The force constants were obtained by the numerical differentiation of the analytical energy gradients. The step size used in numerical differentiation was 0.04 bohr. The force-constant matrix was transformed from the Cartesian coordinate system to the mass-weighted Cartesian coordinate system. Diagonalizing the thus-obtained force-constant matrix, we obtained the $k = 0$ vibrational frequencies and the corresponding mass-weighted normal coordinates as the eigenvalues and eigenvectors [64,65].

The computer implementation of the self-consistent-field part of the method is described in more detail in Chapter 2. The geometry optimization and vibrational frequency calculation were performed for *trans*-transoid polyacetylene by using the 3-21G and the 6-31G(d) basis sets. For the other polymers treated in the present study, only the 3-21G basis set was used. The results of the B3LYP/3-21G calculations on oligomers obtained with the GAUSSIAN 94 program [66] are also discussed in the following.

3.4 Results and discussion

3.4.1 Polyacetylene

The optimized structural parameters of *trans*-transoid and *cis*-transoid polyacetylene are listed in Table 3.2. We have performed the geometry optimization for *trans*-transoid and *cis*-transoid polyacetylene at the B3LYP/3-21G level by the Powell's method previously [26]. The structural parameters optimized in the present study at the B3LYP/3-21G

Table 3.2 Optimized structural parameters of *trans*-transoid and *cis*-transoid polyacetylene. In units of Å (bond length) and degrees (bond angle).

Structural parameter	*Trans*-transoid[a]	*Trans*-transoid[b]	*Cis*-transoid[a]
C=C bond length	1.367	1.369	1.366
C–C bond length	1.428	1.426	1.437
CH bond length	1.089	1.091	1.086
CCC angle	124.3	124.5	126.5
C=CH angle	118.6	118.3	116.7

[a] Calculated with the 3-21G basis set. [b] Calculated with the 6-31G(d) basis set.

level by using analytical energy gradients with a larger auxiliary basis set are almost the same with the previous values. The structural parameters of *trans*-transoid polyacetylene calculated with the 6-31G(d) basis set are in reasonable agreement with those calculated with the 3-21G basis set. The C=C and C–C bond lengths calculated with the 3-21G and the 6-31G(d) basis sets are also consistent with the experimental values directly measured by nutation NMR spectroscopy (1.36 and 1.44 Å) [67]. The calculated C=C bond length (1.366 Å) of *cis*-transoid polyacetylene is also in agreement with the experimental value (1.37 Å) [67]. The structural aspects of polyacetylene obtained by using various exchange-correlation functionals were discussed in Refs. [25,26].

The experimental frequencies and assignments of the infrared- and Raman-active modes of polyacetylene are well established [27–39] particularly for the *trans*-transoid isomer, and on this basis we can assess the performance of the B3LYP crystal orbital method as a method of calculating the vibrational frequencies of conjugated polymers. The calculated $k = 0$ vibrational frequencies of *trans*-transoid polyacetylene and its deuterated analog are shown in Table 3.3. The observed frequencies taken from Refs. [27,33,39] are also shown for comparison. Although the unscaled frequencies are invariably higher than the observed frequencies, the frequencies uniformly scaled with a single scale factor (0.964) are in reasonable agreement with the observed frequencies regardless of the basis set used. As described in the introduction, the HF calculations tend to overestimate the frequencies of the in-phase C=C stretching modes even if the calculated frequencies are scaled [8,9]. The in-phase C=C stretching mode of *trans*-transoid polyacetylene is the ν_2 mode. It should be emphasized that at the B3LYP/3-21G and the B3LYP/6-31G(d) levels the agreement between the calculated (scaled) and observed frequencies for ν_2 is as good as that for the other modes. The largest deviation between the frequencies calculated with the 3-21G basis set and the observed can be seen for the ν_6 mode. We assigned a weak infrared band

Table 3.3 Calculated and observed frequencies of the infrared- and Raman-active modes of *trans*-transoid polyacetylene and its deuterated analog.

Species	Mode[a]		Obs.[b] / cm^{-1}	Calc. (3-21G) / cm^{-1}		Calc. (6-31G(d)) / cm^{-1}	
				Unscaled	×0.964	Unscaled	×0.964
t-$(C_2H_2)_x$	a_g	ν_1	2990	3139	3026	3146	3033
		ν_2	1457	1506	1452	1506	1452
		ν_3	1294	1342	1294	1333	1285
		ν_4	1066	1111	1071	1110	1070
	b_u	ν_5	3013	3161	3047	3159	3045
		ν_6	1170	1260	1215	1212	1168
	a_u	ν_7	1012	1061	1023	1064	1026
	b_g	ν_8	884	945	911	922	889
t-$(C_2D_2)_x$	a_g	ν_1	2230	2328	2244	2336	2252
		ν_2	1347	1379	1329	1386	1336
		ν_3	1201	1226	1182	1233	1189
		ν_4	852	896	864	879	847
	b_u	ν_5	2231	2321	2237	2319	2236
		ν_6	861	925	892	890	858
	a_u	ν_7	746	779	751	781	753
	b_g	ν_8	816	849	818	828	798

[a] The normal modes are classified under the factor group isomorphous to the point group C_{2h}. [b] References [27,33,39].

at 1170 cm^{-1} to this mode in a previous study [3], but other authors [38,39] assigned a band at 1250 cm^{-1} instead of 1170-cm^{-1} band (we confine our discussion to undeuterated *trans*-transoid polyacetylene for the sake of simplicity). The frequency of this mode calculated with the 3-21G basis set (1215 cm^{-1}) is halfway between these two values (1170 cm^{-1} and 1250 cm^{-1}), and cannot confirm either of the assignments. However, the frequency of the ν_6 mode calculated with the 6-31G(d) basis set is 1168 cm^{-1}, which is very close to the observed frequency of 1170 cm^{-1}. Therefore, the present result renders substantial support to our previous assignment [3]. The overall agreement between the frequencies calculated with the 6-31G(d) basis set and the observed is satisfactory, and it is concluded that the force fields generated by the B3LYP/6-31G(d) crystal orbital method are highly reliable. Except for the ν_6 mode, the frequencies calculated at the B3LYP/3-21G level and then scaled are in agreement with the observed ones to an almost similar extent. Thus, the calculated frequencies of *trans*-transoid polyacetylene are relatively insensitive to the inclusion of the polarization functions. The same trend was also observed for the frequencies of *trans*-transoid oligoenes and polyacetylene calculated at the MP2 level and then scaled [3]. Therefore, we expect that the calculations with the 3-21G basis set is tolerable also for the other polymers treated in the present study.

The $k = 0$ vibrational frequencies of *cis*-transoid polyacetylene calculated with the 3-

21G basis set are listed in Table 3.4 together with the observed frequencies of the infrared and Raman bands [27,33,36,37]. Although *cis*-transoid polyacetylene possesses a two-fold screw-axis symmetry, we adopted a C_4H_4 unit as a unit cell (see Fig. 3.1) instead of a C_2H_2 unit in the calculations of the force constants, in order to obtain the frequencies of all the infrared- and Raman-active modes. The calculated frequencies were scaled with the same scale factor (0.964) as that used for *trans*-transoid polyacetylene. The agreement between the scaled and observed frequencies seems to be reasonable again. It should be emphasized that the overall agreement between the calculations and experiments is remarkably improved by using the B3LYP functional instead of the HF method [8]. Nevertheless, there are still discrepancies for some modes. For example, the scaled frequencies of the in-phase C=C stretching modes (ν_2) are lower than the observed ones, particularly for the deuterated species. There are also discrepancies for the ν_{10} and ν_{14} modes of the undeuterated species. We calculated the vibrational frequencies of *cis*-transoid polyacetylene by using the force field extrapolated from those of oligoenes obtained at the B3LYP/6-31G(d) level [4]. The calculated frequencies were scaled uniformly by 0.955. The discrepancies for ν_{10} and ν_{14} are smaller in the previous study using a larger basis set, and hence the discrepancies in the present study might be attributed to the basis set inadequacy. On the contrary, the differences between the calculated and observed frequencies of ν_2 are larger in the previous study than in the present one. The larger differences in the previous study are partly due to the overestimation of the chain-length dependence of some force constants [26], but another possible origin of this discrepancy was also discussed in the previous study [4].

3.4.2 Polymethineimine

Polymethineimine was first synthesized by Wöhrle [40] in 1971. He also observed characteristic infrared bands of this compound at 3170, 1620, and 1410 cm^{-1}. There are a relatively small number of theoretical studies that dealt with the structural properties of this compound [8,68,69], and all of them assumed the *anti*-transoid structure (Fig. 3.1). The actual structure of this compound, however, is not experimentally established yet. The optimized structures of *anti*-transoid polymethineimine were obtained by using the HF crystal orbital method by Karpfen [68] and subsequently by Teramae *et al.* [8]. Teramae *et al.* also calculated the $k = 0$ vibrational frequencies of *anti*-transoid polymethineimine by using the STO-3G basis set. The frequencies calculated at the HF/STO-3G level and

Table 3.4 Calculated and observed frequencies of the infrared- and Raman-active modes of *cis*-transoid polyacetylene and its deuterated analog.

Species	Mode[a]		Observed[b] / cm^{-1}	Calculated[c] / cm^{-1}	
				Unscaled	×0.964
c-$(C_2H_2)_x$	a_g	ν_1	3090	3191	3076
		ν_2	1540	1575	1518
		ν_3	1250	1308	1260
		ν_4	910	912	879
	b_{2g}	ν_5	3030	3153	3040
		ν_6	···	1548	1493
		ν_7	1170	1233	1188
		ν_8	···	839	809
	b_{1u}	ν_9	3044	3168	3054
		ν_{10}	1328	1419	1368
		ν_{11}	448	462	445
	b_{3u}	ν_{12}	3057	3204	3089
		ν_{13}	1483	1534	1479
		ν_{14}	1246	1328	1280
	b_{1g}	ν_{15}	826	842	812
	b_{3g}	ν_{16}	···	979	944
		ν_{17}	···	584	563
	a_u	ν_{18}	(983)[d]	1027	990
		ν_{19}	(295)[d]	306	295
	b_{2u}	ν_{20}	740	774	746
c-$(C_2D_2)_x$	a_g	ν_1	2315	2357	2272
		ν_2	1470	1479	1426
		ν_3	976	1017	981
		ν_4	835	845	815
	b_{2g}	ν_5	2260	2326	2242
		ν_6	···	1388	1338
		ν_7	1040	1058	1020
		ν_8	···	740	713
	b_{1u}	ν_9	2275	2326	2243
		ν_{10}	1050	1112	1072
		ν_{11}	402	417	402
	b_{3u}	ν_{12}	2255	2366	2281
		ν_{13}	···	1513	1458
		ν_{14}	892	947	913
	b_{1g}	ν_{15}	685	698	673
	b_{3g}	ν_{16}	···	851	821
		ν_{17}	···	475	458
	a_u	ν_{18}	(765)[d]	793	765
		ν_{19}	(270)[d]	281	270
	b_{2u}	ν_{20}	548	568	548

[a] The normal modes are classified under the factor group isomorphous to the point group D_{2h}. [b] References [27,33,36,37]. [c] Calculated with the 3-21G basis set. [d] The a_u vibrations are infrared or Raman inactive.

Table 3.5 Optimized structural parameters of *anti*-transoid and *syn*-transoid polymethineimine obtained with the 3-21G basis set. In units of Å (bond length) and degrees (bond angle).

Structural parameter	*Anti*-transoid	*Syn*-transoid
C=N bond length	1.300	1.301
C–N bond length	1.373	1.400
CH bond length	1.108	1.088
CNC angle	119.3	119.1
N=CH angle	121.9	118.6

then uniformly scaled by 0.89 were 3077, 1669, 1351, 1152, and 1001 cm^{-1}. The first three of these frequencies appear to be in qualitative agreement with the observed (3170, 1620, and 1410 cm^{-1}). However, it should be remembered that the frequencies of *trans*-transoid polyacetylene calculated at this level of theory and then uniformly scaled by 0.89 considerably deviated from the observed with the largest deviation being about 340 cm^{-1} [8].

In the present study, the structures were optimized and vibrational frequencies were calculated at the B3LYP/3-21G level not only for *anti*-transoid polymethineimine but also for *syn*-transoid polymethineimine. The optimized structures for these two isomers are listed in Table 3.5. It was found that *anti*-transoid polymethineimine prefers a structure with alternating CN bond lengths, which is in accord with the results obtained by Karpfen [68] and by Teramae *et al.* [8]. It should be remarked, however, that Peierls instability, which is the origin of the bond alternation in *trans*-transoid polyacetylene, cannot be invoked to explain the bond alternation in *anti*-transoid polymethineimine. *Syn*-transoid polymethineimine was also found to have an alternating structure. The CNC and N=CH angles of *syn*-transoid polymethineimine are closer to 120° than the CCC and C=CH angles of *cis*-transoid polyacetylene. This is because hydrogen–hydrogen nonbonded repulsion in *cis*-transoid polyacetylene significantly distorts the sp^2 hybridization, and replacement of a CH group in C_2H_2 unit cell by a nitrogen atom reduces this distortion. The C=N bond lengths of *anti*-transoid and *syn*-transoid polymethineimine (1.300 and 1.301 Å, respectively) are longer than the measured C=N bond length of methylenimine CH_2NH (1.273 Å) [70], and the C–N bond lengths of *anti*-transoid and *syn*-transoid polymethineimine (1.373 and 1.400 Å, respectively) are shorter than the measured C–N bond length of methylamine CH_3NH_2 (1.471 Å) [70]. This is a consequence of the π-electron conjugation in polymethineimine, which renders the single bonds more double-bond-like character and vice versa, in complete analogy to what was observed for polyacetylene.

Table 3.6 Calculated and observed frequencies of the infrared- and Raman-active modes of *anti*-transoid and *syn*-transoid polymethineimine.

Species	Mode[a]		Observed[b] / cm^{-1}	Calculated[c] / cm^{-1}
a-$(CHN)_x$	a'	ν_1	3170	2905
		ν_2	1620	1396
		ν_3	1410	1275
		ν_4	···	916
	a''	ν_5	···	1098
s-$(CHN)_x$	a_1	ν_1	···	3153
		ν_2	···	1396
		ν_3	···	1311
		ν_4	···	842
		ν_5	···	559
	b_1	ν_6	3170	3160
		ν_7	1620	1625
		ν_8	1410	1424
		ν_9	···	1148
		ν_{10}	···	895
	a_2	ν_{11}	*d*	1095
		ν_{12}	*d*	312
	b_2	ν_{13}	···	950
		ν_{14}	···	413

[a] The normal modes are classified under the factor group isomorphous to the point group C_s for *anti*-transoid polymethineimine and C_{2v} for *syn*-transoid polymethineimine. [b] Reference [40]. [c] Calculated with the 3-21G basis set. [d] The a_2 vibrations are infrared inactive.

The calculated frequencies of *anti*-transoid and *syn*-transoid polymethineimine are compared with the observed frequencies [40] in Table 3.6. The vibrational modes are depicted in Figs. 3.2, 3.3, and 3.4. There are only four in-plane modes and one out-of-plane mode at $k = 0$ for the *anti*-transoid isomer. As is clear from the table, it is difficult to assign the observed bands at 1620 cm^{-1} and 1410 cm^{-1} to the calculated modes of *anti*-transoid polymethineimine; there are unacceptable differences between the calculated and the observed frequencies. If we assign the observed band at 1410 cm^{-1} to ν_2 (calculated frequency is 1396 cm^{-1}), the observed band at 1620 cm^{-1} seems to have no counterpart in the calculation. In contrast, if we assume that *syn*-transoid polymethineimine is the one experimentally studied, the three observed bands can be assigned tentatively to the ν_6, ν_7, and ν_8 modes. The differences between the calculated (unscaled) and observed frequencies of these modes are within 14 cm^{-1}. This result suggests the possibility that polymethineimine takes the *syn*-transoid structure.

There is another piece of theoretical evidence that support this possibility; the total energy per CHN unit cell of the *syn*-transoid isomer is lower than that of the *anti*-transoid isomer. The total energies of *anti*-transoid and *syn*-transoid polymethineimine and the

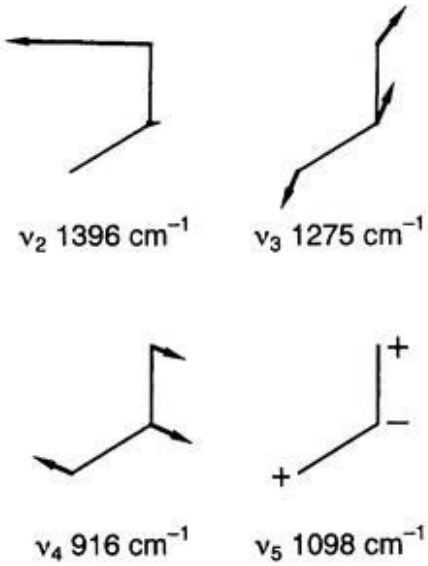

Figure 3.2 The vibrational patterns of *anti*-transoid polymethineimine. The CH stretching mode is excluded. The lines represent a N=CH unit, and the numbers indicate the scaled vibrational frequencies.

total energy differences between these two isomers are shown in Table 3.7. It should be remembered that B3LYP/3-21G calculations reproduced the total energies of the polyacetylene isomers in the experimentally correct order [26]. Since the unit cell of polymethineimine has a nonzero dipole moment, the total energies may converge very slowly with the inclusion of the long-range Coulomb interaction. Thus, we calculated the total energies of the two isomers by taking into account the interactions ($E_{\rm V} + E_{\rm J} + E_{\rm NR}$) up to the twentieth, fiftieth, and hundredth neighboring unit cells. The total energies converge at a value accurate to 5 decimal places when the interactions up to the hundredth neighboring unit cells are taken into account. The total energy of the *syn*-transoid isomer is lower than that of the *anti*-transoid isomer by 15.6 kJ mol^{-1}. The order of the total energies of the polyacetylene isomers is the reverse; *trans*-transoid polyacetylene, which is isoelectronic with *anti*-transoid polymethineimine, is more stable than *cis*-transoid polyacetylene, which is isoelectronic with *syn*-transoid polymethineimine [26].

To examine the similarity and difference between an infinite polymethineimine chain and their oligomers, the geometries of *anti*-transoid and *syn*-transoid oligomers of polymethineimine were optimized and the harmonic frequencies were evaluated at the B3LYP/3-21G level. It turned out that the geometries of *anti*-transoid oligomers of polymethineimine with intermediate chain lengths have slightly curved backbones. Thus, strictly speaking, *anti*-transoid polymethineimine does not have a translational symmetry. However, the

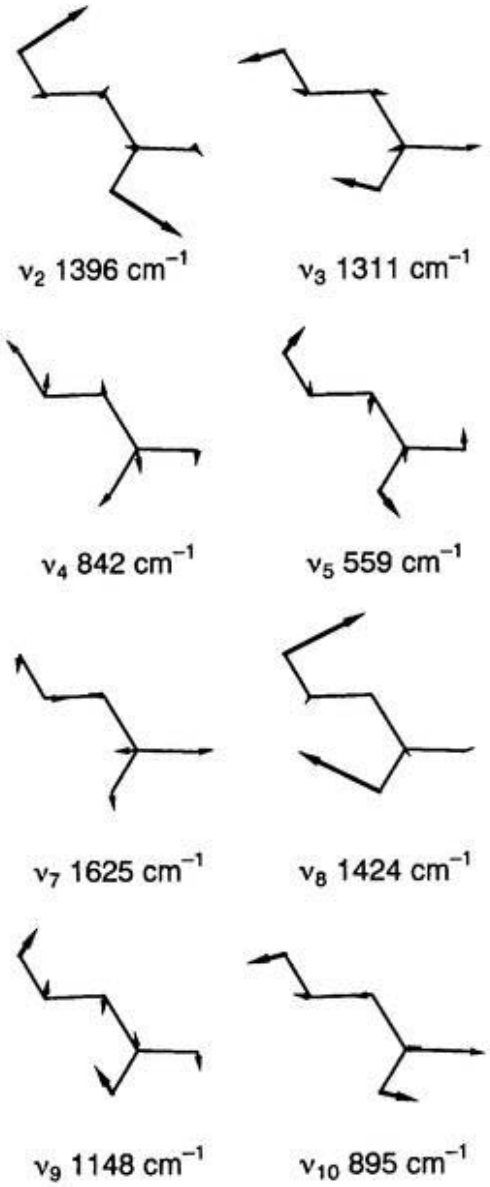

Figure 3.3 The vibrational patterns for the in-plane modes of *syn*-transoid polymethineimine. The CH stretching modes are excluded. The lines represent a CH=N–CH=N unit, and the numbers indicate the scaled vibrational frequencies.

Table 3.7 Total and relative energies of *anti*-transoid and *syn*-transoid polymethineimine calculated with the 3-21G basis set.

Number of neighbors	Total energy[a]		Relative energy[b]
	Anti-transoid	*Syn*-transoid	
20	−92.91903	−92.92493	−15.5
50	−92.91905	−92.92499	−15.6
100	−92.91905	−92.92500	−15.6

[a] In hartrees per CHN unit. [b] Energies relative to the *anti*-transoid isomer in kJ mol^{-1} per CHN unit.

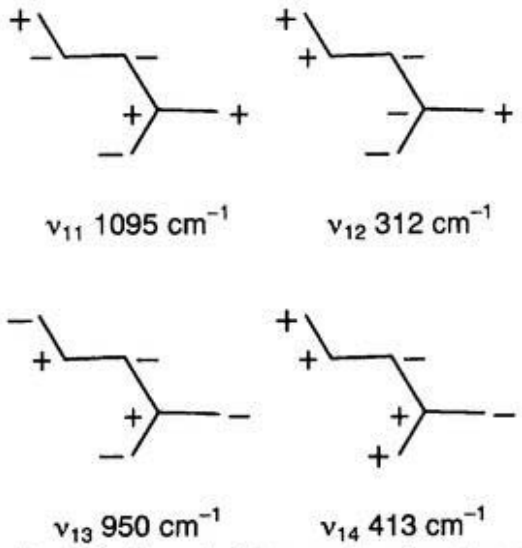

Figure 3.4 The vibrational patterns for the out-of-plane modes of *syn*-transoid polymethineimine. The lines represent a CH=N–CH=N unit, and the numbers indicate the scaled vibrational frequencies.

curvature of the oligomer backbone is small [71], and hence we can safely expect that the present treatment, which assumes a perfect translational symmetry of an infinite *anti*-transoid polymethineimine chain, will not cause serious numerical errors in the total energies, in the structural parameters, and in the vibrational frequencies. We confirmed that the total energies of the *syn*-transoid oligomers with intermediate chain lengths are lower than those of the *anti*-transoid oligomers with the same chain lengths. For instance, the difference in total energy between *anti*-transoid oligomers with 6 and 7 C=N bonds is -92.91849 hartree, and the difference between *syn*-transoid oligomers with 6 and 7 C=N bonds is -92.92336 hartree. The difference between these two values is -12.8 kJ mol^{-1}, which is comparable to the total energy difference between infinite *anti*-transoid and *syn*-transoid polymethineimine chains (-15.6 kJ mol^{-1}).

The calculations on *syn*-transoid oligomers with 6 and 7 C=N bonds also suggested that the vibrational modes which give rise to the most intense infrared bands involve the in-phase C=N stretching vibrations. The corresponding normal mode for *syn*-transoid polymethineimine is probably ν_3, although the correlation between the in-phase modes of oligomers and the $k = 0$ modes of polymer is not straightforward in this case (vide post). The calculated frequency of the ν_3 mode of *syn*-transoid polymethineimine is 1311 cm^{-1}, but no intense band was reported in this wavenumber region and only three infrared bands due to ν_6, ν_7, and ν_8 were observed [40]. Thus, the agreement between the calculated frequencies of ν_6, ν_7, and ν_8 of *syn*-transoid polymethineimine and the observed frequencies

might possibly be coincidental. The observed frequencies seem to be too few to make a definite comparison with the calculations. To conclude that the polymethineimine samples synthesized by Wöhrle consist of the *syn*-transoid chains, the experimental reexamination of the vibrational spectra of polymethineimine is required. The present calculations, nevertheless, indicate that polymethineimine is unlikely to take the *anti*-transoid structure in the actual samples, and the previous assumption that the polymethineimine samples consist of the *anti*-transoid chains is not justified.

It turned out that the vibrational patterns of some $k = 0$ modes of polymethineimine were substantially different from those of the corresponding in-phase modes of oligomers. In other words, the vibrational patterns of some modes change to a great extent with increasing chain length. The change in the vibrational patterns is particularly large for the ν_3 modes of *anti*-transoid and *syn*-transoid polymethineimine and for the in-phase C=N stretching modes of their oligomers. In the in-phase C=N stretching modes of *anti*-transoid and *syn*-transoid oligomers with 7 C=N bonds, the hydrogen and carbon atoms move nearly in the opposite direction, while in the ν_3 modes of *anti*-transoid and *syn*-transoid polymethineimine, the displacements of the carbon and hydrogen atoms are nearly in the same direction (Fig. 3.3). This change in the vibrational patterns of the in-phase C=N stretching modes between oligomers and polymers will be related to the large chain-length dependence of the vibrational frequencies of these modes. The frequencies of the in-phase C=N stretching modes of polymethineimine oligomers exhibit a larger chain-length dependence than the frequencies of the in-phase C=C stretching modes of oligoenes.

3.5 Conclusion

The analytical-energy-gradient scheme based on the density functional crystal orbital method was implemented and applied to the calculations of the normal vibrations of polyacetylene and polymethineimine. The vibrational frequencies of *trans*-transoid and *cis*-transoid polyacetylene calculated with the B3LYP functional and then uniformly scaled were in reasonable agreement with the observed frequencies. This result implies that the present method can reproduce the vibrational spectra of a variety of conjugated polymers with considerable accuracy. The isomeric form of polymethineimine in the actual samples is discussed on the basis of the calculated frequencies and total energies of the *anti*-transoid and *syn*-transoid isomers of polymethineimine. Because of a very small number

of observed frequencies available, it is difficult to conclude unambiguously which isomer the actual samples of polymethineimine consist of. The present calculations, nevertheless, indicate that the total energy of the *syn*-transoid isomer is definitely lower than that of the *anti*-transoid isomer, and the previous assumption that polymethineimine takes the *anti*-transoid structure is ungrounded.

References

[1] C. X. Cui and M. Kertesz, J. Chem. Phys., **93**, 5257 (1990).

[2] P. Pulay, G. Fogarasi, and J. E. Boggs, J. Chem. Phys., **74**, 3999 (1981).

[3] S. Hirata, H. Torii, and M. Tasumi, J. Chem. Phys., **103**, 8964 (1995).

[4] S. Hirata, H. Torii, and M. Tasumi, Bull. Chem. Soc. Jpn., **69**, 3089 (1996).

[5] A. Karpfen, J. Phys. C, **12**, 3227 (1979).

[6] M. J. S. Dewar, Y. Yamaguchi, and S. H. Suck, Chem. Phys., **43**, 145 (1979).

[7] H. Teramae, T. Yamabe, C. Satoko, and A. Imamura, Chem. Phys. Lett., **101**, 149 (1983).

[8] H. Teramae, T. Yamabe, and A. Imamura, J. Chem. Phys., **81**, 3564 (1984).

[9] M. Kofranek, H. Lischka, and A. Karpfen, J. Chem. Phys., **96**, 982 (1992).

[10] R. G. Parr and W. Yang, *Density-Functional Theory of Atoms and Molecules* (Oxford University Press, New York, 1989).

[11] T. Ziegler, Chem. Rev., **91**, 651 (1991).

[12] M. W. Wong, Chem. Phys. Lett., **256**, 391 (1996).

[13] A. P. Scott and L. Radom, J. Phys. Chem., **100**, 16502 (1996).

[14] P. M. Grant and I. P. Batra, Solid State Commun., **29**, 225 (1979).

[15] R. V. Kasowski, W. Y. Hsu, and E. B. Caruthers, J. Chem. Phys., **72**, 4896 (1980).

[16] J. W. Mintmire and C. T. White, Phys. Rev. Lett., **50**, 101 (1983).

[17] M. Springborg, Phys. Rev. B, **33**, 8475 (1986).

[18] J. W. Mintmire and C. T. White, Phys. Rev. B, **35**, 4180 (1987).

[19] J. von Boehm, P. Kuivalainen, and J.-L. Calais, Phys. Rev. B, **35**, 8177 (1987).

[20] P. Vogl and D. K. Campbell, Phys. Rev. Lett., **62**, 2012 (1989).

[21] J. Ashkenazi, W. E. Pickett, H. Krakauer, C. S. Wang, B. M. Klein, and S. R. Chubb, Phys. Rev. Lett., **62**, 2016 (1989).

[22] P. Vogl and D. K. Campbell, Phys. Rev. B, **41**, 12797 (1990).

[23] M. Springborg, J.-L. Calais, O. Goscinski, and L. A. Eriksson, Phys. Rev. B, **44**, 12713 (1991).

[24] J. Paloheimo and J. von Boehm, Phys. Rev. B, **46**, 4304 (1992).

[25] S. Suhai, Phys. Rev. B, **51**, 16553 (1995).

[26] Chapter 2 of the present thesis.

[27] H. Shirakawa and S. Ikeda, Polym. J., **2**, 231 (1971).

[28] H. Shirakawa, T. Ito, and S. Ikeda, Polym. J., **4**, 460 (1973).

[29] I. Harada, M. Tasumi, H. Shirakawa, and S. Ikeda, Chem. Lett., **1978**, 1411.

[30] S. Lefrant, L. S. Lichtmann, H. Temkin, D. B. Fitchen, D. C. Miller, G. E. Whitwell II, and J. M. Burlitch, Solid State Commun., **29**, 191 (1979).

[31] I. Harada, Y. Furukawa, M. Tasumi, H. Shirakawa, and S. Ikeda, J. Chem. Phys., **73**, 4746 (1980).

[32] L. S. Lichtmann, A. Sarhangi, and D. B. Fitchen, Solid State Commun., **36**, 869 (1980).

[33] H. Kuzmany, Phys. Status Solidi B, **97**, 521 (1980).

[34] F. B. Schügerl and H. Kuzmany, J. Chem. Phys., **74**, 953 (1981).

[35] D. B. Fitchen, Mol. Cryst. Liq. Cryst., **83**, 95 (1982).

[36] P. Piaggio, G. Dellepiane, L. Piseri, R. Tubino, and C. Taliani, Solid State Commun., **50**, 947 (1984).

[37] L. S. Lichtmann, E. A. Imhoff, A. Sarhangi, and D. B. Fitchen, J. Chem. Phys., **81**, 168 (1984).

[38] H. Takeuchi, Y. Furukawa, I. Harada, and H. Shirakawa, J. Chem. Phys., **84**, 2882 (1986).

[39] H. Takeuchi, T. Arakawa, Y. Furukawa, I. Harada, and H. Shirakawa, J. Mol. Struct., **158**, 179 (1987).

[40] D. Wöhrle, Tetrahedron Lett., **22**, 1969 (1971).

[41] It is assumed here that the system under consideration is a closed-shell system.

[42] R. Fournier, J. Andzelm, and D. R. Salahub, J. Chem. Phys., **90**, 6371 (1989).

[43] J. A. Pople, P. M. W. Gill, and B. G. Johnson, Chem. Phys. Lett., **199**, 557 (1992).

[44] B. G. Johnson, P. M. W. Gill, and J. A. Pople, J. Chem. Phys., **98**, 5612 (1993).

[45] G. Del Re, J. Ladik, and G. Biczó, Phys. Rev, **155**, 997 (1967).

[46] J. M. André, J. Chem. Phys., **50**, 1536 (1969).

[47] H. Fujita and A. Imamura, J. Chem. Phys., **53**, 4555 (1970).

[48] A. Imamura and H. Fujita, J. Chem. Phys., **61**, 115 (1974).

[49] M. Kertész, Adv. Quantum Chem., **15**, 161 (1982).

[50] J. J. Ladik, *Quantum Theory of Polymers as Solids* (Plenum Press, New York, 1988).

[51] The mixing ratios for the B3LYP functional are as follows: m_1 (Slater exchange) = 0.08, m_1 (Vosko–Wilk–Nusair correlation) = 0.19, m_1 (Becke exchange) = 0.72, m_1 (Lee–Yang–Parr correlation) = 0.81, and m_2 (HF or exact exchange) = 0.20. These optimum values were obtained by A. D. Becke, J. Chem. Phys., **98**, 5648 (1993).

[52] B. I. Dunlap, J. W. D. Connolly, and J. R. Sabin, J. Chem. Phys., **71**, 3396 (1979).

[53] B. I. Dunlap, J. W. D. Connolly, and J. R. Sabin, J. Chem. Phys., **71**, 4993 (1979).

[54] B. G. Johnson and M. J. Frisch, Chem. Phys. Lett., **216**, 133 (1993).

[55] S. Obara and A. Saika, J. Chem. Phys., **84**, 3963 (1986).

[56] J. S. Binkley, J. A. Pople, and W. J. Hehre, J. Am. Chem. Soc., **102**, 939 (1980).

[57] W. J. Hehre, R. Ditchfield, and J. A. Pople, J. Chem. Phys., **56**, 2257 (1972).

[58] P. C. Hariharan and J. A. Pople, Theo. Chim. Acta, **28**, 213 (1973).

[59] A. D. Becke, J. Chem. Phys., **88**, 2547 (1988).

[60] V. I. Lebedev, Zh. Vychisl. Mat. Mat. Fiz. **15**, 48 (1975).

[61] V. I. Lebedev, Zh. Vychisl. Mat. Mat. Fiz. **16**, 293 (1976).

[62] V. I. Lebedev, Sibirsk. Mat. Zh. **18**, 132 (1977).

[63] P. Császár and P. Pulay, J. Mol. Struct., **114**, 31 (1984).

[64] M. Tasumi and T. Shimanouchi, J. Chem. Phys., **43**, 1245 (1965).

[65] L. Piseri and G. Zerbi, J. Mol. Spectrosc., **26**, 254 (1968).

[66] GAUSSIAN 94, Revision D.3, M. J. Frisch, G. W. Trucks, H. B. Schlegel, P. M. W. Gill, B. G. Johnson, M. A. Robb, J. R. Cheeseman, T. A. Keith, G. A. Petersson, J. A. Montgomery, K. Raghavachari, M. A. Al-Laham, V. G. Zakrzewski, J. V. Ortiz, J. B. Foresman, J. Cioslowski, B. B. Stefanov, A. Nanayakkara, M. Challacombe, C. Y. Peng, P. Y. Ayala, W. Chen, M. W. Wong, J. L. Andres, E. S. Replogle, R. Gomperts, R. L. Martin, D. J. Fox, J. S. Binkley, D. J. Defrees, J. Baker, J. P. Stewart, M. Head-Gordon, C. Gonzalez, and J. A. Pople, Gaussian, Inc., Pittsburgh PA, 1995.

[67] C. S. Yannoni and T. C. Clarke, Phys. Rev. Lett., **51**, 1191 (1983).

[68] A. Karpfen, Chem. Phys. Lett., **64**, 299 (1979).

[69] M. Kertesz, J. Koller, and A. Ažman, Chem. Phys. Lett., **69**, 225 (1980).

[70] M. D. Harmony, V. W. Laurie, R. L. Kuczkowski, R. H. Schwendeman, D. A. Ramsay, F. J. Lovas, W. J. Lafferty, and A. G. Maki, J. Phys. Chem. Ref. Data, **8**, 619 (1979).

[71] In an infinite *anti*-transoid polymethineimine chain with a perfect translational symmetry, the adjacent CNC and NCN angles must be the same (119.3°). In the *anti*-transoid oligomer with 7 C=N bonds, adjacent CNC and NCN angles which are located near the center of the molecule were found to be 117.0° and 120.8°, respectively.

Chapter 4

Structures and normal vibrations of polyethylene

So Hirata and Suehiro Iwata, "Density functional crystal orbital study on the normal vibrations and phonon dispersion curves of all-*trans*-polyethylene," J. Chem. Phys., **108**(18), 7901–7908 (1998).

Abstract

Optimized structural parameters and frequencies of the infrared- and Raman-active vibrations are obtained for all-*trans* polyethylene by using the analytical-energy-gradient scheme in the density functional crystal orbital formalism. The Slater–Vosko–Wilk–Nusair (SVWN), the Becke–Lee–Yang–Parr (BLYP), and the Becke3–Lee–Yang–Parr (B3LYP) functionals are used with the 3-21G and 6-31G(d) basis sets. The frequencies calculated with the 6-31G(d) basis set are found to be in better agreement with the observed frequencies than those calculated with the 3-21G basis set regardless of the exchange-correlation functionals used. The root-mean-square errors between the calculated and observed frequencies are 21, 20, and 15 cm^{-1} for the SVWN/6-31G(d), the BLYP/6-31G(d), and the B3LYP/6-31G(d) calculations, respectively (the frequencies obtained from the B3LYP/6-31G(d) calculations are scaled uniformly by 0.966). Optical branches of the phonon dispersion curves are calculated at the SVWN/6-31G(d) level by adopting a C_7H_{14} unit as a reference unit cell. The calculated phonon dispersion curves are in reasonable agreement with the curves experimentally determined and with the curves obtained with an empirical force field except for the skeletal stretching branches. Inelastic neutron scattering (INS) spectrum is calculated by using the force field derived at the SVWN/6-31G(d) level and by taking into account the effects of the Debye–Waller factors and the phonon wings. The overall intensity profile of the observed INS spectrum is well reproduced by the present calculations.

4.1 Introduction

All-*trans* polyethylene (hereafter simply referred to as polyethylene) is one of the polymers whose structures and vibrations are best characterized experimentally. For this reason, polyethylene has also been the subject of a number of theoretical studies, whereby the performance of the theoretical models employed has been evaluated on the basis of the comparison between the calculations and experiments.

For instance, the ab initio crystal orbital method at the Hartree–Fock (HF) level was intensively applied to polyethylene for the purpose of elucidating the electronic structure, equilibrium molecular structure, conformation, and mechanical and vibrational properties [1–15]. Among these applications, the number of the vibrational analyses of the polymer is surprisingly small [9,12]. The first attempt was made by Karpfen [9] to calculate some

vibrational force constants of polyethylene. Fitting with polynomials the total energies of the polymer computed at 41 different structures, he obtained the equilibrium structure and some force constants in the internal coordinate basis. Although the force constants calculated in this manner with roughly double zeta quality basis set were found to be consistent with the empirical force constants of Schachtschneider and Snyder [16], the number of the calculated force constants was insufficient to perform a complete vibrational analysis. Later Teramae *et al.* derived the formulas for the analytical-energy-gradient scheme in the ab initio HF crystal orbital method [12,17], and carried out the vibrational analysis of polyethylene at the HF/STO-3G level [12]. The overall agreement between the observed frequencies and the frequencies calculated and then scaled uniformly with an optimum scale factor was good, considering the extremely small basis set used in the calculation. Nevertheless, the largest deviation between the calculated and observed frequencies was as large as about 64 cm^{-1} [18], and there is room for improvement by using more sophisticated theoretical levels and larger basis sets.

A few groups of researchers pioneered the use of correlated theoretical levels in the ab initio crystal orbital method and performed post-HF calculations on polyethylene [19–24]. Suhai analyzed the effect of electron correlation on the mechanical properties of polyethylene on the basis of the second-order Møller–Plesset perturbation (MP2) calculations [19–21]. So far, however, analytical-energy-gradient schemes have not been implemented in the ab initio crystal orbital method at post-HF levels, and no correlated calculation has been performed on the vibrational frequencies of polyethylene, although it may appear to be computationally feasible.

Density functional theory has also been applied to polyethylene for the study of the electronic structure, conformation, and interchain interactions [25–30]. In the last decade, density functional theory has proven a powerful tool for the vibrational frequency prediction of a wide variety of molecules [31–33]. Wong [31] calculated the vibrational frequencies for a set of 122 molecules with various density functional methods and the MP2 method, and compared them with the experimental frequencies. The overall root-mean-square errors between the observed frequencies and the frequencies calculated and then uniformly scaled were significantly smaller for the density functional methods than for the MP2 method. The best agreement was obtained with the density functional methods using the hybrid functionals such as the Becke3–Lee–Yang–Parr (B3LYP) and the Becke3–Perdew86 (B3P86) functionals. Scott and Radom [32] also calculated the vibrational frequencies for

122 molecules with various theoretical methods and basis sets. The theoretical methods investigated were semiempirical methods, HF, MP2, quadratic configuration interaction with single and double substitutions (QCISD), and several variants of density functional theory. Scott and Radom concluded that the hybrid HF/density functional methods such as the B3LYP/6-31G(d) method performed best for the frequency calculations. These results suggest that density functional theory can also predict the vibrational frequency of polymers with considerable accuracy.

In this chapter, we present the results of the density functional calculations on the vibrational frequencies of polyethylene. The force constants of an infinite polyethylene chain are evaluated by numerical differentiation of the analytical energy gradients. The exchange-correlation functionals employed are the local Slater–Vosko–Wilk–Nusair (SVWN) functional, the gradient-corrected Becke–Lee–Yang–Parr (BLYP) functional, and the hybrid B3LYP functional. The basis sets used are the standard 3-21G and 6-31G(d) basis sets. The combination of these exchange-correlation functionals and the basis sets constitutes one of the most frequently studied sets of density functional models. The performance of these models is evaluated in terms of the maximum and root-mean-square errors between the calculated and observed frequencies of the infrared- and Raman-active vibrations. By adopting a C_7H_{14} reference unit cell, we also calculate the frequencies of the modes in the whole range of the Brillouin zone by using the SVWN/6-31G(d) level of approximation. The optical branches of the phonon dispersion curves are drawn, and are compared with the curves determined experimentally by Snyder and Schachtschneider [34] and with the curves obtained by using the empirical force field of Tasumi *et al.* [35–37]. Inelastic neutron scattering (INS) spectrum of polyethylene is also calculated with the force field derived at the SVWN/6-31G(d) level by taking into account the effects of the Debye–Waller factors and the phonon wings, and is compared with an observed spectrum.

4.2 Method of calculations

In the present study, the linear-combination-of-atomic-orbital (LCAO) density functional crystal orbital method was applied to the geometry optimizations and vibrational frequency calculations of an infinite polyethylene chain. The formalism and computer implementation of the SCF procedure and the analytical-energy-gradient scheme were described previously [38,39]. Polyethylene is a 2_1 helix, and a translational repeat unit (C_2H_4) contains two chemical repeat units (CH_2). The geometry optimizations of the polymer were

performed with the analytical energy gradients by adopting a CH_2 reference unit cell and by making use of the screw-axis symmetry. Three exchange-correlation functionals (SVWN [40,41], BLYP [42–44], and B3LYP [45]) were employed with the 3-21G [46] and 6-31G(d) [47,48] basis sets. Electron density was also expanded by auxiliary basis sets in order to minimize the computational tasks concerning the accumulation of the long-range electron repulsion integrals. Two sets of auxiliary basis sets were used: auxiliary basis set I for the 3-21G calculations and auxiliary basis set II for the 6-31G(d) calculations. These two auxiliary basis sets are identical to those used in Chapter 3. The long-range Coulomb interactions were taken into account by evaluating explicitly the relevant electron repulsion integrals extending to the fortieth neighboring CH_2 unit cells. For the other molecular integrals, interactions up to the eighth neighboring CH_2 unit cells were considered.

The normal modes of polyethylene can be characterized in terms of the wavevector k of the vibrations or the phase difference θ between two adjacent CH_2 groups. The normal modes at $k = 0$ (or at $\theta = 0$ and π) are infrared- or Raman-active for polyethylene. The frequencies and vibrational patterns of the normal modes at any value of k can be calculated by diagonalizing the so-called k-dependent dynamical force-constant matrix $\mathbf{D}(k)$, which is defined by the following equation (see Refs. [37,49]):

$$\mathbf{D}(k) = \mathbf{M}^{-\frac{1}{2}}\mathbf{F}(k)\mathbf{M}^{-\frac{1}{2}}, \tag{4.1}$$

where $\mathbf{M}$ is the diagonal matrix of the atomic masses. The k-dependent force-constant matrix $\mathbf{F}(k)$ is constructed by summing the force-constant matrix $\mathbf{F}_n$ associate with the Cartesian coordinates of atoms belonging to unit cells 0 and n multiplied by a proper set of phase factors [37,49]:

$$\mathbf{F}(k) = \sum_n \mathbf{F}_n \exp(ink a), \tag{4.2}$$

where a is the translational period. For the vibrational frequency calculations of the infrared- and Raman-active modes, we lifted the screw-axis symmetry of the system and adopted a C_2H_4 reference unit cell. The force constants were evaluated by numerical differentiation of the analytical energy gradients. Since the analytical-energy-gradient scheme used in the present study assumes that all the nuclei that are equivalent by the translational symmetry move in phase [12,17,39], the 18×18 force-constant matrix thus obtained corresponds to $\mathbf{F}(0)$. The frequencies of the infrared- and Raman-active vibrations were calculated by diagonalizing the dynamical force-constant matrix $\mathbf{D}(0)$ constructed from $\mathbf{F}(0)$.

The frequencies of the normal modes in the whole range of the Brillouin zone were calculated at the SVWN/6-31G(d) level by extending the reference unit cell for the crystal orbital calculations to a C_7H_{14} unit. The 9×9 force-constant matrices $\mathbf{F}_n(-3 \leq n \leq 3)$ were computed by numerically differentiating the analytical energy gradients for the structures in which the nuclei belonging to the central CH_2 group were displaced from the equilibrium positions. The force-constant matrices $\mathbf{F}_n$ with $|n|$ greater than 3, whose elements are expected to have very small absolute values, were neglected in the normal coordinate analysis. This approximation does not lead to numerical errors in the vibrational frequencies of optical branches; the frequencies of the infrared- and Raman-active vibrations calculated with this approximation are in agreement within 3 cm^{-1} with those calculated by the method described in the preceding paragraph. However, $\mathbf{F}_n$ with $|n|$ greater than 3 were found to be important for normal modes with almost zero vibrational frequencies, and hence the present method cannot treat the acoustic vibrations at $k \approx 0$. In the present study, therefore, we concentrate on the optical branches of the phonon dispersion curves. The frequencies of the modes belonging to the optical branches were calculated by varying the phase difference θ from 0 to π at intervals of 0.01π.

The INS spectrum of polyethylene was simulated by using the force field $\mathbf{F}_n(-3 \leq n \leq 3)$ obtained at the SVWN/6-31G(d) level, and was compared with the high-resolution spectrum observed by Parker [50]. The method of simulation was outlined in Ref. [51]. By taking into account the experimental conditions under which the spectrum was measured [50], we employed the following expression [51–54] for the scattering function $S_H(Q,\nu)$ for the fundamental transitions of the high-frequency vibrations (for the separation of the high-frequency and low-frequency vibrations, the readers are referred to Refs. [55,56]):

$$S_H(Q,\nu) \propto \exp[-2W_H(Q)]g_{HH}(\nu), \tag{4.3}$$

where $\hbar Q$ is the magnitude of neutron momentum transfer, $h\nu$ is the neutron energy transfer, and $\exp[-2W_H(Q)]$ is the Debye–Waller factor. The hydrogen-amplitude-weighted density of states $g_{HH}(\nu)$ for polyethylene was computed as a histogram at 1-cm^{-1} intervals and then convoluted with a Gaussian function with a full width at half maximum being 30 cm^{-1} to take into account the band broadening due to the recoil of the hydrogen nuclei. Since only the scattered neutron with a very small final energy (*ca.* 32 cm^{-1}) were detected in the experiment [50], Q is related to ν by

$$\frac{(\hbar Q)^2}{2m_N} = h\nu, \tag{4.4}$$

where m_N is the mass of a neutron [57]. The effect of phonon wings [55,56] was considered by convoluting the scattering function $S_H(Q,\nu)$ for the high-frequency vibrations with the scattering function $S_L(Q,\nu)$ for the low-frequency vibrations:

$$S(Q,\nu) = S_H(Q,\nu) \otimes S_L(Q,\nu), \tag{4.5}$$

with

$$S_L(Q,\nu) \propto \exp[-2W_L(Q)]g_{HL}(\nu). \tag{4.6}$$

The hydrogen-amplitude-weighted density of states for the low-frequency vibrations $g_{HL}(\nu)$ was approximated by the observed spectrum in the region below 210 cm^{-1}. The contribution of the higher-order phonon wings up to fifth order was calculated by repeatedly convoluting this $g_{HL}(\nu)$ and then collected after proper normalization to give $S_L(Q,\nu)$. Since the observed spectrum was measured at a low temperature (30 K), only the additive contribution of the phonon wings was included in the calculations. The Debye–Waller factor was calculated by using the isotropic approximation:

$$\exp[-2W_H(Q)] = \exp[-Q^2\langle u^2\rangle_H], \tag{4.7}$$

and

$$\exp[-2W_L(Q)] = \exp[-Q^2\langle u^2\rangle_L] \tag{4.8}$$

where $\langle u^2\rangle_H$ and $\langle u^2\rangle_L$ are the mean square amplitude of the hydrogen nuclei due to the high-frequency and low-frequency vibrations, respectively. The values of $\langle u^2\rangle_H$ and $\langle u^2\rangle_L$ used in the present study were 0.012 and 0.020 $Å^2$, respectively. The value of $\langle u^2\rangle_L$ (0.020 $Å^2$) may be compared to the value determined experimentally by Lynch *et al.* [58] at 93 K (0.024 – 0.027 $Å^2$) and by Myers and Randolph [59] at 77 K (0.012 – 0.018 $Å^2$) and at 4.2 K (0.008 – 0.012 $Å^2$).

4.3 Results and discussion

4.3.1 Structural parameters

The optimized structural parameters are listed in Table 4.1 together with the experimental values determined by X-ray diffraction and neutron diffraction techniques [60–64]. The optimized structural parameters seem to be affected to a greater extent by the choice of the basis sets than that of the exchange-correlation functionals except for the CC bond lengths. The CCC angles calculated with the 6-31G(d) basis set (113.6 – 113.7°) are

Table 4.1 *Calculated and observed structural parameters of all-trans polyethylene.* Bond lengths in Å and bond angles in degrees.

	CC bond length	CH bond length	CCC angle	HCH angle
SVWN/3-21G	1.521	1.111	112.7	106.6
SVWN/6-31G(d)	1.511	1.110	113.6	105.4
BLYP/3-21G	1.557	1.107	112.8	107.0
BLYP/6-31G(d)	1.546	1.108	113.7	106.1
B3LYP/3-21G	1.544	1.099	112.8	107.2
B3LYP/6-31G(d)	1.534	1.100	113.7	106.1
X-ray diffraction [60]	1.53		112	
X-ray diffraction [61]	1.534±0.006		112.0±0.4	
X-ray diffraction [62]	1.533±0.022	1.07±0.022	111.9±1.8	107±1.8
X-ray diffraction [63]	1.527±0.007		112±0.8	
Neutron diffraction [64]	1.578±0.005	1.06±0.01 1.10±0.01	107.7±0.5	109.0±1.0

coincident with each other and are invariably larger than those calculated with the 3-21G basis set (112.7 – 112.8°). The measured CCC angles are in excellent agreement with each other except for the value determined by the neutron diffraction study [64], which is substantially smaller than the other values. The CCC angles optimized with the 3-21G basis set (112.7–112.8°) appears to be in a slightly better agreement with the experimental values (112°) than those obtained with the 6-31G(d) basis set (113.6 – 113.7°). The CC bond lengths varies substantially with the exchange-correlation functionals and basis sets employed. The use of the 6-31G(d) basis set decreases the CC bond lengths by about 0.01 Å from the values obtained with the 3-21G basis set. The measured CC bond lengths are generally consistent with each other, although the value determined by the neutron diffraction study [64] considerably deviates from the other values again. The CC bond length optimized at the B3LYP/6-31G(d) level (1.534 Å) is within the experimental errors of the bond lengths measured by the X-ray diffraction studies.

4.3.2 Frequencies of the infrared- and Raman-active vibrations

The calculated frequencies of the infrared- and Raman-active vibrations of polyethylene and polyethylene-d_4 are given in Table 4.2. The frequencies of the infrared and Raman bands were reported in Refs. [65–71] for polyethylene and in Refs. [68,71–74] for polyethylene-d_4. The observed frequencies given in Table 4.2 were taken from Refs. [65–68,74]. The assignments of the observed bands of the undeuterated species are based on the studies of Nielsen and Holland [67], of Tasumi *et al.* [35–37], and of Schachtschneider and Snyder [16], except for the $\nu_3(\pi)$ vibration. These groups assigned a band at 1415

cm^{-1} to $\nu_3(\pi)$, but later Snyder revised the assignment of this vibration and reassigned a weaker Raman band at 1370 cm^{-1} to $\nu_3(\pi)$ [75,76]. The assignments of the observed bands of polyethylene-d_4 are based on the studies of Tasumi *et al.* [37,72]. The normal coordinate analyses of polyethylene using empirical force fields were reviewed by Barnes and Fanconi [77] with emphasis on the interchain interactions.

In Table 4.2, the frequencies calculated with the SVWN and BLYP functionals are directly (without scaling of the force constants or frequencies) compared with the observed frequencies. The frequencies calculated at the B3LYP/3-21G and B3LYP/6-31G(d) levels are scaled uniformly with the scale factors determined by a least-squares fitting procedure (the CH and CD stretching modes were excluded in this procedure). The optimum scale factors are 0.958 for the B3LYP/3-21G level and 0.966 for the B3LYP/6-31G(d) level. The scale factor for the B3LYP/6-31G(d) level (0.966) is close to the values recommended by Wong (0.9613) [31] and by Scott and Radom (0.9614) [32].

As can be seen in Table 4.2, the maximum and root-mean-square errors between the calculated and observed frequencies are larger for the BLYP/3-21G and B3LYP/3-21G calculations than for the SVWN/3-21G calculation. In other words, as long as the 3-21G basis set is used, the gradient correction or exact-exchange mixing does not lead to improved agreement. In contrast, the use of the 6-31G(d) basis set significantly reduces the deviations between the calculated and observed frequencies, particularly for the BLYP and B3LYP calculations. The frequencies calculated with the 6-31G(d) basis set are found to be in good agreement with the observed frequencies with the root-mean-square errors being 21, 20 and 15 cm^{-1} for the SVWN, BLYP, and B3LYP calculations, respectively. Therefore, these three functionals (SVWN, BLYP, and B3LYP) perform equally well for the vibrational frequency predictions of polyethylene provided that the 6-31G(d) basis set is used. The inclusion of polarization function in the basis set has more significant effects on the vibrational frequencies of polyethylene than the choice of the exchange-correlation functionals.

The above-mentioned observation for polyethylene contrasts with what we found for polyacetylene. The SVWN and BLYP predicted the equilibrium structures of *trans*-transoid polyacetylene that were substantially different from the result obtained with the B3LYP functional [38]. The structures optimized with the SVWN and BLYP functionals were found to be even qualitatively incorrect, while the B3LYP functional predicted the structure and vibrational frequencies of *trans*-transoid polyacetylene that were

Table 4.2 Frequencies (in units of cm^{-1}) of the infrared- and Raman-active vibrations of all-*trans* polyethylene and all-*trans* polyethylene-d_4 calculated with the SVWN, BLYP, and B3LYP functionals.

Mode[a]		Obs.[b]	SVWN		BLYP		B3LYP[c]	
			3-21G	6-31G(d)	3-21G	6-31G(d)	3-21G	6-31G(d)
			all-*trans* polyethylene					
a_g	$\nu_1(0)$	2848	2941	2941	2945	2929	2902	2912
	$\nu_2(0)$	1440	1482	1445	1514	1478	1484	1465
	$\nu_4(0)$	1131	1143	1153	1094	1107	1087	1108
b_{1g}	$\nu_3(\pi)$	1370[d]	1344	1384	1348	1370	1334	1374
	$\nu_4(\pi)$	1061	1089	1090	1004	1029	1008	1033
b_{2g}	$\nu_7(\pi)$	1295	1297	1268	1324	1301	1302	1289
b_{3g}	$\nu_6(0)$	2883	2967	2967	2958	2943	2918	2928
	$\nu_7(0)$	1168	1185	1168	1192	1185	1174	1176
a_u	$\nu_8(0)$	1050	1079	1032	1098	1058	1081	1047
b_{1u}	$\nu_6(\pi)$	2919	3025	3014	3016	2994	2973	2976
	$\nu_8(\pi)$	725	734	723	726	724	711	712
b_{2u}	$\nu_1(\pi)$	2851	2964	2960	2963	2946	2919	2927
	$\nu_2(\pi)$	1468	1507	1473	1541	1509	1509	1492
b_{3u}	$\nu_3(0)$	1176	1190	1146	1219	1186	1199	1174
			all-*trans* polyethylene-d_4					
a_g	$\nu_1(0)$	2103	2141	2146	2140	2134	2111	2124
	$\nu_2(0)$	1148	1153	1160	1144	1145	1128	1143
	$\nu_3(0)$	975	1011	985	997	981	984	975
b_{1g}	$\nu_2(\pi)$	1253	1240	1307	1163	1221	1169	1240
	$\nu_4(\pi)$	831	835	817	823	816	814	810
b_{2g}	$\nu_7(\pi)$	917	918	897	936	920	920	912
b_{3g}	$\nu_6(0)$	2199	2197	2199	2193	2183	2164	2172
	$\nu_7(0)$	993	1029	1015	1030	1026	1015	1019
a_u	$\nu_8(0)$	748	763	730	777	748	764	740
b_{1u}	$\nu_6(\pi)$	2195	2240	2232	2234	2218	2202	2204
	$\nu_8(\pi)$	525	530	523	524	523	513	514
b_{2u}	$\nu_1(\pi)$	2089	2152	2151	2150	2140	2119	2126
	$\nu_3(\pi)$	1091	1110	1084	1137	1112	1112	1099
b_{3u}	$\nu_4(0)$	892	900	867	922	897	907	888
Maximum error[e]			42	54	90	41	84	28
Root mean square error[e]			22	21	42	20	32	15

[a] The normal modes are classified under the factor group isomorphous to the point group D_{2h}. The branches of the phonon dispersion curves are numbered in the same way as in Ref. [35]. The ν_5 and ν_9 are the acoustic branches and do not appear in this table. The values in the parentheses are the vibrational phase difference between the adjacent CH_2 groups. [b] The observed frequencies are taken from Refs. [65-68,74]. [c] The frequencies calculated with the 3-21G basis set are uniformly scaled by 0.958, and those calculated with the 6-31G(d) basis set by 0.966. [d] References [75,76]. [e] CH and CD stretching modes are excluded.

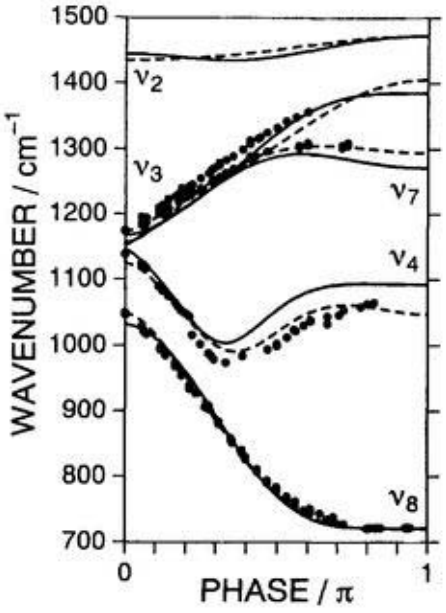

Figure 4.1 Phonon dispersion curves of all-*trans* polyethylene in the 700–1500-cm^{-1} region. Solid curves: calculated at the SVWN/6-31G(d) level. Broken curves: obtained with the force field of Tasumi *et al.* (Refs. [35–37]). Filled circles: the vibrational frequencies of *n*-alkane molecules measured by Snyder and Schachtschneider (Ref. [34]) plotted at appropriate vibrational phase differences.

in good agreement with the experimental results [38,39]. Therefore, the choice of exchange-correlation functionals is of critical importance for *trans*-transoid polyacetylene. The frequencies calculated at the B3LYP/6-31G(d) level were in better agreement with the observed frequencies than those calculated at the B3LYP/3-21G level also for *trans*-transoid polyacetylene, but the basis-set dependence on the calculated frequencies seems to be less significant for polyacetylene than for polyethylene.

As we have seen in the previous paragraphs, the frequencies of the infrared- and Raman-active vibrations of polyethylene calculated at the SVWN/6-31G(d) level are in agreement with the observed frequencies to an extent similar to those calculated at the BLYP/6-31G(d) and B3LYP/6-31G(d) levels. This result suggests that the SVWN calculations, which require much less computational costs than the BYLP and B3LYP calculations, provide a reasonably accurate force field for polyethylene, whereby not only the infrared and Raman spectra but also other vibrational spectra of the polymer can be theoretically interpreted. In what follows, the phonon dispersion curves and INS spectrum of polyethylene calculated with the force field derived at the SVWN/6-31G(d) level are compared with the experimental results.

4.3.3 Phonon dispersion curves

The calculated phonon dispersion curves of polyethylene and polyethylene-d_4 are depicted in Figs. 4.1 and 4.2, respectively. It is known that the vibrational frequencies of n-alkane molecules fall on the phonon dispersion curves of an infinite polyethylene chain at the vibrational phase differences between adjacent CH_2 groups. Snyder and Schachtschneider [34] measured the infrared spectra of a series of n-alkane molecules from C_3H_8 through n-$C_{19}H_{40}$ and suggested the vibrational phase difference for each of the observed vibrational modes. The experimental phonon dispersion curves were reproduced in Fig. 4.1 as filled circles by plotting the frequencies of n-$C_{15}H_{32}$ through n-$C_{19}H_{40}$ observed by Snyder and Schachtschneider [34]. The phonon dispersion curves obtained with the empirical force field of Tasumi *et al.* [35–37] are also drawn in Figs. 4.1 and 4.2 (the force constants tabulated in Ref. [37] were actually used). The phonon dispersion curves of Tasumi *et al.* are in excellent agreement with the plot of Snyder and Schachtschneider (Fig. 4.1). Therefore, they can practically be regarded as the true phonon dispersion curves, except for the ν_3 branch of the undeuterated species at $\theta \approx \pi$ because these authors based their force field determination on the wrong assignment of $\nu_3(\pi)$. Henceforth, the phonon dispersion curves of Snyder and Schachtschneider and of Tasumi *et al.* are simply referred to as experimental curves.

As can be seen in Fig. 4.1, the calculated phonon dispersion curves of the undeuterated species are generally consistent with the experimental ones. The calculated ν_8 branch overlaps the experimental counterpart in the whole region of the Brillouin zone. For the ν_2, ν_3, and ν_7 branches also, the theoretical and experimental curves are in reasonable agreement with each other. However, the calculated ν_4 branch are found to have substantially higher frequencies than the experimental curve particularly for the phase difference of $\theta \geq \pi/3$ with the largest deviation being about 45 cm^{-1}. Therefore, although the force field derived at the SVWN/6-31G(d) level is considered to be close to the true one, there still exist significant differences between them. The deviation found in the ν_4 branch cannot be ascribed to the neglect of the force-constant matrices $\mathbf{F}_n$ with $|n|$ greater than 3, because the ν_4 branch calculated with $\mathbf{F}_n(-3 \leq n \leq 3)$ is practically the same with that calculated with $\mathbf{F}_n(-2 \leq n \leq 2)$. Similar trend can be seen in the calculated phonon dispersion curves of polyethylene-d_4, as shown in Fig. 4.2. The ν_3, ν_4, ν_7, and ν_8 branches of the calculated phonon dispersion curves are in reasonable agreement with the

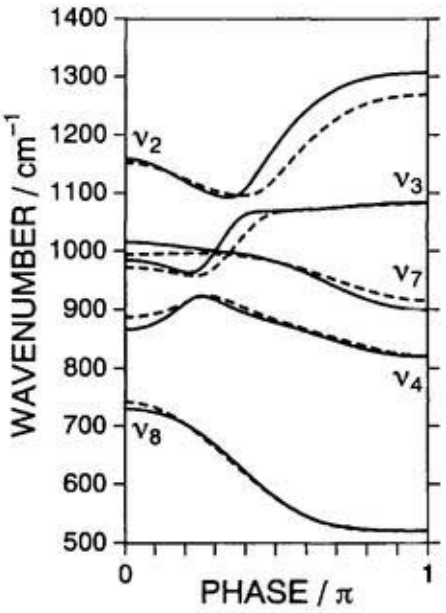

Figure 4.2 Phonon dispersion curves of all-*trans* polyethylene-d_4 in the 500–1400-cm^{-1} region. Solid curves: calculated at the SVWN/6-31G(d) level. Broken curves: obtained with the force field of Tasumi *et al.* (Refs. [35–37]).

experimental counterparts, but the calculated ν_2 branch significantly deviates from the experimental branch in the region of $\theta \geq \pi/3$. It should be pointed out that both the ν_4 branch of the undeuterated species for $\theta \geq \pi/3$ and the ν_2 branch of the perdeuterated species for $\theta \geq \pi/3$ mainly consist of the skeletal stretching vibrations [35]. A large part of the discrepancies observed for these branches are found to be ascribable to the difference in the diagonal and off-diagonal force constants associated with the z-coordinates of the carbon nuclei between the calculated and the empirical force fields (the chain axis is parallel to the z-axis).

4.3.4 Inelastic neutron scattering

In contrast to infrared and Raman spectroscopy, INS spectroscopy can in principle probe the vibrational modes in the whole range of the Brillouin zone. The intensities of the transitions in INS spectra are primarily determined by the momentum transfer and the vibrational amplitudes of hydrogen nuclei [52–54]. INS spectroscopy provides us with information about the phonon dispersion curves of polymers through the hydrogen-amplitude-weighted density of states $g_{\mathrm{H}}(\nu)$. The INS spectra of polyethylene were measured by a number of groups [50,78–82], and are interpreted by Lynch *et al.* [58] and by Kitagawa and Miyazawa [83,84] by making use of the empirical force fields. Recently, high-resolution INS

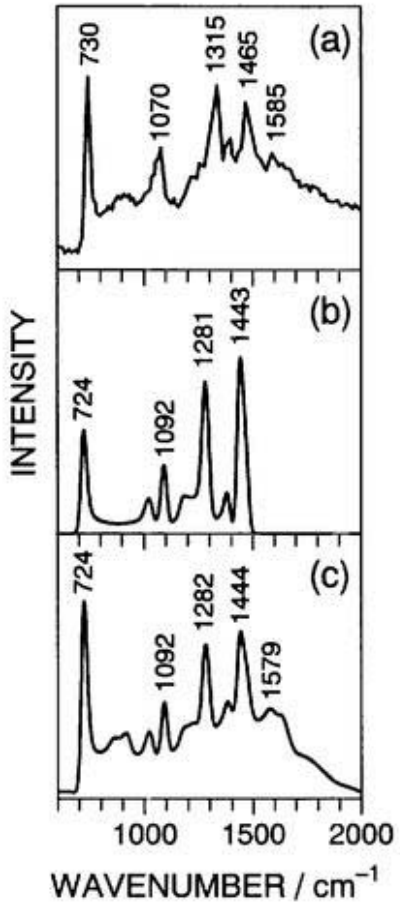

Figure 4.3 (a) Inelastic neutron scattering (INS) spectrum of a randomly oriented all-*trans* polyethylene sample in the 600–2000-cm^{-1} region observed by Parker (Ref. [50]). The approximate peak positions were taken from the original figures. (b) Hydrogen-amplitude-weighted density of states calculated at the SVWN/6-31G(d) level and convoluted with a Gaussian function whose full width at half maximum is 30 cm^{-1}. (c) Calculated INS spectrum in which the effects of the Debye–Waller factors and the phonon wings are taken into account.

spectra of polyethylene were observed by Parker [50]. The spectrum observed by Parker for a randomly oriented sample is reproduced in Fig. 4.3(a).

The $g_H(\nu)$ profile calculated with the force field derived at the SVWN/6-31G(d) level is shown in Fig. 4.3(b). The $g_H(\nu)$ profile seems to provide a qualitative account of the overall intensity profile of the observed spectrum. The intense peaks in the observed INS spectrum at 730, 1070, 1315, and 1465 cm^{-1} are reproduced in the $g_H(\nu)$ profile. The calculated peak positions are in reasonable agreement with the observed ones, although the calculated peak position of 1281 cm^{-1} seems to be too low as compared to the experimental result (1315 cm^{-1}). A weak band at about 1400 cm^{-1} and a shoulder band at about 1250 cm^{-1} in the observed spectrum can also be seen in the $g_H(\nu)$ profile. However, a weak broad band around 900 cm^{-1} and a broad feature in the high frequency side of the 1465-cm^{-1} band in the observed spectrum are not reproduced in the $g_H(\nu)$ profile. The relative intensities of the peaks in the 1300 – 1500-cm^{-1} region to the peak at 730 cm^{-1} are also too large in the $g_H(\nu)$ profile than in the observed spectrum. These deviations are apparently due to the neglect of the Debye–Waller factors and the phonon wings.

The INS spectrum shown in Fig. 4.3(c) is calculated by taking into account the effects of the Debye–Waller factors and the phonon wings. The agreement between the calculated and observed INS spectrum becomes satisfactory. The calculated spectrum accounts for the observed broad band around 900 cm^{-1} and the broad shoulder above 1500 cm^{-1}. Comparison between the calculated INS spectrum and the $g_H(\nu)$ profile indicates that the broad band around 900 cm^{-1} is predominantly due to the phonon wings of the 724-cm^{-1} band and that the contribution from the minimum of the ν_4 branch to this band is negligibly small. It appears that the phonon wings are at least partly responsible for the constant level of scattering in the region of 700 – 1700 cm^{-1}. However, the level of scattering in the higher-frequency region cannot be accounted for by the fundamental transitions and their phonon wings.

In the calculated INS spectrum and the $g_H(\nu)$ profile, there are two bands in the 1000 – 1100-cm^{-1} region, while in the observed spectrum there is only one broad band with an asymmetric shape. The peak at about 1020 cm^{-1} in the calculated spectrum is primarily due to $\nu_8(0)$ with a smaller contribution from the minimum of the ν_4 branch. The calculated peak at 1092 cm^{-1} arises from $\nu_4(\pi)$. The discrepancy in this region is probably due to a larger difference (58 cm^{-1}) in the calculated frequencies between $\nu_4(\pi)$ and $\nu_8(0)$ than the difference actually observed (11 cm^{-1}) and to a very small dispersion

in the calculated ν_4 branch near $\theta = \pi$.

4.4 Conclusion

The density functional crystal orbital method is found to be useful in theoretically interpreting the vibrational spectra of polyethylene. The frequencies of the infrared- and Raman-active vibrations calculated at the SVWN/6-31G(d), BLYP/6-31G(d), and B3LYP /6-31G(d) levels are found to be in agreement with the observed frequencies with the root-mean-square errors being 21, 20, and 15 cm^{-1}, respectively. Provided that the 6-31G(d) basis set is used, not only the gradient-corrected BLYP functional and hybrid B3LYP functional but also the local SVWN functional provides us with a reasonably good force field for polyethylene and probably also for the polymers having similar molecular structures without π-electron conjugation. The phonon dispersion curves and INS spectrum of polyethylene calculated with the force field derived at the SVWN/6-31G(d) level are also in reasonable agreement with the experimental results, although the detailed comparison indicates that there still exist discrepancies between the calculations and experiments. In the present study, the force-constant matrices $\mathbf{F}_n$ with $|n| \leq 3$ were computed by adopting a larger reference unit cell than the chemical repeat unit. This treatment is apparently inefficient and is also found to yield inaccurate results for low-frequency vibrations. It is highly desirable to develop an efficient and accurate analytical-second-derivative scheme in the framework of crystal orbital theory whereby the force-constant matrices $\mathbf{F}_n$ with an arbitrary n [or equivalently $\mathbf{F}(k)$ with an arbitrary k] can be calculated.

References

[1] J.-M. André and G. Leroy, Chem. Phys. Lett., **5**, 71 (1970).

[2] E. Clementi, J. Chem. Phys., **54**, 2492 (1971).

[3] J. M. André, J. Delhalle, S. Delhalle, R. Caudano, J. J. Pireaux, and J. J. Verbist, Chem. Phys. Lett., **23**, 206 (1973).

[4] J. Delhalle, J. M. Andre, S. Delhalle, J. J. Pireaux, R. Caudano, and J. J. Verbist, J. Chem. Phys., **60**, 595 (1974).

[5] J. Delhalle, J.-M. André, S. Delhalle, C. Pivont-Malherbe, F. Clarisse, G. Leroy, and D. Peeters, Theor. Chim. Acta, **43**, 215 (1977).

[6] D. R. Armstrong, J. Jamieson, and P. G. Perkins, Theor. Chim. Acta, **50**, 193 (1978).

[7] J. L. Brédas, J. M. André, and J. Delhalle, Chem. Phys., **45**, 109 (1980).

[8] D. R. Armstrong, J. Jamieson, and P. G. Perkins, Theor. Chim. Acta, **57**, 43 (1980).

[9] A. Karpfen, J. Chem. Phys., **75**, 238 (1981).

[10] R. S. Weidman, K. L. Bedford, and A. B. Kunz, Solid State Commun., **39**, 917 (1981).

[11] H. Teramae, T. Yamabe, and A. Imamura, Theor. Chim. Acta, **64**, 1 (1983).

[12] H. Teramae, T. Yamabe, C. Satoko, and A. Imamura, Chem. Phys. Lett., **101**, 149 (1983).

[13] A. Karpfen and A. Beyer, J. Comp. Chem., **5**, 11 (1984).

[14] J. M. André, D. P. Vercauteren, V. P. Bodart, and J. G. Fripiat, J. Comp. Chem., **5**, 535 (1984).

[15] D. H. Mosley, J. G. Fripiat, B. Champagne, and J.-M. André, Int. J. Quantum Chem. Quantum Chem. Symp., **27**, 793 (1993).

[16] J. H. Schachtschneider and R. G. Snyder, Spectrochim. Acta, **19**, 117 (1963).

[17] H. Teramae, T. Yamabe, and A. Imamura, J. Chem. Phys., **81**, 3564 (1984).

[18] In the original paper of Teramae *et al.*, the calculated frequencies were found to contain considerable numerical errors due to insufficient lattice summations (see Chapter 6). The present author found that the optimum scale factor for the frequencies calculated at the HF/STO-3G level was 0.795 and that the largest deviation between the scaled and observed frequencies was 64 cm^{-1}.

[19] S. Suhai, J. Polym. Sci. Polym. Phys. Ed., **21**, 1341 (1983).

[20] S. Suhai, Int. J. Quantum Chem. Quantum Chem. Symp., **18**, 161 (1984).

[21] S. Suhai, J. Chem. Phys., **84**, 5071 (1986).

[22] G. König and G. Stollhoff, J. Chem. Phys., **91**, 2993 (1989).

[23] Y.-J. Ye, W. Förner, and J. Ladik, Chem. Phys., **178**, 1 (1993).

[24] S. Suhai, Int. J. Quantum Chem. Quantum Chem. Symp., **27**, 131 (1993).

[25] J. E. Falk and R. J. Fleming, J. Phys. C, **6**, 2954 (1973).

[26] R. V. Kasowski, W. Y. Hsu, and E. B. Caruthers, J. Chem. Phys., **72**, 4896 (1980).

[27] M. Springborg and M. Lev, Phys. Rev. B, **40**, 3333 (1989).

[28] M. S. Miao, P. E. Van Camp, V. E. Van Doren, J. J. Ladik, and J. W. Mintmire, Phys. Rev. B, **54**, 10430 (1996).

[29] B. Montanari, and R. O. Jones, Chem. Phys. Lett., **272**, 347 (1997).

[30] H. Meider and M. Springborg, J. Phys. Chem., **101**, 6949 (1997).

[31] M. W. Wong, Chem. Phys. Lett., **256**, 391 (1996).

[32] A. P. Scott and L. Radom, J. Phys. Chem., **100**, 16502 (1996).

[33] M. J. Frisch, G. W. Trucks, and J. R. Cheeseman, in *Recent Developments and Applications of Modern Density Functional Theory*, edited by J. M. Seminario (Elsevier, Amsterdam, 1996).

[34] R. G. Snyder and J. H. Schachtschneider, Spectrochim. Acta, **19**, 85 (1963).

[35] M. Tasumi, T. Shimanouchi, and T. Miyazawa, J. Mol. Spectrosc., **9**, 261 (1962).

[36] M. Tasumi, T. Shimanouchi, and T. Miyazawa, J. Mol. Spectrosc., **11**, 422 (1963).

[37] M. Tasumi and T. Shimanouchi, J. Chem. Phys., **43**, 1245 (1965).

[38] Chapter 2 of the present thesis.

[39] Chapter 3 of the present thesis.

[40] J. C. Slater, *Quantum Theory of Molecules and Solids, Vol. 4: The Self-Consistent Field for Molecules and Solids* (McGraw-Hill, NewYork, 1974).

[41] S. H. Vosko, L. Wilk, and M. Nusair, Can. J. Phys., **58**, 1200 (1980).

[42] A. D. Becke, Phys. Rev. A, **38**, 3098 (1988).

[43] C. Lee, W. Yang, and R. G. Parr, Phys. Rev. B, **37**, 785 (1988).

[44] B. Miehlich, A. Savin, H. Stoll, and H. Preuss, Chem. Phys. Lett., **157**, 200 (1989).

[45] A. D. Becke, J. Chem. Phys., **98**, 5648 (1993).

[46] J. S. Binkley, J. A. Pople, and W. J. Hehre, J. Am. Chem. Soc., **102**, 939 (1980).

[47] W. J. Hehre, R. Ditchfield, and J. A. Pople, J. Chem. Phys., **56**, 2257 (1972).

[48] P. C. Hariharan and J. A. Pople, Theor. Chim. Acta, **28**, 213 (1973).

[49] L. Piseri and G. Zerbi, J. Mol. Spectrosc., **26**, 254 (1968).

[50] S. F. Parker, J. Chem. Soc., Faraday Trans., **92**, 1941 (1996).

[51] S. Hirata, H. Torii, Y. Furukawa, M. Tasumi, and J. Tomkinson, Chem. Phys. Lett., **261**, 241 (1996).

[52] W. Marshall and S. W. Lovesey, *Theory of Thermal Neutron Scattering* (Oxford University Press, London, 1971).

[53] J. Howard and T. C. Waddington, in *Advances in Infrared and Raman Spsctroscopy, Vol. 7*, edited by R. J. H. Clark and R. E. Hester (Heyden, London, 1980) p.86.

[54] J. Tomkinson, C. J. Carlile, S. W. Lovesey, R. Osborn, and A. D. Taylor, in *Spectroscopy of Advanced Materials*, edited by R. J. H. Clark and R. E. Hester (Wiley, Chichester, 1991) p.135.

[55] H. Jobic and H. J. Lauter, J. Chem. Phys., **88**, 5450 (1988).

[56] J. Tomkinson and G. J. Kearley, J. Chem. Phys., **91**, 5164 (1989).

[57] A. Griffin and H. Jobic, J. Chem. Phys., **75**, 5940 (1981).

[58] J. E. Lynch, Jr., G. C. Summerfield, L. A. Feldkamp, and J. S. King, J. Chem. Phys., **48**, 912 (1968).

[59] W. R. Myers and P. D. Randolph, J. Chem. Phys., **49**, 1043 (1968).

[60] C. W. Bunn, Trans. Faraday Soc., **35**, 482 (1939).

[61] H. M. M. Shearer and V. Vand, Acta Cryst., **9**, 379 (1956).

[62] P. W. Teare, Acta Cryst., **12**, 294 (1959).

[63] S. Kavesh and J. M. Schultz, J. Polym. Sci. Part A-2, **8**, 243 (1970).

[64] G. Avitabile, R. Napolitano, B. Pirozzi, K. D. Rouse, M. W. Thomas, and B. T. M. Willis, J. Polym. Sci. Polym. Lett. Ed., **13**, 351 (1975).

[65] S. Krimm, C. Y. Liang, and G. B. B. M. Sutherland, J. Chem. Phys., **25**, 549 (1956).

[66] J. R. Nielsen and A. H. Woollett, J. Chem. Phys., **26**, 1391 (1957).

[67] J. R. Nielsen and R. F. Holland, J. Mol. Spectrosc., **6**, 394 (1961).

[68] R. G. Brown, J. Chem. Phys., **38**, 221 (1963).

[69] M. J. Gall, P. J. Hendra, C. J. Peacock, M. E. A. Cudby, and H. A. Willis, Spectrochim. Acta, **28A**, 1485 (1972).

[70] P. J. Hendra, H. P. Jobic, E. P. Marsden, and D. Bloor, Spectrochim. Acta, **33A**, 445 (1977).

[71] G. Masetti, S. Abbate, M. Gussoni, and G. Zerbi, J. Chem. Phys., **73**, 4671 (1980).

[72] M. Tasumi, T. Shimanouchi, H. Tanaka, and S. Ikeda, J. Polym. Sci. Part A, **2**, 1607 (1964).

[73] D. J. Cutler, P. J. Hendra, J. H. Walker, M. E. A. Cudby, and H. A. Willis, Spectrochim. Acta, **34A**, 391 (1978).

[74] S. F. Parker and H. Herman, Spectrochim. Acta, **53A**, 119 (1997).

[75] R. G. Snyder, J. Mol. Spectrosc., **23**, 224 (1967).

[76] R. G. Snyder, J. Mol. Spectrosc., **31**, 464 (1969).

[77] J. Barnes and B. Fanconi, J. Phys. Chem. Ref. Data, **7**, 1309 (1978).

[78] H. R. Danner, G. J. Safford, H. Boutin, and H. Berger, J. Chem. Phys., **40**, 1417 (1964).

[79] W. Myers, G. C. Summerfield, and J. S. King, J. Chem. Phys., **44**, 184 (1966).

[80] S. F. Trevino, J. Chem. Phys., **45**, 757 (1966).

[81] G. J. Safford, A. W. Naumann, and F. T. Simon, J. Chem. Phys., **45**, 3787 (1966).

[82] H. Jobic, J. Chem. Phys., **76**, 2693 (1982).

[83] T. Kitagawa and T. Miyazawa, J. Chem. Phys., **47**, 337 (1967).

[84] T. Kitagawa and T. Miyazawa, in *Advances in Polymer Science, Vol. 9* (Springer-Verlag, Berlin, 1972) p. 335.

Chapter 5

Structures and normal vibrations of an infinite hydrogen fluoride polymer

So Hirata and Suehiro Iwata, "Ab initio Hartree–Fock and density functional studies on the structures and vibrations of an infinite hydrogen fluoride polymer," J. Phys. Chem. A, in press.

Abstract

Structural parameters, binding energies, and frequencies of the infrared- and Raman-active vibrations are calculated for an infinite zigzag chain of hydrogen fluoride molecules by ab initio crystal orbital theory with the analytical-energy-gradient scheme. The Becke–Lee–Yang–Parr (BLYP), Becke3–Lee–Yang–Parr (B3LYP), and Hartree–Fock (RHF) levels are used in conjunction with the 6-311++G(d,p) basis set. Molecular orbital calculations at the BLYP, B3LYP, RHF, and the second-order Møller–Plesset perturbation (MP2) levels with the same basis set are carried out on linear HF oligomers containing up to six molecules, in order to examine the chain-length dependence of the energetic and structural properties. The predicted chain-length dependence is found to be significantly smaller in the RHF results than in the BLYP and B3LYP results. The RHF level substantially underestimates the downward frequency shifts in the intramolecular H–F stretching modes on going from the monomer to the polymer, while the shifts calculated at the BLYP and B3LYP levels are much closer to the experimental findings, although they are slightly overestimated. The RHF level strongly underestimates the intramolecular H–F bond length and overestimates the intermolecular F···H and F···F distances of the HF polymer, while the structural parameters predicted at the BLYP and B3LYP levels are in good agreement with the experimental results. It is concluded that the RHF level seriously underestimates the cooperative binding effects of consecutive hydrogen bonds, whereas the BLYP and B3LYP levels slightly overestimate this behavior; but these latter levels provide much better description than the former. Vibrational assignment of librational modes of HF crystals is reexamined on the basis of the calculated frequencies. The observed frequencies of the librational and pseudo-translational modes fall between the corresponding frequencies calculated at the RHF and density functional levels.

5.1 Introduction

It is well recognized that the energetic and structural properties of consecutively hydrogen-bonded systems X–H···X–H···X–H exhibit "cooperative," or "non-additive" behavior [1–8]. For instance, the binding energy per hydrogen bond increases as the number of constituent X–H molecules increases. The intermolecular H···X distances shorten and the intramolecular X–H bonds lengthen as the chain becomes longer, which accompanies a decrease in the frequencies of the X–H stretching modes. The dipole moments of

hydrogen-bonded chains are usually larger than a simple vector addition of the dipole moment of a monomer would suggest. Quantitative knowledge of the cooperativity is essential in studying the structures and dynamics of hydrogen-bonded systems in the condensed phase.

The cooperative behavior is most clearly illustrated by the linear or cyclic hydrogen-bonded chains of hydrogen fluoride (HF) molecules [3,5,9–17]. The intermolecular binding in HF clusters is categorized into moderately strong hydrogen bonds [5], and the crystalline HF is constructed from one-dimensional zigzag chains $(HF)_\infty$ of HF molecules [18–20]. The intermolecular F···F distance of $(HF)_\infty$ is $2.49 - 2.50$ Å [18,19], which is substantially shorter than the F···F distance ($2.72 - 2.79$ Å) [21,22] of the neutral dimer $(HF)_2$. The frequencies of the H–F stretching modes decrease by several hundreds of cm^{-1} on going from $(HF)_2$ [23] to $(HF)_\infty$ [20,24–30].

The most intensive investigations on the cooperativity of the hydrogen bonds in HF clusters were carried out by Karpfen and Yanovitskii [14,15]. They examined the chain-length dependence of the H–F and F···F distances, frequencies of the H–F stretching modes, and other properties for neutral, protonated, and deprotonated HF clusters. In these studies, the authors employed the Hartree–Fock approximation with the 4-31G, 6-31G(d,p), and 6-311++G(2d,p) basis sets. The calculated chain-length dependence was found to be systematic, and it turned out that the calculated bond lengths and frequencies converged very slowly to the corresponding values of $(HF)_\infty$. Therefore, it is hardly possible to obtain the structures or vibrational frequencies of $(HF)_\infty$ by extrapolation from those of oligomers with reasonably large basis sets or theoretical levels which incorporate the effects of electron correlation.

An alternative, and in principle more accurate and efficient, method to calculate the structures and vibrational frequencies of infinite chains is provided by ab initio crystal orbital theory [31–34]. Several papers have been published so far which have dealt with $(HF)_\infty$ on the basis of ab initio crystal orbital theory [35–41] or periodic density functional theory using local exchange-correlation functionals [42,43]. Among them, the paper written by Beyer and Karpfen [37] has been the only one which reported the optimized structural parameters and vibrational frequencies of $(HF)_\infty$ with reasonably large basis sets. These authors employed the Hartree–Fock approximation in conjunction with the Gaussian lobe basis sets. The H–F bond length of $(HF)_\infty$ calculated with the largest basis set they used was, however, significantly shorter than the experimental results. Cor-

respondingly, the calculated F···F bond length was much longer than the experimental values and the calculated frequencies of the H–F stretching modes were overestimated by more than 700 cm^{-1}.

It is probable that these discrepancies are ascribed to the neglect of electron correlation. Recently, Karpfen [17] has extended the investigations of HF clusters to second-order Møller–Plesset (MP2) perturbation theory and several variants of density functional theory with the 6-311++G(2d,p) basis set. However, there seems to be no calculation on the structure and vibrational frequencies of $(HF)_\infty$ using correlated theoretical levels with reasonably large basis sets. Such calculations are of great importance, since they directly provide us with quantitative information about the cooperativity of consecutive hydrogen bonds in the solid state. This is especially true for $(HF)_\infty$ because the structures and vibrations of the dimer have thoroughly been investigated both experimentally and theoretically (see, e.g., Refs. [10,17,44,45] and references therein). The performance of a theoretical method as a means to study the hydrogen-bonded systems will be best judged on the basis of the crystal orbital calculations, since the cooperative effects are more pronounced in the condensed phase than in small clusters.

In this chapter, we present the results of ab initio Hartree–Fock and density functional crystal orbital calculations on $(HF)_\infty$. The structural parameters are optimized and frequencies of the infrared- and Raman-active vibrations are calculated using the gradient-corrected Becke–Lee–Yang–Parr (BLYP) [46–48] and the hybrid Becke3–Lee–Yang–Parr (B3LYP) [49] functionals as well as the spin-restricted Hartree–Fock (RHF) [50] approximation in conjunction with the 6-311++G(d,p) basis set. Our choice of the exchange-correlation functionals and basis set has been made on the basis of previous density functional studies of the HF dimer [51–53]. In order to examine the chain-length dependence of the energetic and structural properties, ab initio molecular orbital calculations at the RHF, BLYP, B3LYP, and MP2 levels using the same basis set are carried out for HF oligomers up to the hexamer in the linear chain configuration. The effects of electron correlation, as taken into account at the BLYP and B3LYP levels, on structural parameters, binding energies, and vibrational frequencies are elucidated. The assignment of the observed infrared and Raman bands of HF crystals is also discussed on the basis of the calculated results.

5.2 Method of calculations

5.2.1 Oligomer calculations

Ab initio molecular orbital calculations on the linear HF oligomers up to the hexamer were carried out with the GAUSSIAN 94 program [54]. The geometry optimizations and vibrational frequency calculations were performed at the RHF, BLYP, B3LYP, and MP2 levels with the internally stored 6-311++G(d,p) basis set. We specified the '6d' option, which requests that six Cartesian d-type functions instead of five pure d-type functions be used, in order to make the basis sets used in molecular orbital and crystal orbital calculations identical. All the electrons were correlated in the MP2 calculations.

In the geometry optimizations of the linear oligomers, we assumed the planarity of the molecules and optimized all the remaining structural parameters. Anharmonic vibrational frequencies of the monomer were calculated by the three-term finite-difference method [55] using one-dimensional potential energy curves computed by changing the H–F distance at 0.04 Å intervals in the range of $0.5 - 1.5$ Å.

The intermolecular binding energy of the dimer (trimer) was obtained at each theoretical level as the total energy of the dimer (trimer) minus twice (three times) the total energy of the isolated monomer at their respective optimized structures. We estimated the basis set superposition errors (BSSE's) in the binding energies of the dimer and trimer by the function-counterpoise method of Boys and Bernardi [56], taking into account the structural relaxation of the monomer upon the dimer or trimer formation [57]. The BSSE correction to the binding energy of the trimer was estimated by using Eq. (6) in the paper of Turi and Dannenberg [58].

5.2.2 Polymer calculations

The geometry optimizations and vibrational frequency calculations of infinite zigzag HF chains were carried out using the analytical energy gradients of ab initio crystal orbital theory. Density functional theory using the BLYP and B3LYP functionals as well as RHF theory was employed with the 6-311++G(d,p) basis set. The formulas for the self-consistent-field (SCF) procedures of ab initio crystal orbital theories are given in Refs. [31–34]. Analytical energy gradient formulas for crystal orbital theory were first derived and implemented by Teramae *et al.* [59,60] at the Hartree–Fock level, and we extended them to the density functional and hybrid Hartree–Fock/density functional levels [61]. In our

previous density functional crystal orbital studies [61–63], we expanded the electron density by auxiliary basis sets and evaluated the Coulomb repulsion energies with two- and three-index electron repulsion integrals (ERI's) instead of four-index ERI's [64,65]. In the present study, however, we evaluated the Coulomb repulsion energies with four-index ERI's in order that we can compare the results of the crystal orbital calculations directly with those of the molecular orbital calculations. The contributions of long-range electrostatic interactions to total energies and to Fock matrix elements were evaluated by the multipole expansion technique developed by Delhalle *et al.* [66]. Accordingly, we employed different formulas for the total energies and analytical energy gradients of density functional crystal orbital theory from those given previously [61]. For the sake of completeness, the formulas used in this chapter are given in Appendix.

A translational repeat unit of $(HF)_\infty$ contains two HF molecules. The geometry optimizations of the polymer were performed with the analytical energy gradients by taking an HF unit as the reference unit cell and by making use of the screw-axis symmetry. Four-index ERI's were evaluated by using the eighth, tenth, and sixteenth neighbor approximations for the BLYP, B3LYP, and RHF calculations, respectively. The use of different cut-off radii for different theoretical levels is justified because the exchange-correlation matrix elements decay more rapidly than the exact-exchange matrix elements. The criterion for the convergence of density matrix elements was set to 10^{-8}. The threshold value for the residual energy gradients was 10^{-5} hartree/bohr.

In the vibrational frequency calculations, we adopted a translational repeat unit, i.e., an $(HF)_2$ unit, as the reference unit cell in order to obtain frequencies of all the infrared- and Raman-active modes. Accordingly, we employed the fourth, sixth, and tenth neighbor approximations for the BLYP, B3LYP, and RHF calculations, respectively. Force constants were evaluated by numerical differentiation of the analytical energy gradients. Step size used in the numerical differentiation was 0.04 bohr. We employed the Namur cutoff criterion with multipole expansion corrections [66,67], taking into account the dipole-dipole and charge-quadrupole interaction corrections to total energies and to Fock matrix elements. The other parameters of calculations such as the number of wavevector sampling points and the numerical quadratures and grids used in numerical integration were the same as those used in our previous studies [61–63].

The binding energy of $(HF)_\infty$ was obtained at each theoretical level as the difference between the total energy of the polymer per HF unit and the total energy of the

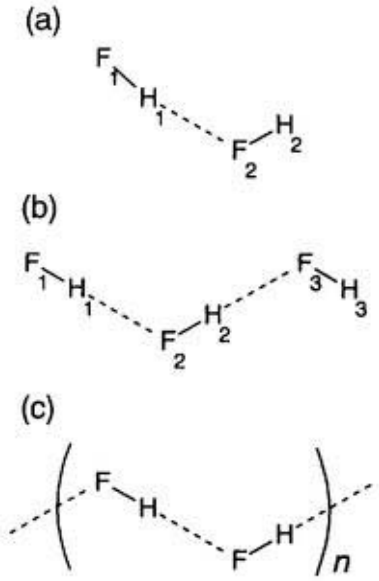

Figure 5.1 Linear hydrogen-bonded (a) dimer, (b) trimer, and (c) polymer of hydrogen fluoride molecules

isolated monomer at their respective optimized geometries. The BSSE's were evaluated by function-counterpoise method [56–58]. We computed the total energy of the monomer with the bond length being equal to that of $(HF)_\infty$ using the basis set of the whole polymer chain. Ghost basis functions were placed within the third nearest HF unit cells at both sides of the reference unit cell.

5.3 Results and discussion

5.3.1 Structures

In Table 5.1, the equilibrium bond lengths of an HF molecule calculated at the BLYP, B3LYP, RHF, and MP2 levels are compared with experimental results [68]. The H–F bond length calculated at the RHF level (0.898 Å) is significantly shorter than the experimental value (0.917 Å), whereas the bond length predicted at the BLYP level (0.933 Å) is too long. At the B3LYP and MP2 levels, the calculated H–F bond lengths agree reasonably well with the experimental value. The errors that are visible in the monomer description at a given theoretical level are carried over to longer oligomers and polymer (vide post).

It has been established by microwave molecular beam experiments [21,22] that the lowest energy configuration of $(HF)_2$ is bent C_s structure with nearly linear F–H$\cdots$F hydrogen bond, as illustrated in Fig. 5.1. All the theoretical models employed in this study (BLYP, B3LYP, RHF, and MP2) correctly reproduce the bent configuration as the global minimum, provided that the 6-311++G(d,p) basis set is used (see also Ref. [51–

Table 5.1 Equilibrium bond length (in units of Å) and harmonic and anharmonic vibrational frequencies (in units of cm^{-1}) of an HF molecule.

	BLYP	B3LYP	RHF	MP2	Experiment
H–F bond length	0.933	0.922	0.898	0.917	0.917[a]
Harmonic frequencies	3939	4098	4491	4200	4138[a]
Anharmonic frequencies	3758	3919	4319	4021	3961[b]

[a] Reference [68]. [b] Reference [73].

Table 5.2 Structural parameters of an open HF dimer. Bond lengths in Å and bond angles in degree.

Structural parameter[a]	BLYP	B3LYP	RHF	MP2	Experiment
F_1–H_1 bond length	0.941	0.929	0.901	0.921	...
$H_1 \cdots F_2$ bond length	1.847	1.832	1.933	1.876	...
F_2–H_2 bond length	0.936	0.925	0.900	0.920	...
$F_1 \cdots F_2$ bond length	2.772	2.748	2.826	2.788	2.79 ± 0.05,[b] 2.72 ± 0.03[c]
$F_2F_1H_1$ angle	8.5	7.9	6.5	6.5	10 ± 6,[c] 7 ± 3[d]
$F_1F_2H_2$ angle	113.6	116.6	126.8	121.0	117 ± 6,[c] 120 ± 2[d]

[a] Atoms are numbered as F_1–$H_1 \cdots F_2$–H_2. [b] Reference [21]. [c] Reference [22]. [d] Reference [69].

53]). The optimized structural parameters of the HF dimer are compiled in Table 5.2 along with the experimental data taken from Refs. [21,22,69]. It is seen from Table 5.2 that the calculated intramolecular H–F bond lengths increase in the same order (RHF < MP2 < B3LYP < BLYP) as the calculated bond lengths of the monomer. The calculated intermolecular H···F and F···F distances are dependent on the theoretical level employed to a larger extent. The F···F distance predicted at the RHF level (2.826 Å) is longer than that obtained at the B3LYP level (2.748 Å) by as much as 0.078 Å, while the F···F distances calculated at the BLYP and MP2 levels fall between these two values. It is difficult to judge which theoretical level yields the best F···F distance on the basis of the comparison between the calculations and experiments due to the large uncertainties in the experimental data. The $F_2F_1H_1$ angles calculated with all of four levels of approximation are within the range of experimental errors. On the other hand, the calculated $F_1F_2H_2$ angles vary substantially with the theoretical levels, and the RHF result seems to be too large as compared with the experimental values.

The most stable structure of $(HF)_3$ in the vapor phase is a cyclic configuration with the C_{3h} symmetry, as has been determined by experimental and theoretical studies (see, e.g., Ref. [17] and references therein). The trimer in the linear open chain configuration (see Fig. 5.1), therefore, corresponds to either a local minimum or a saddle point on the potential energy surface. The BLYP and B3LYP levels predict that the linear $(HF)_3$

Table 5.3 Structural parameters of an open HF trimer. Bond lengths in Å and bond angles in degree.

Structural parameter[a]	BLYP	B3LYP	RHF	MP2
F_1–H_1 bond length	0.944	0.932	0.903	0.923
$H_1 \cdots F_2$ bond length	1.785	1.771	1.879	1.814
F_2–H_2 bond length	0.948	0.935	0.905	0.926
$H_2 \cdots F_3$ bond length	1.756	1.743	1.859	1.789
F_3–H_3 bond length	0.937	0.926	0.901	0.921

[a] Atoms are numbered as $F_1-H_1 \cdots F_2-H_2 \cdots F_3-H_3$.

oligomer is a local minimum, whereas the RHF and MP2 levels indicate that this configuration is a first-order saddle point. The calculated bond distances of $(HF)_3$ are given in Table 5.3. The calculated intramolecular H–F bond lengths depend on the theoretical levels in the way parallel to that found in the monomer and dimer results.

At each theoretical level, the calculated hydrogen-bond distances of the trimer are substantially shorter than that of the dimer. For instance, at the B3LYP level, the calculated $H_1 \cdots F_2$ and $H_2 \cdots F_3$ distances of the trimer are 1.771 and 1.743 Å, respectively, which are shorter by 0.061 and 0.089 Å than the calculated H$\cdots$F distance of the dimer (1.832 Å). These reductions in the hydrogen-bond distances can be regarded as a manifestation of the cooperativity. We observe the similar amounts of reductions at the MP2 (0.062 and 0.087 Å) and at the BLYP level (0.062 and 0.091 Å). However, the values obtained at the RHF level (0.054 and 0.074 Å) are smaller than the those obtained at the correlated levels.

In Fig. 5.2, the intramolecular H–F bond lengths and the H$\cdots$F hydrogen-bond distances are plotted versus the inverse of chain length. Only the longest H–F bond length and the shortest H$\cdots$F distance of each oligomer are used. The corresponding bond lengths of the HF polymer directly obtained from the crystal orbital calculations at the BLYP, B3LYP, and RHF levels are also included. It can be seen that the H–F bond lengths calculated at the BLYP and B3LYP levels change with increasing chain length to a greater extent than those calculated at the RHF level. The BLYP and B3LYP calculations indicate that there is a substantial elongation in the longest H–F bond on going from the hexamer to the polymer, while the RHF calculations show that the bond lengths mostly converge at the hexamer. The chain-length dependence predicted at the MP2 level seems to be intermediate between the density functional results and the RHF result. The chain-length dependence of the H$\cdots$F hydrogen-bond distances is by an order of magnitude larger than

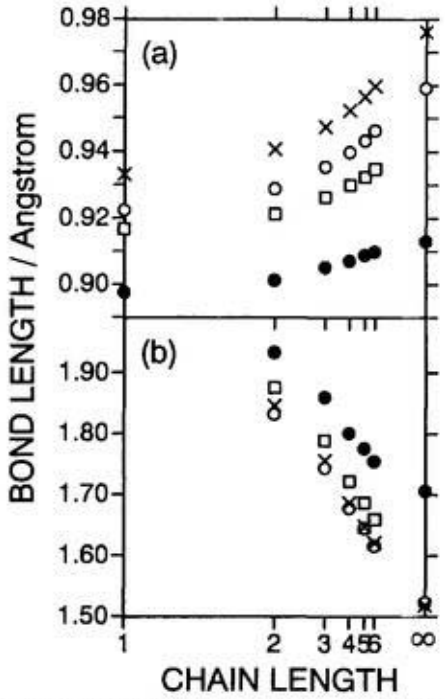

Figure 5.2 Calculated (a) intramolecular H–F bond lengths and (b) H···F hydrogen-bond distances of hydrogen fluoride oligomers and polymer plotted as a function of the inverse of chain length. Crosses: BLYP; open circles: B3LYP; filled circles: RHF; squares: MP2. Only the longest H–F and the shortest H···F distances are used.

that of the intramolecular H–F bond lengths. The H···F distances calculated with the BLYP and B3LYP levels coincide with each other. The RHF level again predicts smaller chain-length dependence than the BLYP and B3LYP levels do. The results obtained from the MP2 calculations seem to be closer to the density functional results than to the RHF results.

The optimized structural parameters of the HF polymer obtained at the RHF, BLYP, and B3LYP levels are compiled in Table 5.4 with the experimental data of crystalline HF taken from Refs. [18,19,70]. In this table, we include the results of previous crystal orbital calculations of Beyer and Karpfen [37] at the RHF level. They employed three different basis sets, i.e., basis sets I, II, and III. Size of the basis sets is in the order: III $\approx$ 6-311++G(d,p) > II > I.

First, we point out that the structural parameters obtained by Beyer and Karpfen with basis set III are in reasonable agreement with our result using the basis set of comparable size, i.e., 6-311++G(d,p). The effects of electron correlation, as taken into account at the BLYP and B3LYP levels, are profound on the structural parameters. The H–F bond lengths calculated at the BLYP and B3LYP levels are 0.976 and 0.959 Å, respec-

Table 5.4 Structural parameters of an infinite HF polymer.
Bond lengths in Å and bond angles in degree.

	Crystal orbital calculation						Experiment
	BLYP[a]	B3LYP[a]	RHF[a]	RHF[b]	RHF[c]	RHF[d]	
H–F bond length	0.976	0.959	0.913	0.918	0.917	0.942	0.97 ± 0.02,[e] 0.95 ± 0.03[f]
F···H bond length	1.519	1.524	1.705	1.69	1.660	1.526	1.53 ± 0.02[e]
F···F bond length	2.495	2.483	2.618	2.60	2.577	2.468	2.50 ± 0.01,[e] 2.49 ± 0.01[g]
FHF angle	178.5	178.6	177.9	178.0	178.1	177.7	176[e]
FFF angle	120.2	122.8	132.0	129.7	130.2	141.9	116,[e] 120.1[g]
Lattice constant	4.326	4.361	4.783	4.707	4.675	4.666	4.26 ± 0.01,[e] 4.32 ± 0.01[g]

[a] Obtained in this study using the 6-311++G(d,p) basis set. [b] Obtained by Beyer and Karpfen [37] with basis set III (see text). [c] Obtained by Beyer and Karpfen [37] with basis set II (see text). [d] Obtained by Beyer and Karpfen [37] with basis set I (see text). [e] Reference [19]. [f] Reference [70]. [g] Reference [18].

tively, which are significantly longer than the RHF value (0.913 Å). The measured H–F bond lengths are 0.97 ± 0.02 Å from the neutron diffraction study [19] and 0.95 ± 0.03 Å from the NMR study [70]. The RHF level underestimates the H–F bond length of $(HF)_\infty$, as it does for the isolated monomer, while the bond lengths obtained from the BLYP and B3LYP calculations are within the experimental errors. Similarly, the RHF level substantially overestimates the F···H and F···F distances, whereas the BLYP and B3LYP levels yield calculated distances which are very close to the experimental data. The H–F, F···H, and F···F lengths calculated at the RHF level with basis set I are apparently in good agreement with the experiments, but this coincidence is fortuitous, and is due to the cancellation of the errors arising from the small basis set used and from the neglect of electron correlation. The FFF angle obtained at the RHF level (132.0 degree) is much larger than the values determined by X-ray diffraction (120.1 degrees) or by neutron diffraction (116 degrees) technique. The BLYP and B3LYP calculations reproduce the experimental angles reasonably well. At the RHF level, the translational period is also greatly overestimated as compared with the experimental results, owing to the too large values of the F···F distance and FFF angle predicted at this level. The BLYP and B3LYP levels, in contrast, reproduce the experimental results quantitatively.

If we take the H–F bond length determined by neutron diffraction technique [19] as a reference value, the discrepancy between the calculated bond length and the reference value amounts to about 0.06 Å at the RHF level. Since the RHF level underestimates the H–F bond length of the isolated monomer by about 0.02 Å, the remaining discrepancy of 0.04 Å is ascribed to the underestimation of the chain-length dependence of the H–F bond length. This result indicates that the inclusion of electron correlation is essential

Table 5.5 Binding energy (in units of kJ mol^{-1}) of an open HF dimer.

	BLYP	B3LYP	RHF	MP2	Experiment
Binding energy	19.9	21.2	18.2	19.6	19.1 ± 1.2^a
Binding energy + ΔZPE[b]	12.6	13.9	11.3	12.6	12.74 ± 0.06^c
BSSE[d]	2.3	2.2	1.7	3.8	...

[a] Reference [71]. [b] Correction due to the zero-point vibrational energy. [c] Reference [72].
[d] Basis set superposition error estimated by the function-counterpoise method.

Table 5.6 Binding energy (in units of kJ mol^{-1}) of an open HF trimer.

	BLYP	B3LYP	RHF	MP2
Binding energy	46.2	48.9	41.5	45.1
Binding energy + ΔZPE[a]	31.5	34.0	27.7	31.0
BSSE[b]	4.9	4.8	3.8	8.9

[a] Correction due to the zero-point vibrational energy. [b] Basis set superposition error estimated by the function-counterpoise method.

in describing the cooperativity of consecutive hydrogen bonds quantitatively. Likewise the discrepancy between the F···F distance of the HF polymer calculated at the RHF level and the observed value is at least partly ascribable to the underestimation of the cooperative behavior.

5.3.2 Binding energies

The calculated binding energies of $(HF)_2$ and $(HF)_3$ are listed in Tables 5.5 and 5.6, respectively. The RHF level predicts the weakest hydrogen bond for $(HF)_2$ and the B3LYP level the strongest hydrogen bond among the theoretical levels employed here. As a consequence, the H···F hydrogen-bond distance calculated at the B3LYP levels is the shortest and that at the RHF level is the longest (vide ante). Since these binding energies inevitably contain the BSSE's, which amount to a few kJ mol^{-1}, all the calculated values for $(HF)_2$ may be too small as compared with the experimental results [71,72]. It should be kept in mind that the calculated structural parameters and vibrational frequencies also contain errors resulting from the BSSE's in the binding energies.

Binding energies per hydrogen bond increase with increasing chain length, which is another manifestation of the cooperativity of hydrogen bonds. At each theoretical level, the calculated binding energy of $(HF)_3$ is substantially larger than twice the calculated binding energy of $(HF)_2$. The ratio of the binding energy of $(HF)_3$ to that of $(HF)_2$ is the smallest in the RHF result (228 %), whereas the ratios obtained with the BLYP, B3LYP,

Table 5.7 Binding energy (in units of kJ mol^{-1}) of an infinite HF polymer.

	BLYP[a]	B3LYP[a]	RHF[a]	RHF[b]	RHF[c]	RHF[d]
Binding energy	35.5	36.4	28.5	27.2	31.8	51.9
BSSE[e]	3.3	3.2	2.5	...	...	...

[a] Obtained in this study using the 6-311++G(d,p) basis set. [b] Obtained by Beyer and Karpfen [37] with basis set III (see text). [c] Obtained by Beyer and Karpfen [37] with basis set II (see text). [d] Obtained by Beyer and Karpfen [37] with basis set I (see text). [e] Basis set superposition error estimated by the function-counterpoise method.

and MP2 levels are within the range of 230 – 232 %. We consider that this result also reflects underestimation of the cooperativity at the RHF level.

The calculated binding energies of the HF polymer are listed in Table 5.7. Again, we observe a reasonable agreement between the RHF/6-311++G(d,p) result (28.5 kJ mol^{-1}) obtained in this study and the RHF/basis set III result (27.2 kJ mol^{-1}) of Beyer and Karpfen. The BLYP and B3LYP levels predict substantially larger binding energies than the RHF level does. The differences between the density functional results and the RHF result, which amount to 7 – 8 kJ mol^{-1}, are at least partly traced back to the underestimation of the chain-length dependence of the binding energies at the RHF level.

5.3.3 Vibrational frequencies

The calculated harmonic and anharmonic frequencies of the H–F stretching mode of an HF molecule are compared with the observed frequencies [68,73] in Table 5.1. The frequencies calculated at the RHF level are overestimated by about 350 cm^{-1}, which is consistent with the too short H–F bond length predicted at this level of theory. At the MP2 level, the calculated frequencies become closer to the observed ones although they are still overestimated by 60 cm^{-1}. The frequencies computed at the BLYP level are too low as compared with the observed frequencies. The results obtained at the B3LYP level are between those obtained at the RHF and BLYP levels, and are in reasonably good agreement with the experimental results as well as with the MP2 results. The differences between the harmonic and anharmonic frequencies predicted at the BLYP, B3LYP, RHF, and MP2 levels are 181, 179, 172, and 179 cm^{-1}, respectively, and are in good agreement with the observed frequency difference of 177 cm^{-1}.

In Table 5.8, the calculated harmonic frequencies of $(HF)_2$ are compared with the measured frequencies [23,74–77]. The frequencies of the H–F stretching modes shift downward

Table 5.8 Vibrational frequencies (in units of cm^{-1}) of an open HF dimer. The values in parentheses are the frequency shifts from the monomer.

Mode	BLYP	B3LYP	RHF	MP2	Experiment
$\nu_1(A')$	3901 (38)	4061 (37)	4455 (36)	4163 (37)	3929 (32)[a]
$\nu_2(A')$	3785 (154)	3962 (136)	4411 (80)	4106 (94)	3868 (93)[a]
$\nu_3(A')$	579	572	503	538	...
$\nu_4(A'')$	455	456	435	421	370,[b] 400[c]
$\nu_5(A')$	222	210	192	203	189[c]
$\nu_6(A')$	157	154	141	146	128[c]

[a] Reference [23]. [b] Reference [74]. [c] References [75–77].

on going from the monomer to the dimer. All the theoretical levels reproduce reasonably well the observed frequency shift for ν_1 mode (32 cm^{-1}), which primarily consists of the stretching motion of the proton acceptor molecule. The ν_2 mode is approximately regarded as the stretching motion of the proton donor molecule, and the large frequency shift (93 cm^{-1}) observed for this mode reflects the strong hydrogen-bond interactions between the two HF molecules. The RHF level predicts too small a frequency shift (80 cm^{-1}) as compared with the experimental value, indicating that this level of theory underestimates the hydrogen-bond interactions. The frequency shifts predicted at the BLYP and B3LYP levels are, on the other hand, substantially overestimated. The MP2 level provides the calculated frequency shift of 94 cm^{-1} which is in good agreement with the experimental value. These results suggest that the BLYP and B3LYP levels tend to overestimate the hydrogen-bond interactions, while the MP2 level describe these interactions reasonably well. The calculated frequencies of the intermolecular vibrations increase in the same order (RHF < MP2 < B3LYP < BLYP) as the frequency shifts increase, except for the out-of-plane (ν_4) mode. At all the theoretical levels, the calculated frequencies of the intermolecular vibrations are higher than the observed [74–77]. It should be noted, however, that the "BSSE-free" frequencies would be lower than these calculated frequencies.

The convergence behavior of the vibrational frequencies of the HF oligomers is depicted in Fig. 5.3. In the $2800 - 4600$ cm^{-1} region, the lowest-frequency mode of each oligomer corresponds to the in-phase H–F stretching vibration, whose infrared intensity is the largest in each oligomer. These in-phase H–F stretching vibrations approach the symmetric H–F stretching mode of the polymer as the chain length increases. The highest-frequency mode of each oligomer, on the other hand, is the localized motion of a terminal HF molecule, and its frequency is relatively insensitive to the chain length. The corre-

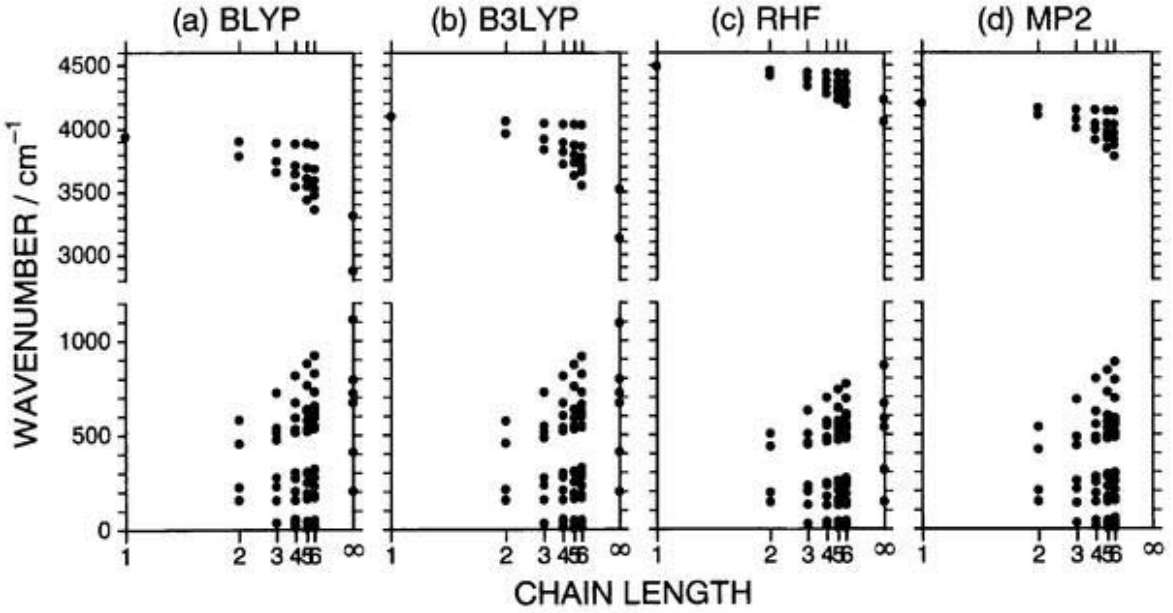

Figure 5.3 Vibrational frequencies of hydrogen fluoride oligomers and polymer calculated at the (a) BLYP, (b) B3LYP, (c) RHF, and (d) MP2 levels plotted as a function of the inverse of chain length.

sponding mode does not exist in the polymer. The absolute values of the H–F stretching frequencies depend strongly on the theoretical levels and are in the order BLYP < B3LYP < MP2 < RHF. This order is determined by the errors that already appear in the monomer results. The chain-length dependence is substantially smaller in the RHF results than in the results obtained at the correlated levels. The chain-length dependence predicted at the BLYP and B3LYP levels is almost the same with each other in magnitude, while that at the MP2 level is again intermediate between the density functional results and the RHF result. The vibrational frequencies in the region below 1200 cm^{-1} are primarily determined by the hydrogen-bond interactions. The RHF level yields invariably lower frequencies for these modes than the other three levels. Among the BLYP, B3LYP, and MP2 results, in contrast, not only the absolute values but also the chain-length dependence of the calculated frequencies in this region agree well with one another.

The calculated frequencies of the infrared- and Raman-active vibrations of $(HF)_\infty$ and $(DF)_\infty$ are compared with the observed frequencies of HF and DF crystals in Table 5.9. Normal coordinates of these modes are depicted in Fig. 5.4. Infrared spectra of HF crystals were first reported by Giguère and Zengin [24], and subsequently by Sastri and Hornig [20] and by Kittelberger and Hornig [25]. Raman spectra were measured by Anderson *et al.* [26,27], and the external-pressure dependence of the spectra has also been studied by Lee *et al.* [28], by Jansen *et al.* [29], and by Pinnick *et al.* [30]. Boutin *et al.* [78] and

Table 5.9 Frequencies (in unit of cm^{-1}) of the infrared- and Raman-active vibrations of an infinite HF polymer.

	Crystal orbital calculation					Experiment		
Mode	BLYP[a]	B3LYP[a]	RHF[a]	RHF[b]	RHF[c]	Infrared[d]	Raman[e]	Raman[f]
				$(HF)_\infty$				
$S(B_1)$	3310	3521	4226	4170	3675	3406	3386	3376 ± 5
$S(A_1)$	2874	3128	4054	3967	3357	3067	3045	3027 ± 6
$L(B_1)$	1112	1093	866	1007	1025	$975 - 1025$	943	...
$L(B_2)$	792	795	665	716	867	792	742	776 ± 1
$L(A_2)$	721	722	585	563	729	inactive	687	722 ± 1
$L(A_1)$	671	668	537	604	702	553	569	566 ± 1
$T(B_1)$	410	409	312	386	490	366	364	...
$T(A_1)$	203	198	144	150	161	202	188	188 ± 2
				$(DF)_\infty$				
$S(B_1)$	2400	2553	3063	3023	2666	2530	2511	2506 ± 4
$S(A_1)$	2089	2272	2940	2874	2432	2294	2281	2272 ± 6
$L(B_1)$	803	790	627	728	741	720	703	...
$L(B_2)$	574	576	482	519	628	572	552	564 ± 4
$L(A_2)$	511	512	415	399	516	inactive	492	515 ± 3
$L(A_1)$	478	476	383	429	498	403	417	409 ± 3
$T(B_1)$	402	400	305	378	479	355	359	...
$T(A_1)$	201	196	142	149	160	210	190	192 ± 2

[a] Obtained in this study using the 6-311++G(d,p) basis set. [b] Obtained by Beyer and Karpfen [37] with basis set II (see text). [c] Obtained by Beyer and Karpfen [37] with basis set I (see text). [d] Reference [25]. [e] Reference [26]. [f] Reference [30].

Axmann *et al.* [79] recorded the inelastic neutron scattering from HF crystals in the region below 600 cm^{-1}. The experimental data in Table 5.9 are taken from Refs. [25,26,30]. The normal modes are classified into stretching (S), librational (L), and pseudo-translational (T) vibrations according to their vibrational patterns. Among them, the assignment of the observed bands has been established for the stretching and pseudo-translational vibrations [25]. For the librational modes, no consensus on the assignment has been reached among the authors [25–27,30,79,80].

In Table 5.9, we include the results obtained by Beyer and Karpfen at the RHF level with basis sets I and II. We can find systematic basis-set dependence of the calculated frequencies in the results of Beyer and Karpfen and our results; as the basis set becomes larger, frequencies of the stretching modes become higher and frequencies of the librational and pseudo-translational modes become lower. There are substantial changes in the vibrational frequencies on going from basis set II of Beyer and Karpfen to the 6-311++G(d,p) basis set.

In the H–F stretching region ($3000 - 3600$ cm^{-1}) of the HF crystals, four infrared absorption bands have been observed [20,24,25]. Among them, two weaker bands were

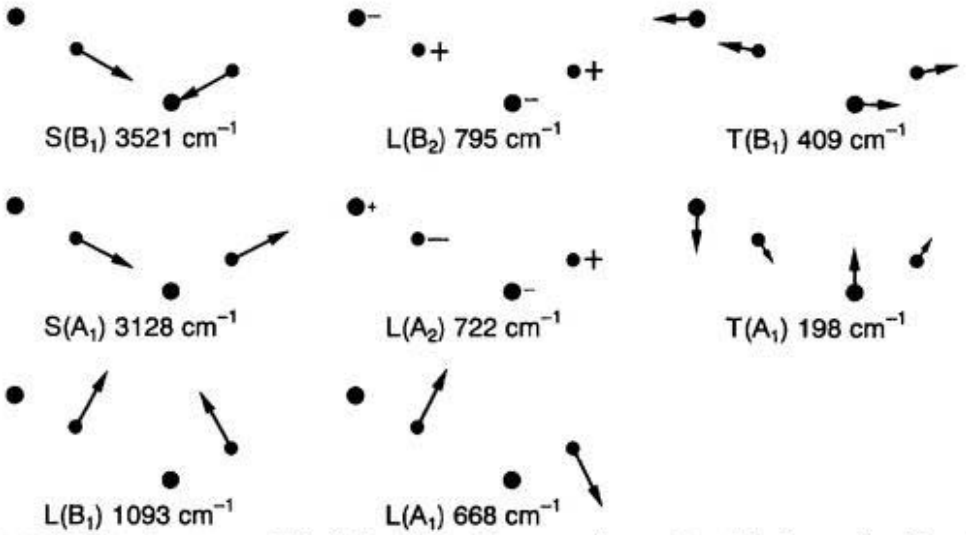

Figure 5.4 Vibrational patterns of the infrared- and Raman-active modes of hydrogen fluoride polymer. Larger filled circles represent fluorine nuclei and smaller ones hydrogen nuclei. The numbers indicate the frequencies calculated at the B3LYP level.

assigned as combination bands of the other two intense fundamental absorption bands and a lattice band near 200 cm^{-1} [25]. The two fundamental absorption bands in this frequency region are the symmetric $S(A_1)$ and antisymmetric $S(B_1)$ intramolecular H–F (D–F) stretching vibrations, the former being more intense than the latter.

It is seen from the table that the frequencies of $S(A_1)$ and $S(B_1)$ modes calculated at the RHF level are too high as compared with the experiments. The deviations between the calculations and experiments are as large as about 1000 cm^{-1} for the $S(A_1)$ mode of $(HF)_\infty$. The splitting of these two modes is also greatly underestimated at this level. The observed splittings are 340 cm^{-1} for $(HF)_\infty$ and 230 cm^{-1} for $(DF)_\infty$, whereas the RHF level yields 172 and 123 cm^{-1}. The predicted too small splittings indicate that the RHF level underestimates the hydrogen-bond interactions. As expected from Fig. 5.3, the RHF level also underestimates the downward shift in the stretching frequencies from the isolated monomer to the polymer. From the experimental side, the frequency shift is 894 $(= 3961 - 3067)$ cm^{-1} for the $S(A_1)$ mode of $(HF)_\infty$. The shift calculated at the RHF level is 437 cm^{-1}, which amounts to only 49 % of the experimental value. The BLYP level, on the contrary, yields the calculated splittings [436 and 311 cm^{-1} for $(HF)_\infty$ and $(DF)_\infty$, respectively], which are larger than the experimental values (340 and 230 cm^{-1}). Therefore, the BLYP level overestimates the hydrogen-bond interactions. Furthermore, the downward shift in the frequencies of the H–F stretching mode from the monomer

to the polymer is also overestimated; the BLYP calculations predict too large a shift of 1065 cm^{-1} as compared with the experimental value (894 cm^{-1}), although the deviation becomes much smaller at the BLYP level than at the RHF level. The use of the B3LYP functional leads to significantly improved agreements in this frequency region. The calculated frequencies of the $S(A_1)$ and $S(B_1)$ modes seem reasonable as compared with the experiments. The calculated splittings of these two modes [393 and 281 cm^{-1} for $(HF)_\infty$ and $(DF)_\infty$, respectively] become much closer to the experimental values (340 and 230 cm^{-1}), and the calculated downward shift (970 cm^{-1}) is also in better agreement with the observed value (894 cm^{-1}) than that obtained at the RHF or BLYP level. Therefore, the chain-length dependence predicted at the B3LYP level is reasonable although it is still slightly overestimated.

There are two pseudo-translational vibrations in the region below 400 cm^{-1}. In the $T(A_1)$ mode, the HF units move nearly perpendicular to the chain axis, while in the $T(B_1)$ mode, the displacements are along the chain axis (see Fig. 5.4). The frequencies of these modes calculated at the RHF level are lower than the experimental values, while those obtained at the BLYP and B3LYP levels, which agree with each other, are higher than the observed. As expected from their vibrational patterns, the frequencies of the pseudo-translational modes are relatively insensitive to the deuteration. The observed frequency of the $T(B_1)$ mode of $(DF)_\infty$ is slightly lower than that of $(HF)_\infty$. The calculated frequencies are consistent with this observed small downward shift upon deuteration. In contrast to $T(B_1)$ mode, the frequency of $T(A_1)$ mode becomes higher upon deuteration. This upward shift cannot be explained by the single chain approximation employed in this study; the interchain interactions probably play a role in this upward shift.

The $T(A_1)$ mode can be regarded as the in-phase stretching motion of the H···F hydrogen bonds. This motion is expected to couple strongly with the intramolecular H–F stretching (S) modes, because the changes in the H···F hydrogen-bond distances substantially affect the shape of the potential energy curves along the H–F stretching coordinates. The weak bands observed in the $2000 - 4000$ cm^{-1} region of HF and DF crystals are combination tones of $S(A_1)$ and $T(A_1)$ and of $S(B_1)$ and $T(A_1)$ [25]. Marechal and Witkowski [81] have analyzed the broad and complex infrared spectral band profiles of general hydrogen-bonded systems in terms of the coupling between the intramolecular high-frequency X–H stretching modes and the low-frequency X–H···Y hydrogen-bond stretching modes. The theoretical model developed by Marechal and Witkowski is capa-

ble of predicting the spectral band profiles and their changes upon isotopic substitution, and Wójcik has successfully applied the model to various hydrogen-bonded complexes and crystals [82,83]. We point out that this model can also be invoked to explain the observed behavior of the combination bands in HF and DF crystals. For instance, the phenomena that the combination bands in DF crystals are much less intense than in HF crystals and that the combination bands associated with $T(B_1)$ modes are not observed are readily accounted for by this model.

Four fundamental normal modes are expected in the librational ($400 - 2000$ cm^{-1}) region. However, there have been found more than four peaks in the observed infrared and Raman spectra in this region, and some of these peaks are very broad, which complicates the assignments. The frequencies of the librational modes calculated at the BLYP and B3LYP levels are in good agreement with each other, while those calculated at the RHF level are significantly lower than the density functional results. The assignment made on the basis of these calculated frequencies is given in Table 5.9. The observed frequency of each librational mode falls within the frequency region bracketed by the density functional and RHF results. The RHF level invariably underestimates the frequencies of the librational modes. The frequencies calculated at the BLYP and B3LYP levels are in reasonable agreement with the observed frequencies, although some of them are significantly overestimated. These results are consistent with our previous conclusion that the RHF level underestimates the chain-length dependence of the frequencies, whereas the BLYP and B3LYP levels slightly overestimate it.

Our assignment generally agrees with the previous one made by Anderson *et al.* [26,27] except for a few modes. In the paper published in 1980, Anderson *et al.* [26] assigned a Raman band at 742 cm^{-1} to $L(B_1)$ and a band at 943 cm^{-1} to $L(B_2)$ for $(HF)_\infty$ and likewise for $(DF)_\infty$. Pinnick *et al.* [30] supported this assignment. Our calculations indicate that the frequencies of $L(B_1)$ modes are higher than those of the $L(B_2)$ modes, and accordingly in the table we have reversed the assignment of these modes made by Anderson *et al.* In the paper of 1981, Anderson *et al.* [27] changed their assignment in the librational frequency region, such that the assignment of $L(B_1)$ and $L(B_2)$ modes is the same as ours. However, they also reversed the assignment of $L(A_1)$ and $L(A_2)$ modes on the basis of their normal coordinate analysis. Our calculations suggest, however, that their previous assignment for $L(A_1)$ and $L(A_2)$ modes is more reasonable. The intensities of the infrared bands at 792 cm^{-1} of HF crystals and at 572 cm^{-1} of DF crystals are strongly

dependent on the conditions of crystallization. Kittelberger and Hornig [25] suggested that these bands manifested itself due to the formation of imperfect crystals and are disorder-induced modes. Pinnick *et al.* [30], however, argued that these modes are true fundamental librational modes on the basis of the morphology of the crystal growth. The frequencies of $L(B_2)$ modes calculated at the B3LYP level are 795 cm^{-1} for $(HF)_\infty$ and 576 cm^{-1} for $(DF)_\infty$, respectively, and are in good agreement with the observed frequencies of these modes. This result seems to support the view of Pinnick *et al.*

5.4 Conclusion

Optimized structures and vibrational frequencies are obtained for linear HF oligomers and an infinite zigzag HF polymer using ab initio molecular orbital and crystal orbital theories. It is demonstrated that electron correlation, as taken into account at the BLYP and B3LYP levels, has profound effects not only on the absolute values of the structural parameters, binding energies, and vibrational frequencies but also on their chain-length dependence, which results from the cooperativity of the consecutive hydrogen bonds. The RHF level significantly underestimates the cooperativity. Too short an H–F bond length, too long F···H and H···H distances, and too high frequencies of the H–F and D–F stretching modes of $(HF)_\infty$ and $(DF)_\infty$ predicted at the RHF level are at least partly ascribable to this deficiency. The chain-length dependence of the structural parameters and vibrational frequencies predicted at the BLYP and B3LYP levels is reasonable as compared with the experimental data or the results obtained from the MP2 calculations. The BLYP level yields too low frequencies for the H–F stretching mode of the isolated monomer, and this tendency is carried over to the results for $(HF)_\infty$ and $(DF)_\infty$. The B3LYP functional reproduces the H–F stretching frequencies of the monomer and polymer reasonably well. The downward frequency shifts in the stretching modes are overestimated at the BLYP and B3LYP levels, but the agreements are significantly better at the BLYP and B3LYP levels than at the RHF level. The BLYP and B3LYP levels reproduce the structural parameters of $(HF)_\infty$ with considerable accuracy. On this basis, we conclude that the BLYP and B3LYP levels describe reasonably well but slightly overestimate the cooperativity of the consecutive hydrogen bonds, whereas the RHF level greatly underestimates this property.

Vibrational assignment of the infrared and Raman bands in the librational frequency region is reexamined on the basis of the present calculations. We reversed the assignment of $L(B_1)$ and $L(B_2)$ modes made by Anderson *et al.* [26]. The frequencies of the librational

and pseudo-translational modes calculated at the RHF levels are lower than the observed. The BLYP and B3LYP levels reproduce the experimental results reasonably well, but they tend to overestimate the frequencies of some modes. Consequently, the observed frequency of each mode falls between the corresponding frequencies calculated at the RHF and density functional levels. These results are consistent with the underestimation of the chain-length dependence of the vibrational frequencies at the RHF levels and the slight overestimation at the BLYP and B3LYP levels.

Appendix: Analytical energy gradient formulas without auxiliary fitting of electron density

In the framework of spin-restricted hybrid Hartree–Fock/density functional crystal orbital theory of polymers [63,84], Kohn–Sham crystal (Bloch) orbitals are expressed as linear combinations of atomic orbitals $\chi_\mu^{(q)}(\mathbf{r})$ in the form

$$\psi_n^{[k]}(\mathbf{r}) = \frac{1}{\sqrt{K}} \sum_\mu \sum_q C_{\mu n}^{[k]} \exp(ikqa) \chi_\mu^{(q)}(\mathbf{r}), \tag{5.1}$$

where a is the translational period, and K is the number of unit cells in the system. The crystal orbital $\psi_n^{[k]}(\mathbf{r})$ and crystal orbital coefficient $C_{\mu n}^{[k]}$ are characterized by energy band n and quasi-momentum k, which are indicated by subscripts and square-bracketed superscripts, respectively. The atomic orbital $\chi_\mu^{(q)}(\mathbf{r})$ is a real spatial function centered in unit cell q.

By using the above-mentioned symmetry-adapted basis functions and applying Ritz variation principle to the total energy expectation value, we obtain the following k-dependent Hartree–Fock–Roothaan equation [31–34]:

$$\mathbf{F}^{[k]}\mathbf{C}^{[k]} = \mathbf{S}^{[k]}\mathbf{C}^{[k]}\epsilon^{[k]}, \tag{5.2}$$

where $\epsilon^{[k]}$ is a diagonal matrix of one-electron energies. The elements of the k-dependent Fock and overlap matrices are defined as

$$F_{\mu\nu}^{[k]} = \sum_q F_{\mu\nu}^{(q)} \exp(ikqa), \tag{5.3}$$

and

$$S_{\mu\nu}^{[k]} = \sum_q S_{\mu\nu}^{(q)} \exp(ikqa), \tag{5.4}$$

where

$$F_{\mu\nu}^{(q)} = H_{\mu\nu}^{(q)} + \sum_{\lambda,\sigma}\sum_{r,s} P_{\lambda\sigma}^{(s-r)} \left(\mu^{(0)}\nu^{(q)}|\lambda^{(r)}\sigma^{(s)}\right) + m_1 X_{\mu\nu}^{(q)} - \frac{m_2}{2}\sum_{\lambda,\sigma}\sum_{r,s} P_{\lambda\sigma}^{(s-r)} \left(\mu^{(0)}\lambda^{(r)}|\nu^{(q)}\sigma^{(s)}\right) + M_{\mu\nu}^{(q)}, \quad (5.5)$$

and

$$S_{\mu\nu}^{(q)} = \int \chi_\mu^{(0)}(\mathbf{r})\chi_\nu^{(q)}(\mathbf{r})d\mathbf{r}. \quad (5.6)$$

Lattice summations in Eq. (5.5) are truncated after several terms, and the long-range electrostatic contributions $M_{\mu\nu}^{(q)}$ to the Fock matrix elements are estimated by the multipole expansion technique [66]. The matrix H in Eq. (5.5) is the one-electron part of the Fock matrix, whose elements are given by

$$H_{\mu\nu}^{(q)} = \int \chi_\mu^{(0)}(\mathbf{r})\left(-\frac{1}{2}\nabla^2\right)\chi_\nu^{(q)}(\mathbf{r})d\mathbf{r} - \sum_A\sum_r \int \chi_\mu^{(0)}(\mathbf{r})\frac{Z_A}{|\mathbf{r}-\mathbf{R}_A^{(r)}|}\chi_\nu^{(q)}(\mathbf{r})d\mathbf{r}, \quad (5.7)$$

where Z_A is the charge of nucleus A at position $\mathbf{R}_A^{(r)}$. The elements of the density matrix $P_{\mu\nu}^{(q)}$ are defined as

$$P_{\mu\nu}^{(q)} = \frac{2}{K}\sum_j^{\text{occ.}}\sum_k^{\text{BZ}} C_{\mu j}^{[k]*} C_{\nu j}^{[k]} \exp(ikqa), \quad (5.8)$$

where the summations are over all the occupied states in the first Brillouin zone. Two-electron integrals $\left(\mu^{(0)}\nu^{(q)}|\lambda^{(r)}\sigma^{(s)}\right)$ in Eq. (5.5) are

$$\left(\mu^{(0)}\nu^{(q)}|\lambda^{(r)}\sigma^{(s)}\right) = \int\int \chi_\mu^{(0)}(\mathbf{r}_1)\chi_\nu^{(q)}(\mathbf{r}_1)\frac{1}{r_{12}}\chi_\lambda^{(r)}(\mathbf{r}_2)\chi_\sigma^{(s)}(\mathbf{r}_2)d\mathbf{r}_1 d\mathbf{r}_2. \quad (5.9)$$

Parameters m_1 and m_2 in Eq. (5.5) denote the mixing ratios of exchange-correlation energy and exact-exchange energy, respectively. In practice, more than one exchange-correlation functional is used in hybrid exchange-correlation functionals such as in the B3LYP functional [49]. We assume that the exchange-correlation functional has the form

$$f = f\left[\rho, \nabla\rho\right], \quad (5.10)$$

where ρ and $\nabla\rho$ are electron density and its gradient. The elements of the exchange-correlation part $X_{\mu\nu}^{(q)}$ of the Fock matrix are given by [85,86]

$$X_{\mu\nu}^{(q)} = \int \left\{\chi_\mu^{(0)} v_{\text{xc}}\chi_\nu^{(q)} + \nabla\chi_\mu^{(0)}\cdot\mathbf{g}_{\text{xc}}\chi_\nu^{(q)} + \chi_\mu^{(0)}\mathbf{g}_{\text{xc}}\cdot\nabla\chi_\nu^{(q)}\right\} d\mathbf{r}, \quad (5.11)$$

with

$$v_{\mathrm{xc}} = \frac{\partial f}{\partial \rho}, \tag{5.12}$$

$$\mathbf{g}_{\mathrm{xc}} = \left\{ \frac{\partial f}{\partial \gamma_{\alpha\alpha}} + \frac{1}{2}\frac{\partial f}{\partial \gamma_{\alpha\beta}} \right\} \nabla\rho, \tag{5.13}$$

$$\gamma_{\alpha\alpha} = \nabla\rho_\alpha \cdot \nabla\rho_\alpha, \tag{5.14}$$

$$\gamma_{\alpha\beta} = \nabla\rho_\alpha \cdot \nabla\rho_\beta, \tag{5.15}$$

where α and β denote spins.

The total energy per unit cell is then expressed as

$$\begin{aligned} E = & \sum_{\mu,\nu}\sum_{q} P_{\mu\nu}^{(q)} H_{\mu\nu}^{(q)} + \frac{1}{2}\sum_{\mu,\nu}\sum_{\lambda,\sigma}\sum_{q,r,s} P_{\mu\nu}^{(q)} P_{\lambda\sigma}^{(s-r)} \left(\mu^{(0)}\nu^{(q)}|\lambda^{(r)}\sigma^{(s)}\right) \\ & + m_1 \int_{\mathrm{cell}} f\left[\rho, \nabla\rho\right] d\mathbf{r} - \frac{m_2}{4}\sum_{\mu,\nu}\sum_{\lambda,\sigma}\sum_{q,r,s} P_{\mu\nu}^{(q)} P_{\lambda\sigma}^{(s-r)} \left(\mu^{(0)}\lambda^{(r)}|\nu^{(q)}\sigma^{(s)}\right) \\ & + E_{\mathrm{ME}} + E_{\mathrm{NR}}, \end{aligned} \tag{5.16}$$

where E_{ME} and E_{NR} are multipole expansion correction and nuclear repulsion energy per unit cell, respectively. The energy gradients with respect to an in-phase ($k = 0$) nuclear coordinate Q can be obtained by directly differentiating Eq. (5.16). The evaluation of the derivatives of orbital coefficients can be avoided by using the orthonormality condition of crystal orbitals [59–61].

$$\begin{aligned} \frac{\partial E}{\partial Q} = & \sum_{\mu,\nu}\sum_{q} P_{\mu\nu}^{(q)} \frac{\partial H_{\mu\nu}^{(q)}}{\partial Q} + \frac{1}{2}\sum_{\mu,\nu}\sum_{\lambda,\sigma}\sum_{q,r,s} P_{\mu\nu}^{(q)} P_{\lambda\sigma}^{(s-r)} \frac{\partial}{\partial Q}\left(\mu^{(0)}\nu^{(q)}|\lambda^{(r)}\sigma^{(s)}\right) \\ & + m_1 \sum_{\mu,\nu}\sum_{q} P_{\mu\nu}^{(q)} \int \left\{ \chi_\mu^{(0)} v_{\mathrm{xc}} \frac{\partial \chi_\nu^{(q)}}{\partial Q} + \frac{\partial \chi_\mu^{(0)}}{\partial Q} v_{\mathrm{xc}} \chi_\nu^{(q)} + \nabla\chi_\mu^{(0)} \cdot \mathbf{g}_{\mathrm{xc}} \frac{\partial \chi_\nu^{(q)}}{\partial Q} \right. \\ & \left. + \frac{\partial \nabla\chi_\mu^{(0)}}{\partial Q} \cdot \mathbf{g}_{\mathrm{xc}} \chi_\nu^{(q)} + \chi_\mu^{(0)} \mathbf{g}_{\mathrm{xc}} \cdot \frac{\partial \nabla\chi_\nu^{(q)}}{\partial Q} + \frac{\partial \chi_\mu^{(0)}}{\partial Q} \mathbf{g}_{\mathrm{xc}} \cdot \nabla\chi_\nu^{(q)} \right\} d\mathbf{r} \\ & - \frac{m_2}{4}\sum_{\mu,\nu}\sum_{\lambda,\sigma}\sum_{q,r,s} P_{\mu\nu}^{(q)} P_{\lambda\sigma}^{(s-r)} \frac{\partial}{\partial Q}\left(\mu^{(0)}\lambda^{(r)}|\nu^{(q)}\sigma^{(s)}\right) + \frac{\partial E_{\mathrm{NR}}}{\partial Q} \\ & - \sum_{\mu,\nu}\sum_{q} W_{\mu\nu}^{(q)} \frac{\partial S_{\mu\nu}^{(q)}}{\partial Q}, \end{aligned} \tag{5.17}$$

where W is the energy-weighted density matrix, whose elements are defined as

$$W_{\mu\nu}^{(q)} = \frac{2}{K}\sum_{j}^{\mathrm{occ.}}\sum_{k}^{\mathrm{BZ}} \epsilon_j^{[k]} C_{\mu j}^{[k]*} C_{\nu j}^{[k]} \exp(ikqa). \tag{5.18}$$

Since the first (and higher) derivatives of total energy are expected to converge much faster than the total energy itself, we neglect the gradient contributions from the multipole

expansion correction. For instance, the leading term in the expression for the dipole-dipole interaction energy is proportional to $1/r^3$ with r being the distance between the centers of two dipoles. The forces resulting from the dipole-dipole interaction are then proportional to $1/r^4$, and hence they converge more rapidly than the interaction energy itself with increasing r.

The analytical energy gradient with respect to the translational period a can be calculated by using Eq. (5.17) and the following relation [59–61]:

$$\frac{\partial}{\partial a} = \sum_A \sum_q q \frac{\partial}{\partial Q_z^{A(q)}}. \tag{5.19}$$

Here $Q_z^{A(q)}$ denotes the z-coordinate, which we assume to be parallel to the chain axis, of nucleus A in unit cell q. The differentiation of exchange-correlation part of the energy with respect to a gives rise to a two-dimensional (surface) integral [61]. This two-dimensional integral can be transformed to three-dimensional (volume) integrals by virtue of Gauss theorem [61], and these three-dimensional integrals are conveniently evaluated by using the atomic partitioning scheme of Becke [87].

References

[1] H. S. Frank, Proc. Roy. Soc. (London) A, **247,** 481 (1958).

[2] J. Del Bene and J. A. Pople, J. Chem. Phys., **52,** 4858 (1970).

[3] J. E. Del Bene and J. A. Pople, J. Chem. Phys., **55,** 2296 (1971).

[4] J. E. Del Bene and J. A. Pople, J. Chem. Phys., **58,** 3605 (1973).

[5] P. Schuster, G. Zundel, and C. Sandorfy, *The Hydrogen Bond, Vol. 1–3* (North-Holland, Amsterdam, 1976).

[6] G. A. Jeffrey, M. E. Gress, and S. Takagi, J. Am. Chem. Soc., **99,** 609 (1977).

[7] Y.-C. Tse and M. D. Newton, J. Am. Chem. Soc., **99,** 611 (1977).

[8] G. A. Jeffrey and W. Saenger, *Hydrogen Bonding in Biological Structures* (Springer-Verlag, Berlin, 1991).

[9] Z. Latajka and S. Scheiner, Chem. Phys., **122,** 413 (1988).

[10] D. J. Nesbitt, Chem. Rev., **88,** 843 (1988).

[11] G. Chałasiński, S. M. Cybulski, M. M. Szczęśniak, and S. Scheiner, J. Chem. Phys., **91,** 7048 (1989).

[12] A. Karpfen, Int. J. Quantum Chem. Quantum Chem. Symp., **24,** 129 (1990).

[13] M. Quack, J. Stohner, and M. A. Suhm, J. Mol. Struct., **294,** 33 (1993).

[14] A. Karpfen and O. Yanovitskii, J. Mol. Struct. (THEOCHEM), **307,** 81 (1994).

[15] A. Karpfen and O. Yanovitskii, J. Mol. Struct. (THEOCHEM), **314,** 211 (1994).

[16] K. R. Liedl, R. T. Kroemer, and B. M. Rode, Chem. Phys. Lett., **246,** 455 (1995).

[17] A. Karpfen, in *Molecular Interactions,* edited by S. Scheiner (Wiley, 1997), p. 265.

[18] M. Atoji and W. N. Lipscomb, Acta Cryst., **7,** 173 (1954).

[19] M. W. Johnson, E. Sándor, and E. Arzi, Acta Cryst. B, **31,** 1998 (1975).

[20] M. L. N. Sastri and D. F. Hornig, J. Chem. Phys., **39,** 3497 (1963).

[21] T. R. Dyke, B. J. Howard, and W. Klemperer, J. Chem. Phys., **56,** 2442 (1972).

[22] B. J. Howard, T. R. Dyke, and W. Klemperer, J. Chem. Phys., **81,** 5417 (1984).

[23] A. S. Pine and W. J. Lafferty, J. Chem. Phys., **78,** 2154 (1983).

[24] P. A. Giguère and N. Zengin, Can. J. Chem., **36,** 1013 (1958).

[25] J. S. Kittelberger and D. F. Hornig, J. Chem. Phys., **46,** 3099 (1967).

[26] A. Anderson, B. H. Torrie, and W. S. Tse, Chem. Phys. Lett., **70,** 300 (1980).

[27] A. Anderson, B. H. Torrie, and W. S. Tse, J. Raman Spectrosc., **10,** 148 (1981).

[28] S. A. Lee, D. A. Pinnick, S. M. Lindsay, and R. C. Hanson, Phys. Rev. B, **34,** 2799 (1986).

[29] R. W. Jansen, R. Bertoncini, D. A. Pinnick, A. I. Katz, R. C. Hanson, O. F. Sankey, and M. O'Keeffe, Phys. Rev. B, **35,** 9830 (1987).

[30] D. A. Pinnick, A. I. Katz, and R. C. Hanson, Phys. Rev. B, **39,** 8677 (1989).

[31] G. Del Re, J. Ladik, and G. Biczó, Phys. Rev., **155,** 997 (1967).

[32] J. M. André, J. Chem. Phys., **50,** 1536 (1969).

[33] M. Kertész, Adv. Quantum Chem., **15,** 161 (1982).

[34] J. J. Ladik, *Quantum Theory of Polymers as Solids* (Plenum, New York, 1988).

[35] M. Kertész, J. Koller, and A. Ažman, Chem. Phys. Lett., **36,** 576 (1975)

[36] A. Karpfen, A. Beyer, and P. Schuster, Int. J. Quantum Chem., **19,** 1113 (1981).

[37] A. Beyer and A. Karpfen, Chem. Phys., **64,** 343 (1982).

[38] Y. J. I'haya, S. Narita, Y. Fujita, and H. Ujino, Int. J. Quantum Chem. Quantum Chem. Symp., **18,** 153 (1984).

[39] C.-M. Liegener and J. Ladik, Phys. Rev. B, **35,** 6403 (1987).

[40] S. Berski and Z. Latajka, J. Mol. Struct. (THEOCHEM), **389,** 147 (1997).

[41] I. Mayer, G. Räther, and S. Suhai, Chem. Phys. Lett., **270,** 211 (1997).

[42] M. Springborg, Phys. Rev. Lett., **59,** 2287 (1987).

[43] M. Springborg, Phys. Rev. B, **38,** 1483 (1988).

[44] S. Scheiner, in *Theoretical Models of Chemical Bonding, Part 4,* edited by Z. B. Maksić (Springer-Verlag, Berlin, 1991), p. 171.

[45] D. G. Truhlar, in *Dynamics of Polyatomic Van der Waals Complexes,* edited by N. Halberstadt and K. C. Janda (Plenum, New York, 1990), p. 159.

[46] A. D. Becke, Phys. Rev. A, **38,** 3098 (1988).

[47] C. Lee, W. Yang, and R. G. Parr, Phys. Rev. B, **37,** 785 (1988).

[48] B. Miehlich, A. Savin, H. Stoll, and H. Preuss, Chem. Phys. Lett., **157,** 200 (1989).

[49] A. D. Becke, J. Chem. Phys., **98,** 5648 (1993).

[50] In order to avoid confusion, we use different abbreviations for hydrogen fluoride (HF) and for Hartree–Fock (RHF) in this chapter.

[51] Z. Latajka and Y. Bouteiller, J. Chem. Phys., **101,** 9793 (1994).

[52] Y. Jeanvoine, F. Bohr, and M. F. Ruiz-López, Can. J. Chem., **73,** 710 (1995).

[53] P. Hobza, J. Šponer, and T. Reschel, J. Comput. Chem., **16,** 1315 (1995).

[54] GAUSSIAN 94, Revision E.2, M. J. Frisch, G. W. Trucks, H. B. Schlegel, P. M. W. Gill, B. G. Johnson, M. A. Robb, J. R. Cheeseman, T. Keith, G. A. Petersson, J. A. Montgomery, K. Raghavachari, M. A. Al-Laham, V. G. Zakrzewski, J. V. Ortiz, J. B. Foresman, J. Cioslowski, B. B. Stefanov, A. Nanayakkara, M. Challacombe, C. Y. Peng, P. Y. Ayala, W. Chen, M. W. Wong, J. L. Andres, E. S. Replogle, R. Gomperts, R. L. Martin, D. J. Fox, J. S. Binkley, D. J. Defrees, J. Baker, J. P. Stewart, M. Head-Gordon, C. Gonzalez, and J. A. Pople, Gaussian, Inc., Pittsburgh PA, 1995.

[55] B. W. Shore, J. Chem. Phys., **59,** 6450 (1973).

[56] S. F. Boys and F. Bernardi, Mol. Phys., **19,** 553 (1970).

[57] I. Mayer and P. R. Surján, Chem. Phys. Lett., **191,** 497 (1992).

[58] L. Turi and J. J. Dannenberg, J. Phys. Chem., **97,** 2488 (1993).

[59] H. Teramae, T. Yamabe, C. Satoko, and A. Imamura, Chem. Phys. Lett., **101,** 149 (1983).

[60] H. Teramae, T. Yamabe, and A. Imamura, J. Chem. Phys., **81,** 3564 (1984).

[61] Chapter 3 of the present thesis.

[62] Chapter 2 of the present thesis.

[63] Chapter 4 of the present thesis.

[64] B. I. Dunlap, J. W. D. Connolly, and J. R. Sabin, J. Chem. Phys., **71,** 3396 (1979).

[65] B. I. Dunlap, J. W. D. Connolly, and J. R. Sabin, J. Chem. Phys., **71,** 4993 (1979).

[66] J. Delhalle, L. Piela, J.-L. Brédas, and J.-M. André, Phys. Rev. B, **22,** 6254 (1980).

[67] J. M. André, D. P. Vercauteren, V. P. Bodart, and J. G. Fripiat, J. Comput. Chem., **5,** 535 (1984).

[68] K. P. Huber and G. Herzberg, *Molecular Spectra and Molecular Structure IV. Constants of Diatomic Molecules* (Van Nostrand Reinhold, New York, 1979).

[69] H. S. Gutowsky, C. Chuang, J. D. Keen, T. D. Klots, and T. Emilsson, J. Chem. Phys., **83,** 2070 (1985).

[70] S. P. Habuda and Yu. V. Gagarinsky, Acta Cryst. B, **27,** 1677 (1971).

[71] A. S. Pine and B. J. Howard, J. Chem. Phys., **84,** 590 (1986).

[72] D. C. Dayton, K. W. Jucks, and R. E. Miller, J. Chem. Phys., **90,** 2631 (1989).

[73] G. Guelachvili, Opt. Commun., **19,** 150 (1976).

[74] K. von Puttkamer and M. Quack, Chem. Phys., **139,** 31 (1989).

[75] L. Andrews and G. L. Johnson, J. Phys. Chem., **88,** 425 (1984).

[76] R. D. Hunt and L. Andrews, J. Chem. Phys., **82,** 4442 (1985).

[77] L. Andrews, S. R. Davis, and R. D. Hunt, Mol. Phys., **77,** 993 (1992).

[78] H. Boutin, G. J. Safford, and V. Brajovic, J. Chem. Phys., **39,** 3135 (1963).

[79] A. Axmann, W. Biem, P. Borsch, F. Hoßfeld, and H. Stiller, Discuss. Faraday Soc., **48,** 69 (1969).

[80] R. Tubino and G. Zerbi, J. Chem. Phys., **51,** 4509 (1969).

[81] Y. Marechal and A. Witkowski, J. Chem. Phys., **48,** 3697 (1968).

[82] M. J. Wójcik, Int. J. Quantum. Chem., **10,** 747 (1976).

[83] M. J. Wójcik, Int. J. Quantum. Chem., **29,** 855 (1986).

[84] S. Suhai, Phys. Rev. B, **51,** 16553 (1995).

[85] J. A. Pople, P. M. W. Gill, and B. G. Johnson, Chem. Phys. Lett., **199,** 557 (1992).

[86] B. G. Johnson, P. M. W. Gill, and J. A. Pople, J. Chem. Phys., **98,** 5612 (1993).

[87] A. D. Becke, J. Chem. Phys., **88,** 2547 (1988).

Chapter 6

Analytical second derivatives for ab initio Hartree–Fock crystal orbital theory

So Hirata and Suehiro Iwata, "Analytical second derivatives in ab initio Hartree–Fock crystal orbital theory of polymers," J. Mol. Struct. (THEOCHEM) (Special issue for Prof. Shigeru Huzinaga), in press.

Abstract

In the framework of ab initio Hartree–Fock crystal orbital theory of polymers, the formulas for the analytical second derivatives of energy with respect to in-phase ($k = 0$) nuclear coordinates are derived. The coupled perturbed Hartree–Fock (CPHF) equation is iteratively solved by using the direct (recomputation of two-electron integrals) atomic-orbital-based algorithm. Frequencies of the Brillouin zone center ($k = 0$) vibrations of all-*trans* polyethylene are calculated by using the STO-3G, 3-21G, and 6-31G(d) basis sets. The dependence of the frequencies on the number of neighbors included in the lattice summations, on the number of momentum sampling points in the first Brillouin zone, and on the convergence criterion for the CPHF solutions is examined. In our implementation, the use of analytical second derivatives is more efficient than the use of the finite differences of analytical first derivatives.

6.1 Introduction

Analytical first and second derivatives of the electronic energy with respect to nuclear coordinates are essential in the calculations of equilibrium geometries and vibrational frequencies of molecules on the basis of ab initio molecular orbital theory [1–5]. Force constants of a molecule can be obtained either as the finite differences of analytical first derivatives or as analytical second derivatives. At the Hartree–Fock (HF) level of theory, the use of analytical second derivatives has turned out to be less expensive than the use of finite differences, owing to the efficient algorithms for solving the coupled perturbed Hartree–Fock (CPHF) equation [6–11] and for evaluating the derivatives of two-electron integrals [12–20]. The second-derivative method has become the standard approach and the vibrational analyses of molecules based on this method are now routinely carried out.

In ab initio crystal orbital theory of polymers, however, only the analytical-first-derivative scheme has so far been implemented in the framework of HF theory [21,22]. Very recently, we have developed the analytical-first-derivative scheme for density functional and hybrid HF/density functional theories, and applied it to the vibrational analyses of polyacetylene, polymethineimine, and polyethylene [23,24]. No work has been carried out on the higher-order analytical derivatives at the HF level or the analytical derivatives at HF-based correlated levels. The objectives of the present study are to describe the formulas and computer implementation of the analytical-second-derivative scheme in

the framework of ab initio HF crystal orbital theory and to study the dependence of the frequencies calculated with this scheme on several parameters, namely, the number of neighbors included in the lattice summations, the number of momentum sampling points in the first Brillouin zone, and the convergence criterion for the CPHF solutions. Equilibrium geometries and vibrational frequencies are calculated for all-*trans* polyethylene (hereafter simply referred to as polyethylene) by using the STO-3G, 3-21G, and 6-31G(d) basis sets. Polyethylene is an ideal polymer for our purpose, because the size of the translational repeat unit is small and the normal vibrations have thoroughly been studied both experimentally and theoretically, and are well understood [25–27]. Efficiency of the second-derivative method and the finite-difference method is also discussed in terms of the execution times.

There have been only a limited number of vibrational analyses for polymers, based on crystal orbital theory, in which the force constants have been evaluated by the numerical differentiation of the analytical first derivatives [21–24] or by the double numerical differentiation of the total energies [28–32]. These studies are primarily concerned with the frequencies of the Brillouin zone center ($k = 0$) vibrations, which can directly be compared with the positions of the lines appearing in the infrared and Raman spectra of polymers. Since $k = 0$ vibrations do not lift the translational symmetry of the system, we can take full advantage of the symmetry throughout the calculations. In fact, the frequencies of $k = 0$ vibrations are conveniently calculated by taking the smallest translational repeat unit as a reference unit cell. The evaluation of the frequencies of $k \neq 0$ vibrations is, on the other hand, computationally much more demanding than that of $k = 0$ vibrations, since the translational period becomes much longer if the nuclei are displaced along the normal coordinates of $k \neq 0$ vibrations. In principle, the frequencies of $k \neq 0$ vibrations cannot be observed by infrared or Raman spectroscopy, and hence they are usually studied by other experimental techniques such as inelastic neutron scattering spectroscopy. Therefore, the separate treatment of $k = 0$ and $k \neq 0$ vibrations is justified both in the experimental and theoretical viewpoints.

In this chapter, we confine ourselves to the second derivatives of the electronic energy with respect to in-phase ($k = 0$) nuclear coordinates. Thus, we are primarily concerned with the frequencies of the infrared- and Raman-active vibrations of polymers. The frequencies of $k \neq 0$ vibrations can also be obtained by the second-derivative method described here by taking a chain of several repeat units ("supercell") as a reference unit cell.

We have already employed the supercell approach in combination with the finite-difference method to study the phonon dispersion curves and inelastic neutron scattering of polyethylene [24]. However, the finite displacement of a nucleus in a supercell significantly lowers the translational symmetry, and the entire calculation becomes highly redundant and requires much more computational resources than the calculation of $k = 0$ frequencies. In the second-derivative method, the nuclei are fixed at the equilibrium positions, and hence the notion of the supercell may be introduced at a later stage of the calculation, e.g., at the process of solving the CPHF equation. Although we focus our attention on $k = 0$ vibrations in this chapter, we hope that the second-derivative method described here will be the first stage of a program to develop an efficient supercell approach, whereby the frequencies of $k \neq 0$ vibrations can be computed with minimum redundant work.

6.2 Formulas for the analytical second derivatives

In this section, we describe the formulas for the analytical second derivatives of energy in the framework of ab initio HF crystal orbital theory. Since the derivation of the formulas for infinite polymer chains and that for molecules [6,7] have much in common, we shall make as much use of the results for molecules as possible without showing the derivation.

In the crystal orbital method [33–36], the crystal orbitals of an infinite polymer chain are described as linear combinations of atomic orbitals $\chi_\mu^{(q)}(\mathbf{r})$:

$$\psi_n^{[k]}(\mathbf{r}) = \frac{1}{\sqrt{K}} \sum_\mu \sum_q C_{\mu n}^{[k]} \exp(ikqa) \chi_\mu^{(q)}(\mathbf{r}), \tag{6.1}$$

where a is the translational period, and K is the number of unit cells in the system and it approaches infinity. We assume here that the system under consideration is a closed-shell system and $\chi_\mu^{(q)}(\mathbf{r})$ is a real spatial orbital. The crystal orbital $\psi_n^{[k]}(\mathbf{r})$ and crystal orbital coefficient $C_{\mu n}^{[k]}$ are characterized by energy band n, which is indicated by subscripts, and by quasi-momentum k, which is specified by square-bracketed superscripts. The atomic orbital $\chi_\mu^{(q)}(\mathbf{r})$ is located in unit cell q and bears the following relation:

$$\chi_\mu^{(q)}(\mathbf{r}) = \chi_\mu^{(0)}(\mathbf{r} - qa). \tag{6.2}$$

The use of the above-mentioned symmetry-adapted basis functions and the periodic boundary conditions reduces the Hartree–Fock equation of an infinite polymer chain to a set of k-dependent pseudoeigenvalue equations:

$$\mathbf{F}^{[k]}\mathbf{C}^{[k]} = \epsilon^{[k]}\mathbf{S}^{[k]}\mathbf{C}^{[k]}. \tag{6.3}$$

The k-dependent Fock and overlap matrices are constructed from the corresponding molecular integrals in the atomic orbital basis:

$$F_{\mu\nu}^{[k]} = \sum_q F_{\mu\nu}^{(q)} \exp(ikqa), \tag{6.4}$$

and

$$S_{\mu\nu}^{[k]} = \sum_q S_{\mu\nu}^{(q)} \exp(ikqa). \tag{6.5}$$

The elements of the Fock and overlap matrices between the atomic orbitals $\chi_\mu^{(0)}(\mathbf{r})$ and $\chi_\nu^{(q)}(\mathbf{r})$ are given, respectively, by

$$F_{\mu\nu}^{(q)} = H_{\mu\nu}^{(q)} + \sum_{\lambda,\sigma}\sum_{r,s} P_{\lambda\sigma}^{(s-r)} \left(\mu^{(0)}\nu^{(q)}||\lambda^{(r)}\sigma^{(s)}\right), \tag{6.6}$$

and

$$S_{\mu\nu}^{(q)} = \int \chi_\mu^{(0)}(\mathbf{r})\chi_\nu^{(q)}(\mathbf{r})d\mathbf{r}. \tag{6.7}$$

The matrices introduced in Eq. (6.6) are the one-electron core Hamiltonian matrix

$$\begin{aligned} H_{\mu\nu}^{(q)} &= \int \chi_\mu^{(0)}(\mathbf{r}) \left(-\frac{1}{2}\nabla^2\right) \chi_\nu^{(q)}(\mathbf{r})d\mathbf{r} \\ &\quad - \sum_A \sum_r \int \chi_\mu^{(0)}(\mathbf{r}) \frac{Z_A}{|\mathbf{r} - \mathbf{R}_A^{(r)}|} \chi_\nu^{(q)}(\mathbf{r})d\mathbf{r}, \end{aligned} \tag{6.8}$$

and the density matrix

$$P_{\mu\nu}^{(q)} = \frac{2}{K} \sum_j^{\text{occ.}} \sum_k^{\text{BZ}} C_{\mu j}^{[k]*} C_{\nu j}^{[k]} \exp(ikqa). \tag{6.9}$$

Here the summation $\sum_j$ is over occupied energy bands and $\sum_k$ is over k points in the first Brillouin zone. Note that the number of k points in the first Brillouin zone is equal to K. Two-electron integrals over atomic orbitals in Eq. (6.6) are antisymmetrized, namely,

$$\left(\mu^{(0)}\nu^{(q)}||\lambda^{(r)}\sigma^{(s)}\right) = \left(\mu^{(0)}\nu^{(q)}|\lambda^{(r)}\sigma^{(s)}\right) - \frac{1}{2}\left(\mu^{(0)}\sigma^{(s)}|\lambda^{(r)}\nu^{(q)}\right), \tag{6.10}$$

with

$$\left(\mu^{(0)}\nu^{(q)}|\lambda^{(r)}\sigma^{(s)}\right) = \int\int \chi_\mu^{(0)}(\mathbf{r}_1)\chi_\nu^{(q)}(\mathbf{r}_1)\frac{1}{r_{12}}\chi_\lambda^{(r)}(\mathbf{r}_2)\chi_\sigma^{(s)}(\mathbf{r}_2)d\mathbf{r}_1 d\mathbf{r}_2. \tag{6.11}$$

By using the matrices defined above, the total energy per unit cell can be obtained as

$$E = \sum_{\mu,\nu}\sum_q P_{\mu\nu}^{(q)} H_{\mu\nu}^{(q)} + \frac{1}{2}\sum_{\mu,\nu}\sum_{\lambda,\sigma}\sum_{q,r,s} P_{\mu\nu}^{(q)} P_{\lambda\sigma}^{(s-r)} \left(\mu^{(0)}\nu^{(q)}||\lambda^{(r)}\sigma^{(s)}\right) + E_{\text{NR}}, \tag{6.12}$$

where $E_{\rm NR}$ is the nuclear repulsion energy per unit cell. Direct differentiation of the total energy with respect to a nuclear coordinate x gives the expression which contains the derivatives of density matrix elements. However, at this point the explicit evaluation of these derivatives can be avoided by making use of the orthonormality condition of the crystal orbitals, and the final expression is written as [21,22]

$$\begin{aligned}\frac{\partial E}{\partial x} &= \sum_{\mu,\nu}\sum_{q} P_{\mu\nu}^{(q)} \frac{\partial H_{\mu\nu}^{(q)}}{\partial x} + \frac{1}{2}\sum_{\mu,\nu}\sum_{\lambda,\sigma}\sum_{q,r,s} P_{\mu\nu}^{(q)} P_{\lambda\sigma}^{(s-r)} \frac{\partial}{\partial x}\left(\mu^{(0)}\nu^{(q)}||\lambda^{(r)}\sigma^{(s)}\right) \\ &+ \frac{\partial E_{\rm NR}}{\partial x} - \sum_{\mu,\nu}\sum_{q} W_{\mu\nu}^{(q)} \frac{\partial S_{\mu\nu}^{(q)}}{\partial x}, \end{aligned} \tag{6.13}$$

where we introduced the energy-weighted density matrix

$$W_{\mu\nu}^{(q)} = \frac{2}{K}\sum_{j}^{\rm occ.}\sum_{k}^{\rm BZ} \epsilon_j^{[k]} C_{\mu j}^{[k]*} C_{\nu j}^{[k]} \exp(ikqa). \tag{6.14}$$

It should be emphasized that Eq. (6.13) is derived on the assumption that the nuclear displacement along the coordinate x does not lift the translational symmetry. In other words, nuclei in the whole polymer chain move in-phase along the coordinate x. Differentiation of Eq. (6.13) with respect to a second in-phase coordinate y leads to an expression for the second derivatives of the total energy:

$$\begin{aligned}\frac{\partial^2 E}{\partial x \partial y} &= \sum_{\mu,\nu}\sum_{q} P_{\mu\nu}^{(q)} \frac{\partial^2 H_{\mu\nu}^{(q)}}{\partial x \partial y} + \frac{1}{2}\sum_{\mu,\nu}\sum_{\lambda,\sigma}\sum_{q,r,s} P_{\mu\nu}^{(q)} P_{\lambda\sigma}^{(s-r)} \frac{\partial^2}{\partial x \partial y}\left(\mu^{(0)}\nu^{(q)}||\lambda^{(r)}\sigma^{(s)}\right) \\ &+ \frac{\partial^2 E_{\rm NR}}{\partial x \partial y} - \sum_{\mu,\nu}\sum_{q} W_{\mu\nu}^{(q)} \frac{\partial^2 S_{\mu\nu}^{(q)}}{\partial x \partial y} + \sum_{\mu,\nu}\sum_{q} \frac{\partial P_{\mu\nu}^{(q)}}{\partial y}\frac{\partial H_{\mu\nu}^{(q)}}{\partial x} \\ &+ \sum_{\mu,\nu}\sum_{\lambda,\sigma}\sum_{q,r,s} \frac{\partial P_{\mu\nu}^{(q)}}{\partial y} P_{\lambda\sigma}^{(s-r)} \frac{\partial}{\partial x}\left(\mu^{(0)}\nu^{(q)}||\lambda^{(r)}\sigma^{(s)}\right) \\ &- \sum_{\mu,\nu}\sum_{q} \frac{\partial W_{\mu\nu}^{(q)}}{\partial y}\frac{\partial S_{\mu\nu}^{(q)}}{\partial x}. \end{aligned} \tag{6.15}$$

This expression involves the derivatives of density matrix $\partial P_{\mu\nu}^{(q)}/\partial y$ and energy-weighted density matrix $\partial W_{\mu\nu}^{(q)}/\partial y$. Evaluation of these derivatives can no longer be avoided.

In order to evaluate the derivatives of density matrix and energy-weighted density matrix, we have to know the derivatives of the crystal orbital coefficients $\partial C_{\mu n}^{[k]}/\partial y$. The complete set of these derivatives $\partial C_{\mu n}^{[k]}/\partial y$ is obtained as a solution to the CPHF equation. The molecular CPHF equation was first derived by Gerratt and Mills [6], and has been described by a number of authors [2,3,5,7–11]. Following the notation of Pople *et al.* [7],

we can write the equation as

$$(\epsilon_i - \epsilon_a)\, u_{ai}^{(1)} = Q_{ai}^{(1)} + 2 \sum_{b}^{\text{virt.}} \sum_{j}^{\text{occ.}} \{u_{bj}^{(1)*}\, (ai||bj) + u_{bj}^{(1)}\, (ai||jb)\}. \tag{6.16}$$

This equation has to be solved to find $u_{ai}^{(1)}$, which can be used to give the derivatives of the molecular orbital coefficients by the following relation:

$$\frac{\partial C_{\mu n}}{\partial y} = \sum_{m}^{\text{all}} C_{\mu m} u_{mn}^{(1)} \tag{6.17}$$

The superscript '(1)' has been retained in this chapter in order to keep our notation in accordance with that of Pople *et al.* [7]. In Eqs. (6.16) and (6.17) and in what follows, we represent the occupied molecular orbitals by i, j, h, l and virtual molecular orbitals by a, b. We also use m, n for the entire set of molecular orbitals. Thus, $u_{ai}^{(1)}$ is a vector of length $V \times O$ with V being the number of virtual orbitals and O being the number of occupied orbitals. Note that the vectors of the type $u_{ij}^{(1)}$ and $u_{ab}^{(1)}$ are not determined uniquely (nor required) since the HF wave function is invariant to the linear transformations among the occupied orbitals [5]. Two-electron integrals in Eq. (6.16) are defined over molecular orbitals.

We can formally regard Eq. (6.16) as the CPHF equation for infinite polymer chains by simply considering that i is a composite index of energy band i and momentum k_i, and likewise for j, a, and b. If we use capital letters I, J, A, and B for these composite indices, we can write the CPHF equation for polymers as

$$(\epsilon_I - \epsilon_A)\, u_{AI}^{(1)} = Q_{AI}^{(1)} + 2 \sum_{B}^{\text{virt.}} \sum_{J}^{\text{occ.}} \{u_{BJ}^{(1)*}\, (AI||BJ) + u_{BJ}^{(1)}\, (AI||JB)\}, \tag{6.18}$$

with

$$Q_{AI}^{(1)} = \mathcal{H}_{AI}^{(1)} + \mathcal{J}_{AI}^{(1)} - \epsilon_I \mathcal{S}_{AI}^{(1)} - 2 \sum_{H,L}^{\text{occ.}} \mathcal{S}_{HL}^{(1)}\, (AI||LH)\,. \tag{6.19}$$

This matrix equation is, however, highly redundant in that the dimension of the matrices can be reduced considerably by making use of the translational invariance of molecular integrals as we will show below.

The matrices $\mathcal{H}^{(1)}$ and $\mathcal{J}^{(1)}$ in Eq. (6.19) are the one- and two-electron part, respectively, of the so-called skeleton (core) first derivative Fock matrix [5] in the crystal orbital basis. The definitions of these matrices are obtained from the molecular counterparts [7] by simple replacements,

$$C_{\mu m} \rightarrow \frac{1}{\sqrt{K}} C_{\mu M} \exp(ik_m pa), \tag{6.20}$$

and so forth. Hereafter the crystal orbital coefficients and one-electron energies for composite indices are understood, respectively, as

$$C_{\mu M} = C_{\mu m}^{[k_m]}, \tag{6.21}$$

$$\epsilon_M = \epsilon_m^{[k_m]}. \tag{6.22}$$

The definition of $\mathcal{H}^{(1)}$ is written as

$$\begin{aligned}\mathcal{H}_{MN}^{(1)} &= \frac{1}{K}\sum_{\mu,\nu}\sum_{p,q} C_{\mu M}^* C_{\nu N} \frac{\partial H_{\mu\nu}^{(q-p)}}{\partial y} \exp\{i(k_n q - k_m p)a\} \\ &= \sum_{\mu,\nu}\sum_{p,q} C_{\mu M}^* C_{\nu N} \frac{\partial H_{\mu\nu}^{(q-p)}}{\partial y} \exp\{ik_n(q-p)a\} \\ &\quad \times \frac{1}{K}\exp\{i(k_n - k_m)pa\}. \end{aligned} \tag{6.23}$$

As indicated by the last line, the summation over p can be carried out separately. Since both k_n and k_m are confined in the first Brillouin zone, the summation $(1/K)\sum_p \exp\{i(k_n - k_m)pa\}$ gives a non-vanishing result only if $k_n = k_m$. Therefore, Eq. (6.23) can be simplified to

$$\mathcal{H}_{MN}^{(1)} = \sum_{\mu,\nu}\sum_{q} C_{\mu M}^* C_{\nu N} \frac{\partial H_{\mu\nu}^{(q)}}{\partial y} \exp(ik_n qa) \qquad (\text{for } k_n = k_m), \tag{6.24}$$

and

$$\mathcal{H}_{MN}^{(1)} = 0 \qquad (\text{for } k_n \neq k_m). \tag{6.25}$$

In a similar way, we can show that $\mathcal{J}^{(1)}$ and $\mathcal{S}^{(1)}$ vanish if $k_n \neq k_m$. Thus, their definitions are given by

$$\mathcal{J}_{MN}^{(1)} = \sum_{\mu,\nu}\sum_{\lambda,\sigma}\sum_{q,r,s} C_{\mu M}^* C_{\nu N} P_{\lambda\sigma}^{(s-r)} \frac{\partial}{\partial y}\left(\mu^{(0)}\nu^{(q)}||\lambda^{(r)}\sigma^{(s)}\right)\exp(ik_n qa), \tag{6.26}$$

and

$$\mathcal{S}_{MN}^{(1)} = \sum_{\mu,\nu}\sum_{q} C_{\mu M}^* C_{\nu N} \frac{\partial S_{\mu\nu}^{(q)}}{\partial y} \exp(ik_n qa), \tag{6.27}$$

for $k_n = k_m$, and

$$\mathcal{J}_{MN}^{(1)} = 0, \tag{6.28}$$

$$\mathcal{S}_{MN}^{(1)} = 0, \tag{6.29}$$

for $k_n \neq k_m$.

Two-electron integrals over crystal orbitals are obtained by the integral transformation of two-electron integrals over atomic orbitals as

$$\begin{aligned}(AI||MN) &= \frac{1}{K^2}\sum_{\mu,\nu,\lambda,\sigma}\sum_{p,q,r,s} C^*_{\mu A}C_{\nu I}C^*_{\lambda M}C_{\sigma N} \\ &\quad \times \exp\{i(-k_a p + k_i q - k_m r + k_n s)a\}\left(\mu^{(p)}\nu^{(q)}||\lambda^{(r)}\sigma^{(s)}\right) \\ &= \frac{1}{K^2}\sum_{p}\exp\{i(-k_a + k_i - k_m + k_n)pa\}\sum_{\mu,\nu,\lambda,\sigma}\sum_{q,r,s} C^*_{\mu A}C_{\nu I}C^*_{\lambda M}C_{\sigma N} \\ &\quad \times \exp[i\{k_i(q-p) - k_m(r-p) + k_n(s-p)\}a] \\ &\quad \times \left(\mu^{(p)}\nu^{(q)}||\lambda^{(r)}\sigma^{(s)}\right). \qquad (6.30)\end{aligned}$$

The summation $\sum_p \exp\{i(-k_a + k_i - k_m + k_n)pa\}$ gives a non-vanishing result only if $(-k_a + k_i - k_m + k_n)a$ is an integral multiple of 2π. Since we confine k points in the first Brillouin zone, there is always one and only one k_a which satisfies this condition for any given k_i, k_m, and k_n [37,38]. For example,

$$\sum_p \exp\{i(-k_a + k_i - k_m + k_n)pa\} = K \qquad (\text{for } k_a = k_i \text{ and } k_m = k_n), \qquad (6.31)$$

and

$$\sum_p \exp\{i(-k_a + k_i - k_m + k_n)pa\} = 0 \qquad (\text{for } k_a \neq k_i \text{ and } k_m = k_n). \qquad (6.32)$$

It follows from Eqs. (6.29) and (6.32) that the summation in Eq. (6.19) vanishes if $k_a \neq k_i$. Remembering that $\mathcal{H}^{(1)}_{AI}$, $\mathcal{J}^{(1)}_{AI}$, and $\mathcal{S}^{(1)}_{AI}$ also vanish if $k_a \neq k_i$, we can show that

$$Q^{(1)}_{AI} = 0 \quad \text{and} \quad u^{(1)}_{AI} = 0 \qquad (\text{for } k_a \neq k_i). \qquad (6.33)$$

This is expected since the perfect translational symmetry is retained if the nuclei move along the normal coordinates of $k = 0$ vibrations, and hence the Fock and overlap matrix elements between crystal orbitals with different k's remain always zero. However, this does not imply that the CPHF equation for an infinite polymer chain can be solved separately for each k. The two-electron integrals $(AI||BJ)$ and $(AI||JB)$ in Eq. (6.18) survive if $k_a = k_i$ and $k_b = k_j$, and hence $u^{(1)}_{BJ}$ with momentum k_b can influence $u^{(1)}_{AI}$ with momentum k_a (which may differ from k_b) through two-electron integrals.

It follows from these considerations that the two-electron integrals required in the CPHF equation are only of the type

$$\begin{aligned}\left(a^{[k_1]}i^{[k_1]}||m^{[k_2]}n^{[k_2]}\right) &= \frac{1}{K}\sum_{\mu,\nu,\lambda,\sigma}\sum_{q,r,s} C^{[k_1]*}_{\mu a}C^{[k_1]}_{\nu i}C^{[k_2]*}_{\lambda m}C^{[k_2]}_{\sigma n} \\ &\quad \times \exp\{i(k_1 q - k_2 r + k_2 s)a\}\left(\mu^{(0)}\nu^{(q)}||\lambda^{(r)}\sigma^{(s)}\right), \qquad (6.34)\end{aligned}$$

where we explicitly specify the energy band (a,i,m,n) and momentum (k_1,k_2) indices instead of using the composite indices (A,I,M,N). Thus, the dimension of the two-electron integrals is reduced by a factor of K^2 on going from Eq. (6.18) to Eq. (6.34). The lengths of $u_{AI}^{(1)}$ and $Q_{AI}^{(1)}$ vectors are likewise reduced from $V \times O \times K^2$ to $V \times O \times K$. We may rewrite the CPHF equation for polymers in a more useful form as

$$\begin{aligned}\left(\epsilon_i^{[k_1]} - \epsilon_a^{[k_1]}\right) u_{ai}^{(1)[k_1]} &= Q_{ai}^{(1)[k_1]} + 2\sum_{b}^{\text{virt.}}\sum_{j}^{\text{occ.}}\sum_{k_2}^{\text{BZ}}\left\{u_{bj}^{(1)[k_2]*}\left(a^{[k_1]}{}_i{}^{[k_1]}||b^{[k_2]}{}_j{}^{[k_2]}\right)\right. \\ &\left. + u_{bj}^{(1)[k_2]}\left(a^{[k_1]}{}_i{}^{[k_1]}||j^{[k_2]}{}_b{}^{[k_2]}\right)\right\}, \end{aligned} \tag{6.35}$$

with

$$\begin{aligned} Q_{ai}^{(1)[k_1]} &= \mathcal{H}_{ai}^{(1)[k_1]} + \mathcal{J}_{ai}^{(1)[k_1]} - \epsilon_i^{[k_1]}\mathcal{S}_{ai}^{(1)[k_1]} \\ &\quad -2\sum_{h,l}^{\text{occ.}}\sum_{k_2}^{\text{BZ}}\mathcal{S}_{hl}^{(1)[k_2]}\left(a^{[k_1]}{}_i{}^{[k_1]}||l^{[k_2]}{}_h{}^{[k_2]}\right). \end{aligned} \tag{6.36}$$

Now the definitions of the skeleton (core) derivative matrices are

$$\mathcal{H}_{mn}^{(1)[k]} = \sum_{\mu,\nu}\sum_{q} C_{\mu m}^{[k]*} C_{\nu n}^{[k]} \frac{\partial H_{\mu\nu}^{(q)}}{\partial y} \exp(ikqa), \tag{6.37}$$

and

$$\begin{aligned} \mathcal{J}_{mn}^{(1)[k]} &= \sum_{\mu,\nu}\sum_{\lambda,\sigma}\sum_{q,r,s} C_{\mu m}^{[k]*} C_{\nu n}^{[k]} P_{\lambda\sigma}^{(s-r)} \\ &\quad \times \frac{\partial}{\partial y}\left(\mu^{(0)}\nu^{(q)}||\lambda^{(r)}\sigma^{(s)}\right)\exp(ikqa), \end{aligned} \tag{6.38}$$

and

$$\mathcal{S}_{mn}^{(1)[k]} = \sum_{\mu,\nu}\sum_{q} C_{\mu m}^{[k]*} C_{\nu n}^{[k]} \frac{\partial S_{\mu\nu}^{(q)}}{\partial y} \exp(ikqa). \tag{6.39}$$

Once Eq. (6.35) is solved to find $u_{ai}^{(1)[k_1]}$ vector, the derivatives of density matrix can be obtained with the aid of the expression

$$\begin{aligned} \frac{\partial P_{\mu\nu}^{(q)}}{\partial y} &= -\frac{2}{K}\sum_{i}^{\text{occ.}}\sum_{j}^{\text{occ.}}\sum_{k}^{\text{BZ}}\mathcal{S}_{ij}^{(1)[k]} C_{\mu j}^{[k]*} C_{\nu i}^{[k]} \exp(ikqa) \\ &\quad +\frac{2}{K}\sum_{i}^{\text{occ.}}\sum_{a}^{\text{virt.}}\sum_{k}^{\text{BZ}}\left(u_{ai}^{(1)[k]*} C_{\mu a}^{[k]*} C_{\nu i}^{[k]} + u_{ai}^{(1)[k]} C_{\mu i}^{[k]*} C_{\nu a}^{[k]}\right)\exp(ikqa). \end{aligned} \tag{6.40}$$

This expression is obtained by straightforward generalization of the molecular counterpart [7], and hence we do not describe its derivation here. The expression for the derivatives

of energy-weighted density matrix can be obtained by similar generalization as

$$\frac{\partial W_{\mu\nu}^{(q)}}{\partial y} = \frac{2}{K}\sum_{i}^{\text{occ.}}\sum_{j}^{\text{occ.}}\sum_{k}^{\text{BZ}}\left\{\mathcal{F}_{ij}^{(1)[k]} - \left(\epsilon_i^{[k]} + \epsilon_j^{[k]}\right)\mathcal{S}_{ij}^{(1)[k]}\right\} C_{\mu j}^{[k]*} C_{\nu i}^{[k]} \exp(ikqa)$$
$$+\frac{2}{K}\sum_{i}^{\text{occ.}}\sum_{a}^{\text{virt.}}\sum_{k}^{\text{BZ}}\epsilon_i^{[k]}\left(u_{ai}^{(1)[k]*} C_{\mu a}^{[k]*} C_{\nu i}^{[k]} + u_{ai}^{(1)[k]} C_{\mu i}^{[k]*} C_{\nu a}^{[k]}\right)\exp(ikqa), \quad (6.41)$$

with

$$\mathcal{F}_{ij}^{(1)[k_1]} = \mathcal{H}_{ij}^{(1)[k_1]} + \mathcal{J}_{ij}^{(1)[k_1]} - 2\sum_{h,l}^{\text{occ.}}\sum_{k_2}^{\text{BZ}}\mathcal{S}_{hl}^{(1)[k_2]}\left(i^{[k_1]}j^{[k_1]}||l^{[k_2]}h^{[k_2]}\right)$$
$$+2\sum_{a}^{\text{virt.}}\sum_{l}^{\text{occ.}}\sum_{k_2}^{\text{BZ}}\left\{u_{al}^{(1)[k_2]*}\left(i^{[k_1]}j^{[k_1]}||a^{[k_2]}l^{[k_2]}\right)\right.$$
$$\left.+\, u_{al}^{(1)[k_2]}\left(i^{[k_1]}j^{[k_1]}||l^{[k_2]}a^{[k_2]}\right)\right\}. \quad (6.42)$$

For infinitely long polymers, there is an extra in-phase nuclear coordinate arising from the periodic boundary conditions, namely, the translational period a. The first derivative of energy with respect to the translational period plays an important role in the geometry optimization of polymers [21–23]. In this chapter, we do not deal with the analytical second derivatives involving this degree of freedom, because they are not required in the vibrational analyses of polymers. They may, however, be useful as elements of the Hessian matrix in the geometry optimization or in analyzing the experimental data such as longitudinal elastic moduli [39,40].

6.3 Computer implementation

The straightforward implementation of the analytical second derivative formulas described in the previous section will lead to the crystal-orbital-based algorithm, which involves the transformation of two-electron integrals from the atomic-orbital basis to the crystal-orbital basis. The transformation requires storage for two-electron integrals over atomic orbitals as well as those over crystal orbitals. Because the number of two-electron integrals easily exceeds several gigabytes even if we deal with a polymer with a relatively small unit cell and a modest basis set, it is particularly important in ab initio crystal orbital theory to use the direct algorithm [41] and avoid the use of external storage and I/O operation involving two-electron integrals completely.

As in the direct atomic-orbital-based analytical-second-derivative method for mole-

cules [8,10], the summation of the form

$$Z_{ai}^{[k_1]} = \sum_m \sum_n \sum_{k_2}^{\mathrm{BZ}} X_{mn}^{(1)[k_2]} \left(a^{[k_1]} i^{[k_1]} || m^{[k_2]} n^{[k_2]} \right) \tag{6.43}$$

appearing in Eqs. (6.35), (6.36), and (6.42) can be accomplished by using two-electron integrals over atomic orbitals. In the above equation, $X_{mn}^{(1)[k]}$ denotes either $u_{mn}^{(1)[k]}$ in Eqs. (6.35) and (6.42) or $S_{mn}^{(1)[k]}$ in Eqs. (6.36) and (6.42). Using Eq. (6.34), we can rewrite this equation with two-electron integrals over atomic orbitals as

$$\begin{aligned} Z_{ai}^{[k_1]} &= \frac{1}{K} \sum_m \sum_n \sum_{k_2}^{\mathrm{BZ}} \sum_{\mu,\nu,\lambda,\sigma} \sum_{q,r,s} X_{mn}^{(1)[k_2]} C_{\mu a}^{[k_1]*} C_{\nu i}^{[k_1]} C_{\lambda m}^{[k_2]*} C_{\sigma n}^{[k_2]} \\ &\quad \times \exp\{i(k_1 q - k_2 r + k_2 s)a\} \left(\mu^{(0)} \nu^{(q)} || \lambda^{(r)} \sigma^{(s)} \right). \end{aligned} \tag{6.44}$$

At first sight, this summation appears to be hopeless, but it can be carried out in three separate steps, namely,

$$Z_{ai}^{[k_1]} = \sum_{\mu,\nu} \sum_q C_{\mu a}^{[k_1]*} C_{\nu i}^{[k_1]} Y_{\mu\nu}^{(q)} \exp(i k_1 q a), \tag{6.45}$$

and

$$Y_{\mu\nu}^{(q)} = \sum_{\lambda,\sigma} \sum_{r,s} V_{\lambda\sigma}^{(s-r)} \left(\mu^{(0)} \nu^{(q)} || \lambda^{(r)} \sigma^{(s)} \right), \tag{6.46}$$

and

$$V_{\lambda\sigma}^{(s-r)} = \frac{1}{K} \sum_m \sum_n \sum_{k_2}^{\mathrm{BZ}} X_{mn}^{(1)[k_2]} C_{\lambda m}^{[k_2]*} C_{\sigma n}^{[k_2]} \exp\{i k_2 (s-r) a\}. \tag{6.47}$$

Likewise the summation in Eq. (6.38) is decomposed into two separate steps in actual calculations.

The CPHF equation is solved in an iterative manner using a set of trial vectors $\{t_{ai(1)}^{[k_1]}, t_{ai(2)}^{[k_1]}, \cdots, t_{ai(n)}^{[k_1]}\}$ [7]. The initial trial vector is given by

$$t_{ai(1)}^{[k_1]} = \frac{Q_{ai}^{(1)[k_1]}}{\epsilon_i^{[k_1]} - \epsilon_a^{[k_1]}}, \tag{6.48}$$

and other vectors are generated consecutively by

$$\begin{aligned} t_{ai(n+1)}^{[k_1]} &= \frac{2}{\epsilon_i^{[k_1]} - \epsilon_a^{[k_1]}} \sum_b^{\mathrm{virt.}} \sum_j^{\mathrm{occ.}} \sum_{k_2}^{\mathrm{BZ}} \left\{ t_{bj(n)}^{[k_2]*} \left(a^{[k_1]} i^{[k_1]} || b^{[k_2]} j^{[k_2]} \right) \right. \\ &\quad \left. + t_{bj(n)}^{[k_2]} \left(a^{[k_1]} i^{[k_1]} || j^{[k_2]} b^{[k_2]} \right) \right\}. \end{aligned} \tag{6.49}$$

The number of the trial vectors is increased stepwise until a solution vector obtained by a linear combination of the trial vectors satisfies the CPHF equation within a predefined error:

$$u_{ai}^{(1)[k_1]} = c_1 t_{ai(1)}^{[k_1]} + c_2 t_{ai(2)}^{[k_1]} + \cdots + c_n t_{ai(n)}^{[k_1]}. \tag{6.50}$$

The coefficients $c_1, c_2, \cdots, c_n$ are determined by the direct inversion in the iterative subspace (DIIS) method [7,42], such that the norm of the residuum vector in the CPHF equation [left-hand side minus right-hand side of Eq. (6.35)] becomes the smallest. The summation in Eq. (6.49) is carried out by the direct algorithm just described, and hence two-electron integrals over atomic orbitals are repeatedly evaluated every time a new trial vector is generated.

We employed the standard STO-3G [43], 3-21G [44], and 6-31G(d) [45,46] basis sets as atomic orbitals. Geometry optimization was performed for polyethylene in the Cartesian coordinate basis with the aid of the analytical energy gradients. In the geometry optimization processes, we adopted a CH_2 unit as a reference unit cell and took into account the screw-axis symmetry of the system. One- and two-electron integrals over atomic orbitals were evaluated by using the sixth neighbor approximation for the STO-3G calculations and the twelfth neighbor approximation for the 3-21G and 6-31G(d) calculations. The Nth neighbor approximation means that we consider the basis functions in N unit cells at each side of the central (reference) unit cell. We employed the Namur cutoff procedure [47,48] without long-range correction. Teramae demonstrated that the Namur cutoff criterion gave the fastest convergence in the total energy of polyethylene calculated at the HF/STO-3G level [49]. The criterion for the convergence of density matrix in the SCF iteration was set to 10^{-8}. Two-electron integrals were calculated repeatedly in every self-consistent-field (SCF) iteration. At the optimized geometry, the largest absolute value of the energy gradient was less than 3×10^{-5} hartree/bohr.

In the vibrational analyses of polyethylene, we took a C_2H_4 unit, which is the smallest translational repeat unit, as a reference unit cell. The force constants were evaluated by the analytical-second-derivative method. At the HF/STO-3G level, force constants were obtained by the finite-difference method as well. The step size used in the numerical differentiation of the analytical first derivatives was set to 0.04 bohr (nuclei are displaced from the equilibrium positions by ± 0.02 bohr in the x, y, and z directions). The lattice summations were taken up to the sixth and eighth neighboring C_2H_4 units for the 3-21G and 6-31G(d) calculations, respectively. For the STO-3G calculations, we examined the dependence of the frequencies on the number of neighboring C_2H_4 units (N) included in the lattice summations, on the number of momentum sampling points (K) in the first Brillouin zone, and on the convergence criterion (10^{-C}) for the CPHF solutions. For the 3-21G and 6-31G(d) calculations, K and C were set to 20 and 9, respectively. The momentum

sampling points were evenly spaced, and we counted only one of the two sampling points at the Brillouin zone boundaries ($k = \pm\pi/a$). This definition of K exactly matches the formulas given in the previous section. It should be noted that K must be larger than $2N$ to obtain correct total energies [49].

6.4 Illustrative calculations

6.4.1 Optimized structures of polyethylene

As is well recognized, it is important to obtain fully optimized structural parameters before carrying out the vibrational frequency calculations. The optimized structural parameters of polyethylene are listed in Table 6.1 along with the experimental data obtained by X-ray diffraction studies [50–53].

At the HF/STO-3G level, several groups have already reported the structural parameters of polyethylene obtained by using the crystal orbital method [21,39] or the oligomer (cluster) method [54]. Karpfen optimized the structural parameters by computing total energies at 41 different structures by the crystal orbital method and fitting the thus-obtained potential energy surface with a polynomial [39]. The structural parameters of Karpfen are generally in good agreement with those estimated from the calculations of n-C_7H_{16} molecule by Crist *et al.* [54], although there can be seen a slight difference in the CC bond length. Teramae *et al.* implemented the analytical gradients in ab initio HF crystal orbital theory and optimized the structural parameters of polyethylene with them [21]. The structural parameters of Teramae *et al.* are, however, significantly different from those of Karpfen and of Crist *et al.*

We repeated the geometry optimization at the HF/STO-3G level by using both the crystal orbital method and the oligomer method. The optimization by the crystal orbital method was carried out with the aid of the analytical gradients starting from the geometry of Karpfen. The geometry optimization of oligomers (n-$C_{15}H_{32}$ and n-$C_{16}H_{34}$) were performed with the GAUSSIAN 94 program [55]. The structural parameters near the center of n-$C_{16}H_{34}$ are converged at least to first six significant figures with the chain length of oligomers and with the position of the structural parameters. As can be seen in Table 6.1, the structural parameters obtained by the crystal orbital method and by the oligomer method are in agreement with each other to first four significant figures, and hence the structural parameters obtained in this study are considered to be reliable. The CC bond

Table 6.1 Structural parameters of all-*trans* polyethylene. Bond lengths in Å and bond angles in degree.

	CC bond length	CH bond length	CCC angle	HCH angle
		HF/STO-3G		
This work[a]	1.545	1.088	112.4	107.1
This work[b]	1.545	1.088	112.4	107.1
Reference [21] [a]	1.565	1.102	115.3	104.7
Reference [39] [a]	1.547	1.089	112.6	107.0
Reference [54] [b]	1.543	1.089	112.4	107.1
		HF/3-21G		
This work[a]	1.541	1.087	112.5	107.2
		HF/6-31G(d)		
This work[a]	1.530	1.089	113.3	106.2
		Experiments		
Reference [50]	1.53		112	
Reference [51]	1.534 ± 0.006		112.0 ± 0.4	
Reference [52]	1.533 ± 0.022	1.07 ± 0.022	111.9 ± 1.8	107 ± 1.8
Reference [53]	1.527 ± 0.007		112 ± 0.8	

[a] Crystal orbital calculations. [b] Oligomer (cluster) calculations.

lengths calculated in this study are between the values obtained by Karpfen and by Crist *et al.*

The basis-set dependence of the structural parameters obtained at the HF level is parallel to that found in our previous density functional results [24]: the CC bond length and the CCC angle increase and the HCH angle decreases on going from the 3-21G basis set to the 6-31G(d) basis set. The optimized structural parameters obtained at the HF/6-31G(d) level are in good agreement with the experimental results except that the calculated CCC angle is slightly larger than the experimental values. Vibrational frequency calculations of polyethylene discussed below are based on the optimized structural parameters obtained by the crystal orbital method in this study.

6.4.2 Frequencies of $k = 0$ vibrations of polyethylene

The convergence behavior of $k = 0$ frequencies with the number of neighboring C_2H_4 units (N) is shown in Table 6.2. The frequencies are calculated at the HF/STO-3G level by using the second-derivative method. The values of K and C indicated in the table are sufficiently large, and the frequencies are practically converged with these parameters (see below). The frequencies obtained with $N = 1$ are not converged, but the differences between them and those obtained with $N = 3$ are less than 5 cm^{-1}. The frequencies calculated with $N = 2$ are already in agreement with those obtained with $N = 3$ within 1 cm^{-1}, and they can be regarded as being converged. The total energies of polyethylene

Table 6.2 Dependence of the $k = 0$ frequencies of all-*trans* polyethylene on the number of neighbors (N) included in the lattice summations. Frequencies calculated at the HF/STO-3G level in units of cm^{-1}.

Mode[a]		Finite-difference method	Second-derivative method ($K = 8, C = 9$)[b]		
			$N = 1$	$N = 2$	$N = 3$
a_g	$\nu_1(0)$	3601	3601	3601	3601
	$\nu_2(0)$	1826	1826	1827	1827
	$\nu_4(0)$	1342	1341	1342	1342
b_{1g}	$\nu_3(\pi)$	1766	1771	1766	1766
	$\nu_4(\pi)$	1261	1264	1261	1261
b_{2g}	$\nu_7(\pi)$	1566	1566	1565	1565
b_{3g}	$\nu_6(0)$	3708	3708	3708	3708
	$\nu_7(0)$	1435	1436	1436	1436
a_u	$\nu_8(0)$	1277	1276	1277	1277
b_{1u}	$\nu_6(\pi)$	3732	3732	3732	3732
	$\nu_8(\pi)$	833	832	834	834
b_{2u}	$\nu_1(\pi)$	3607	3604	3606	3607
	$\nu_2(\pi)$	1855	1855	1855	1855
b_{3u}	$\nu_3(0)$	1437	1440	1438	1437

[a] The normal vibrations are classified under the factor group isomorphous to the point group D_{2h}. For the labeling of the normal vibrations, see Ref. [24]. [b] N and K represent the number of neighbors (C_2H_4 units) included in the lattice summations and the number of momentum sampling points in the first Brillouin zone, respectively. The convergence criterion for the CPHF solutions is set to 10^{-C}.

calculated with $N = 1$, 2, and 3 are -77.15798, -77.16042, and -77.16041 hartree per C_2H_4 unit, respectively. It should be noted that the total energy calculated with $N = 1$ is accurate to only two decimal places in hartree. Thus, the N-dependence of the frequencies is much smaller than that of the total energy.

Teramae also examined the N-dependence of $k = 0$ frequencies of all-*trans* polyacetylene at the HF/STO-3G level by using the finite-difference method [49]; if the Namur cutoff was employed, the frequencies of polyacetylene converged within 1 cm^{-1} at $N = 3$, but there could be seen considerable differences (12 cm^{-1} at maximum) between $N = 2$ and $N = 3$. Therefore, the convergence of the frequencies is slightly faster for polyethylene than for polyacetylene. This is probably due to the π-conjugation in polyacetylene, which renders the force constants considerably long-range.

In Table 6.2, $k = 0$ frequencies of polyethylene calculated by the finite-difference method are also given. They are in good agreement with those obtained by the second-derivative method (with $N = 3$) with the largest deviation being less than 1 cm^{-1}. Therefore, the numerical accuracy of the finite-difference method used in our previous calculations [23,24] is no less high than that of the second-derivative method.

The dependence of the frequencies on the number of momentum sampling points (K) is shown in Table 6.3. It is seen immediately that the frequencies of polyethylene at

Table 6.3 Dependence of the $k = 0$ frequencies of all-*trans* polyethylene on the number of momentum sampling points (K) in the first Brillouin zone. Frequencies calculated at the HF/STO-3G level in units of cm^{-1}.

Mode[a]		Second-derivative method ($N = 3, C = 9$)[b]		
		$K = 8$	$K = 12$	$K = 20$
a_g	$\nu_1(0)$	3601	3601	3601
	$\nu_2(0)$	1827	1827	1827
	$\nu_4(0)$	1342	1342	1342
b_{1g}	$\nu_3(\pi)$	1766	1766	1766
	$\nu_4(\pi)$	1261	1261	1261
b_{2g}	$\nu_7(\pi)$	1565	1565	1565
b_{3g}	$\nu_6(0)$	3708	3708	3708
	$\nu_7(0)$	1436	1436	1436
a_u	$\nu_8(0)$	1277	1277	1277
b_{1u}	$\nu_6(\pi)$	3732	3732	3732
	$\nu_8(\pi)$	834	834	834
b_{2u}	$\nu_1(\pi)$	3607	3607	3607
	$\nu_2(\pi)$	1855	1855	1855
b_{3u}	$\nu_3(0)$	1437	1437	1437

[a,b] See the corresponding footnotes of Table 6.2.

the HF/STO-3G level are already converged at $K = 8$. The K-dependence of the total energy is also negligibly small as long as K is larger than $2N$; the total energy calculated with $K = 8$ is accurate to 5 decimal places in hartree. Thus, it is normally adequate to take K which is only slightly larger than $2N$, in order to obtain the converged results for the frequencies and total energies of polymers. It should be noted, however, that there are cases where the equilibrium structures (and hence the vibrational frequencies also) of polymers are strongly dependent on K and a small K leads to numerically incorrect results. For example, it was demonstrated that the bond alternation in all-*trans* polyacetylene was dependent on K if some kinds of density functionals were used [56–58]. These density functionals tended to predict unrealistically small band gaps, and it was necessary to take a large number of momentum sampling points in the vicinity of the band gap in order to calculate correctly the magnitude of the bond alternation, which was strongly coupled to the band gap.

Table 6.4 gives the dependence of the frequencies on the convergence criterion of the CPHF solutions. The frequencies calculated with $C = 6$ and $C = 9$ are the same within 1 cm^{-1}. The differences between frequencies calculated with $C = 3$ and $C = 6$ are not negligible with the largest deviation being 12 cm^{-1}. Thus, it is sufficient to take $C = 6$ in the frequency calculations. The number of trial vectors required to obtain the convergence of 10^{-C} for the CPHF solutions is roughly proportional to C. For example, the number

Table 6.4 Dependence of the $k = 0$ frequencies of all-*trans* polyethylene on the convergence criterion (10^{-C}) for the CPHF solutions. Frequencies calculated at the HF/STO-3G level in units of cm^{-1}.

Mode[a]		Second-derivative method ($N = 3, K = 8$)[b]		
		$C = 3$	$C = 6$	$C = 9$
a_g	$\nu_1(0)$	3599	3601	3601
	$\nu_2(0)$	1826	1827	1827
	$\nu_4(0)$	1342	1342	1342
b_{1g}	$\nu_3(\pi)$	1765	1766	1766
	$\nu_4(\pi)$	1261	1261	1261
b_{2g}	$\nu_7(\pi)$	1565	1565	1565
b_{3g}	$\nu_6(0)$	3707	3708	3708
	$\nu_7(0)$	1436	1436	1436
a_u	$\nu_8(0)$	1277	1277	1277
b_{1u}	$\nu_6(\pi)$	3732	3732	3732
	$\nu_8(\pi)$	846	834	834
b_{2u}	$\nu_1(\pi)$	3607	3607	3607
	$\nu_2(\pi)$	1854	1855	1855
b_{3u}	$\nu_3(0)$	1439	1437	1437

[a,b] See the corresponding footnotes of Table 6.2.

of trial vectors is 2, 5, and 8 for $C = 3$, 6, and 9, respectively, for the calculations on polyethylene at the HF/STO-3G level. Since in the direct algorithm, two-electron integrals are repeatedly evaluated as the trial vectors are added to Eq. (6.50), the time required to solve the CPHF equation increases linearly with increasing C.

The frequencies of $k = 0$ vibrations calculated with the STO-3G, 3-21G, and 6-31G(d) basis sets are compared with the experimental data [59–63] in Table 6.5. The calculated frequencies are scaled uniformly by a single scale factor for each basis set. The scale factors, which are given in the table, are determined by a least-squares fitting procedure, such that the root-mean-square errors between the scaled and observed frequencies become the smallest.

It can be seen that the unscaled frequencies are larger by 10 to 30 % than the observed ones regardless of the basis set used. Uniform scaling of the calculated frequencies significantly improves the agreement between the calculated and observed frequencies, and the root-mean-square errors between the scaled and observed frequencies are 37, 33, and 23 cm^{-1} for the STO-3G, 3-21G, and 6-31G(d) calculations, respectively. The use of larger basis sets systematically improves the agreement between the calculated and observed frequencies. In fact, the scaled frequencies obtained with the 6-31G(d) basis set are in reasonably good agreement with the observed frequencies. It was also found in our previous density functional results [24] that the basis-set dependence of the calculated frequencies of polyethylene was larger than the dependence on density functionals.

Table 6.5 Basis-set dependence of the $k = 0$ frequencies of all-*trans* polyethylene calculated at the HF level. Frequencies in units of cm^{-1}.

Mode[a]		Obs.[b]	STO-3G		3-21G		6-31G(d)	
			Unscaled	×0.7952	Unscaled	×0.8991	Unscaled	×0.8995
			normal species					
a_g	$\nu_1(0)$	2848	3601	2864	3189	2867	3186	2866
	$\nu_2(0)$	1440	1827	1453	1657	1490	1638	1473
	$\nu_4(0)$	1131	1342	1067	1207	1085	1236	1112
b_{1g}	$\nu_3(\pi)$	1370	1766	1404	1510	1358	1571	1413
	$\nu_4(\pi)$	1061	1261	1003	1098	987	1138	1024
b_{2g}	$\nu_7(\pi)$	1295	1565	1244	1459	1312	1444	1299
b_{3g}	$\nu_6(0)$	2883	3708	2948	3200	2877	3193	2872
	$\nu_7(0)$	1168	1436	1142	1314	1181	1318	1186
a_u	$\nu_8(0)$	1050	1277	1015	1205	1083	1162	1045
b_{1u}	$\nu_6(\pi)$	2919	3732	2968	3257	2928	3246	2920
	$\nu_8(\pi)$	725	834	663	789	709	781	703
b_{2u}	$\nu_1(\pi)$	2851	3607	2868	3201	2878	3194	2873
	$\nu_2(\pi)$	1468	1855	1475	1676	1507	1661	1494
b_{3u}	$\nu_3(0)$	1176	1437	1143	1350	1214	1314	1182
			perdeuterated species					
a_g	$\nu_1(0)$	2103	2644	2102	2323	2089	2329	2095
	$\nu_2(0)$	1148	1425	1133	1262	1135	1284	1155
	$\nu_3(0)$	975	1172	932	1089	979	1080	972
b_{1g}	$\nu_2(\pi)$	1253	1620	1288	1310	1178	1417	1275
	$\nu_4(\pi)$	831	972	773	896	806	893	803
b_{2g}	$\nu_7(\pi)$	917	1107	880	1032	928	1021	918
b_{3g}	$\nu_6(0)$	2199	2765	2199	2377	2137	2372	2134
	$\nu_7(0)$	993	1232	980	1133	1019	1138	1024
a_u	$\nu_8(0)$	748	903	718	852	766	822	739
b_{1u}	$\nu_6(\pi)$	2195	2767	2200	2413	2170	2404	2163
	$\nu_8(\pi)$	525	602	479	570	513	564	507
b_{2u}	$\nu_1(\pi)$	2089	2623	2086	2323	2089	2321	2088
	$\nu_3(\pi)$	1091	1365	1085	1235	1110	1223	1100
b_{3u}	$\nu_4(0)$	892	1087	864	1022	919	994	894
root-mean-square error			424	37	187	33	185	23

[a] See the corresponding footnote of Table 6.2. [b] Taken from Refs. [59–63].

Table 6.6 Execution times (CPU + I/O times in seconds) for all-*trans* polyethylene at the HF/STO-3G level ($N = 3$, $K = 8$, $C = 6$). All the calculations were performed on an HP Exemplar workstation of our laboratory. The compile options were "+DS2.0a +DA2.0N +O3 +Onolimit +Odataprefetch".

Step	first derivatives	Second derivatives[a]	
		conventional[b]	direct[c]
SCF	3032	287	3032
First derivatives of two-electron integrals	2864	...	...
Two-electron integral transformation	...	839	...
First and second derivatives of two-electron integrals	...	23791	24032
CPHF	...	210	3587
total[d]	5908	25288	31341

[a] Only the symmetrically distinct force constants were calculated. [b] Crystal-orbital-based algorithm involving the transformation of two-electron integrals. [c] Atomic-orbital-based algorithm in which two-electron integrals are recomputed in every SCF and CPHF iteration. [d] Total execution times include small steps which have not been tabulated separately.

6.4.3 Comparison of the execution times

The execution times (the sum of the CPU and I/O times) for the various steps of first and second derivative calculations on polyethylene at the HF/STO-3G level are given in Table 6.6. The second derivative calculations were carried out using both the direct atomic-orbital-based algorithm and the conventional crystal-orbital-based algorithm, which involves the integral transformation.

It is sufficient to calculate the symmetrically distinct force constants to obtain all the $k = 0$ frequencies. Those force constants are obtained by a single calculation using the second-derivative method with the total times given in the table. If the finite-difference method is used, it is necessary to carry out first derivative calculations at 11 different structures to obtain all the symmetrically distinct force constants. Therefore, the total time required to obtain all the $k = 0$ frequencies by the finite-different method is about 65000 ($\approx 11 \times 5908$) seconds, which is about twice as long as the times required in the second-derivative method. This result indicates that the vibrational frequency calculations using the second-derivative method are efficient and practical for polymers, as has already been proved for molecules [7,10].

The second derivative calculation using the direct algorithm is only 1.3 times as costly as that using the conventional algorithm. We are currently using old algorithms for integral evaluation, and more than 80 % of the total execution times of the second derivative calculations are consumed by the step of the integral second derivative evaluation. If

efficient algorithms for integral evaluation are used, the CPHF step will become relatively more important and the ratio of the cost of the calculation using the direct algorithm to that using the conventional algorithm may become slightly larger [10]. Nevertheless, because of the intensive use of the external storage in the conventional algorithm, there seems to be no advantage in using the conventional algorithm instead of using the direct algorithm for the vibrational frequency calculations of polymers.

6.5 Conclusion

We have developed the analytical-second-derivative scheme for ab initio HF crystal orbital theory of polymers. We have found that the frequencies of $k = 0$ vibrations of polyethylene calculated by using this scheme converge fast with the number of neighbors included in the lattice summations and with the number of momentum sampling points. We can safely expect that the frequencies are practically converged if we take sufficiently large values for these parameters that the total energies converge to 5 decimal places in hartree. It has also been found adequate to take 10^{-6} as the convergence criterion for the CPHF solutions. Comparison of the total execution times has indicated that the second-derivative method is more efficient than the finite-difference method for the vibrational frequency calculations of polymers.

References

[1] G. Fogarasi and P. Pulay, Ann. Rev. Phys. Chem., **35,** 191 (1984).

[2] R. D. Amos, in *Ab Initio Methods in Quantum Chemistry I,* edited by K. P. Lawley (Wiley, New York, 1987), p.99.

[3] P. Pulay, in *Ab Initio Methods in Quantum Chemistry II,* edited by K. P. Lawley (Wiley, New York, 1987), p.241.

[4] J. Gauss and D. Cremer, Adv. Quantum Chem., **23,** 205 (1992).

[5] Y. Yamaguchi, Y. Osamura, J. D. Goddard, and H. F. Schaefer III, *A New Dimension to Quantum Chemistry: Analytic Derivative Methods in Ab Initio Molecular Electronic Structure Theory,* (Oxford University Press, New York, 1994).

[6] J. Gerratt and I. M. Mills, J. Chem. Phys., **49,** 1719 (1968); **49,** 1730 (1968).

[7] J. A. Pople, R. Krishnan, H. B. Schlegel, and J. S. Binkley, Int. J. Quantum Chem. Quantum Chem. Symp., **13,** 225 (1979).

[8] Y. Osamura, Y. Yamaguchi, and H. F. Schaefer III, J. Chem. Phys., **77,** 383 (1982).

[9] C. E. Dykstra and P. G. Jasien, Chem. Phys. Lett., **109,** 388 (1984).

[10] M. Frisch, M. Head-Gordon, and J. Pople, Chem. Phys., **141,** 189 (1990).

[11] C. Ochsenfeld and M. Head-Gordon, Chem. Phys. Lett., **270,** 399 (1997).

[12] M. Dupuis, J. Rys, and H. F. King, J. Chem. Phys., **65,** 111 (1976).

[13] H. F. King and M. Dupuis, J. Comput. Phys., **21,** 144 (1976).

[14] L. E. McMurchie and E. R. Davidson, J. Comput. Phys., **26,** 218 (1978).

[15] J. A. Pople and W. J. Hehre, J. Comput. Phys., **27,** 161 (1978).

[16] H. B. Schlegel, J. S. Binkley, and J. A. Pople, J. Chem. Phys., **80,** 1976 (1984).

[17] S. Obara and A. Saika, J. Chem. Phys., **84,** 3963 (1986).

[18] M. Head-Gordon and J. A. Pople, J. Chem. Phys., **89,** 5777 (1988).

[19] P. M. W. Gill, M. Head-Gordon, and J. A. Pople, J. Phys. Chem., **94,** 5564 (1990).

[20] P. M. W. Gill, Adv. Quantum Chem., **25,** 141 (1994).

[21] H. Teramae, T. Yamabe, C. Satoko, and A. Imamura, Chem. Phys. Lett., **101,** 149 (1983).

[22] H. Teramae, T. Yamabe, A. Imamura, J. Chem. Phys., **81,** 3564 (1984).

[23] Chapter 3 of the present thesis.

[24] Chapter 4 of the present thesis.

[25] T. Kitagawa and T. Miyazawa, in *Advances in Polymer Science,* (Springer-Verlag, Berlin, 1972), Vol. 9, p.335.

[26] J. Barnes and B. Fanconi, J. Phys. Chem. Ref. Data, **7,** 1309 (1978).

[27] D. I. Bower and W. F. Maddams, *The Vibrational Spectroscopy of Polymers,* (Cambridge University Press, Cambridge, 1989).

[28] A. Karpfen, J. Phys. C, **12,** 3227 (1979).

[29] A. Beyer and A. Karpfen, Chem. Phys., **64,** 343 (1982).

[30] A. Karpfen, Chem. Phys., **79,** 211 (1983).

[31] M. Kofranek, H. Lischka, and A. Karpfen, J. Chem. Phys., **96,** 982 (1992).

[32] J.-Q. Sun and R. J. Bartlett, J. Chem. Phys., **108,** 301 (1998).

[33] G. Del Re, J. Ladik, and G. Biczó, Phys. Rev., **155,** 997 (1967).

[34] J. M. André, J. Chem. Phys., **50,** 1536 (1969).

[35] M. Kertész, Adv. Quantum Chem., **15,** 161 (1982).

[36] J. J. Ladik, *Quantum Theory of Polymers as Solids,* (Plenum, New York, 1988).

[37] S. Suhai, Chem. Phys. Lett., **96,** 619 (1983); Phys. Rev. B, **27,** 3506 (1983).

[38] J.-Q. Sun and R. J. Bartlett, J. Chem. Phys., **104,** 8553 (1996).

[39] A. Karpfen, J. Chem. Phys., **75,** 238 (1981).

[40] S. Suhai, J. Polym. Sci. Polym. Phys. Ed., **21,** 1341 (1983); Int. J. Quantum Chem. Quantum Chem. Symp., **18,** 161 (1984); J. Chem. Phys., **84,** 5071 (1986).

[41] J. Almlöf, K. Faegri, Jr., and K. Korsell, J. Comput. Chem., **3,** 385 (1982).

[42] P. Pulay, J. Chem. Phys., **78,** 5043 (1983).

[43] W. J. Hehre, R. F. Stewart, and J. A. Pople, J. Chem. Phys., **51,** 2657 (1969).

[44] J. S. Binkley, J. A. Pople, and W. J. Hehre, J. Am. Chem. Soc., **102,** 939 (1980).

[45] W. J. Hehre, R. Ditchfield, and J. A. Pople, J. Chem. Phys., **56,** 2257 (1972).

[46] P. C. Hariharan and J. A. Pople, Theor. Chim. Acta, **28,** 213 (1973).

[47] J. Delhalle, L. Piela, J.-L. Brédas, and J.-M. André, Phys. Rev. B, **22,** 6254 (1980).

[48] J. M. André, D. P. Vercauteren, V. P. Bodart, and J. G. Fripiat, J. Comput. Chem., **5,** 535 (1984).

[49] H. Teramae, Theor. Chim. Acta, **94,** 311 (1996).

[50] C. W. Bunn, Trans. Faraday Soc., **35,** 482 (1939).

[51] H. M. M. Shearer and V. Vand, Acta Cryst., **9,** 379 (1956).

[52] P. W. Teare, Acta Cryst., **12,** 294 (1959).

[53] S. Kavesh and J. M. Schultz, J. Polym. Sci. Part A-2, **8,** 243 (1970).

[54] B. Crist, M. A. Ratner, A. L. Brower, and J. R. Sabin, J. Appl. Phys., **50,** 6047 (1979).

[55] GAUSSIAN 94, Revision D.3, M. J. Frisch, G. W. Trucks, H. B. Schlegel, P. M. W. Gill, B. G. Johnson, M. A. Robb, J. R. Cheeseman, T. A. Keith, G. A. Petersson, J. A. Montgomery, K. Raghavachari, M. A. Al-Laham, V. G. Zakrzewski, J. V. Ortiz, J. B. Foresman, J. Cioslowski, B. B. Stefanov, A. Nanayakkara, M. Challacombe, C. Y. Peng, P. Y. Ayala, W. Chen, M. W. Wong, J. L. Andres, E. S. Replogle, R. Gomperts, R. L. Martin, D. J. Fox, J. S. Binkley, D. J. Defrees, J. Baker, J. P. Stewart, M. Head-Gordon, C. Gonzalez, and J. A. Pople, Gaussian, Inc., Pittsburgh PA, 1995.

[56] J. W. Mintmire and C. T. White, Phys. Rev. B, **35,** 4180 (1987).

[57] J. Ashkenazi, W. E. Pickett, H. Krakauer, C. S. Wang, B. M. Klein, and S. R. Chubb, Phys. Rev. Lett., **62,** 2016 (1989).

[58] J. Paloheimo and J. von Boehm, Phys. Rev. B, **46,** 4304 (1992).

[59] S. Krimm, C. Y. Liang, and G. B. B. M. Sutherland, J. Chem. Phys., **25,** 549 (1956).

[60] J. R. Nielsen and A. H. Woollett, J. Chem. Phys., **26,** 1391 (1957).

[61] J. R. Nielsen and R. F. Holland, J. Mol. Spectrosc., **6**, 394 (1961).

[62] R. G. Brown, J. Chem. Phys., **38**, 221 (1963).

[63] S. F. Parker and H. Herman, Spectrochim. Acta, **53A**, 119 (1997).

Chapter 7

Analytical energy gradients for ab initio second-order Møller–Plesset perturbation crystal orbital theory

So Hirata and Suehiro Iwata, "Analytical energy gradients in second-order Møller–Plesset perturbation theory for extended systems," J. Chem. Phys., in press.

Abstract

The spin-restricted formulas for the analytical gradients of the second-order Møller–Plesset perturbation (MP2) energy are presented within the framework of ab initio crystal orbital theory of infinite one-dimensional lattices (polymers). The coupled perturbed Hartree–Fock equation for polymers is solved iteratively using the atomic-orbital-based algorithms. The MP2 energy and its gradient contributions are evaluated by the disk-based algorithms with the aid of the two-particle density matrix. The analytical-gradient method at the MP2 level as well as the analytical first- and second-derivative methods at the Hartree–Fock (HF) level is applied to calculate the equilibrium structures and harmonic vibrational frequencies of all-*trans* polyacetylene. The deviations of the calculated frequencies from the observed ones for the in-phase C=C stretching modes are reduced by about 70 % on going from HF/6-31G to MP2/6-31G theory.

7.1 Introduction

Vibrational spectra of a number of polymers and some crystalline materials can be interpreted theoretically in terms of the normal vibrations of isolated chains of infinite lengths [1]. Among these normal vibrations, of particular importance are those with wavevector $k = 0$, since they give rise to infrared absorption bands and Raman scattering lines [1]. In $k = 0$ vibrations, the corresponding atoms in all the unit cells vibrate in phase with each other. In other words, the perfect translational symmetry is retained in these vibrations. Because of this property of $k = 0$ vibrations and the selection rules of infrared and Raman spectroscopy, ab initio crystal orbital theory [2–5], which takes full advantage of the periodicity of polymers, is an ideal means to interpret and predict the infrared and Raman spectra of polymers.

In fact, it has been demonstrated by Teramae *et al.* [6,7] that the frequencies of the infrared- and Raman-active vibrations of polymers could be evaluated efficiently with the aid of the analytical gradients of Hartree–Fock (HF) energies with respect to in-phase ($k = 0$) nuclear displacements. At the HF level of approximation, we have recently implemented the analytical second derivatives of energy with respect to in-phase nuclear displacements [8]. In addition, we, and also Sun and Bartlett, have carried out the crystal orbital calculations on the normal vibrations of polymers, in which the effects of electron correlation have been explicitly taken into account [9–11]. We have derived the formulas

for the analytical energy gradients in density functional and hybrid HF/density functional crystal orbital theories, and have developed an efficient code based on these formulas [9]. The method has been applied to the vibrational frequency calculations of polyacetylene, polymethineimine, and polyethylene [9,11]. On the basis of second-order Møller–Plesset perturbation (MP2) crystal orbital theory, Sun and Bartlett [10] have recently carried out a vibrational analysis of *anti*-transoid form of polymethineimine. However, these authors have evaluated the force constants by double numerical differentiation of the total energies without using an analytical-derivative method.

In this chapter, we describe the formulas and computer implementation of analytical gradients of MP2 energy within the framework of ab initio crystal orbital theory. The formulation consists of three parts. The first part reiterates briefly the gradient contributions from the HF energy. The original derivation of this part can be found in the papers of Teramae *et al.* [6,7]. The second part involves the polymer version of the coupled perturbed Hartree–Fock (CPHF) equation, which we have already implemented in the analytical-second-derivative codes of ab initio HF crystal orbital theory [8]. In the third part, the formulas for the MP2 correction and gradient contributions due to this correction are described. The formulas for MP2 energy for infinite systems were first derived and implemented by Suhai [12] and MP2 single point calculations have already been performed for a number of polymers by him [12–19] and other authors [10,20–27]. Here we present the results of vibrational analyses based on the MP2 analytical-gradient method, taking all-*trans* polyacetylene [28] (hereafter simply referred to as polyacetylene) as an example. The vibrational spectra of polyacetylene have been studied intensively [29–38] and the assignments of the infrared and Raman bands have been established [29,30,39]. It is known that some of the structural parameters and normal modes of polyacetylene are strongly affected by electron correlation [9,12,18,40–42]. We shall demonstrate that the differences between the calculated and observed frequencies for these normal modes are significantly reduced on going from HF theory to MP2 theory. The efficiency of the present implementation of the analytical-gradient method is also discussed in terms of the execution times.

7.2 Formulas for the MP2 gradients

7.2.1 HF part of the total energy and gradients

In the spin-restricted HF crystal orbital method [2–5], the total wave function of an infinite one-dimensional lattice is a Slater determinant built from doubly occupied crystal (Bloch) orbitals. Each crystal orbital is then expressed as a linear combination of atomic orbitals $\chi_\mu^{(q)}(\mathbf{r})$ in the form

$$\psi_n^{[k]}(\mathbf{r}) = \frac{1}{\sqrt{K}} \sum_\mu \sum_q C_{\mu n}^{[k]} \exp(ikqa) \chi_\mu^{(q)}(\mathbf{r}), \tag{7.1}$$

where a is the translational period, and K is the number of unit cells in the system and it approaches infinity. The crystal orbital $\psi_n^{[k]}(\mathbf{r})$ and crystal orbital coefficient $C_{\mu n}^{[k]}$ are characterized by energy band n and quasi-momentum k, which are indicated by subscripts and square-bracketed superscripts, respectively. The atomic orbital $\chi_\mu^{(q)}(\mathbf{r})$ is a real spatial function centered in unit cell q.

Applying Ritz variation principle to the HF energy expectation value with the orthonormality condition

$$\int \psi_m^{[k]}(\mathbf{r}) \psi_n^{[k]}(\mathbf{r}) \mathrm{d}\mathbf{r} = \delta_{mn}, \tag{7.2}$$

we obtain the following k-dependent Hartree–Fock–Roothaan equation:

$$\mathbf{F}^{[k]} \mathbf{C}^{[k]} = \mathbf{S}^{[k]} \mathbf{C}^{[k]} \epsilon^{[k]}, \tag{7.3}$$

where $\epsilon^{[k]}$ is a diagonal matrix of one-electron energies. The elements of the k-dependent Fock and overlap matrices are Fourier lattice sums of the corresponding molecular integrals in the atomic orbital basis:

$$F_{\mu\nu}^{[k]} = \sum_q F_{\mu\nu}^{(q)} \exp(ikqa), \tag{7.4}$$

and

$$S_{\mu\nu}^{[k]} = \sum_q S_{\mu\nu}^{(q)} \exp(ikqa). \tag{7.5}$$

The elements of the Fock and overlap matrices between the atomic orbitals $\chi_\mu^{(0)}(\mathbf{r})$ and $\chi_\nu^{(q)}(\mathbf{r})$ are defined, respectively, as

$$F_{\mu\nu}^{(q)} = H_{\mu\nu}^{(q)} + \sum_{\lambda,\sigma} \sum_{r,s} P_{\lambda\sigma}^{(s-r)} \left(\mu^{(0)} \nu^{(q)} || \lambda^{(r)} \sigma^{(s)} \right), \tag{7.6}$$

and

$$S_{\mu\nu}^{(q)} = \int \chi_\mu^{(0)}(\mathbf{r}) \chi_\nu^{(q)}(\mathbf{r}) d\mathbf{r}. \tag{7.7}$$

The elements of the one-electron part of the Fock matrix are given by

$$H_{\mu\nu}^{(q)} = \int \chi_{\mu}^{(0)}(\mathbf{r}) \left(-\frac{1}{2}\nabla^2\right) \chi_{\nu}^{(q)}(\mathbf{r}) d\mathbf{r} - \sum_{A}\sum_{r} \int \chi_{\mu}^{(0)}(\mathbf{r}) \frac{Z_A}{|\mathbf{r} - \mathbf{R}_A^{(r)}|} \chi_{\nu}^{(q)}(\mathbf{r}) d\mathbf{r}, \tag{7.8}$$

where Z_A is the charge of nucleus A at position $\mathbf{R}_A^{(r)}$. The density matrix elements $P_{\mu\nu}^{(q)}$ are defined by summation over all the occupied states in the first Brillouin zone:

$$P_{\mu\nu}^{(q)} = \frac{2}{K} \sum_{j}^{\text{occ.}} \sum_{k}^{\text{BZ}} C_{\mu j}^{[k]*} C_{\nu j}^{[k]} \exp(ikqa). \tag{7.9}$$

Note that the number of k points in the first Brillouin zone is equal to K. Two-electron integrals $\left(\mu^{(0)}\nu^{(q)}||\lambda^{(r)}\sigma^{(s)}\right)$ in Eq. (7.6) are antisymmetrized combinations of regular two-electron integrals over atomic orbitals

$$\left(\mu^{(0)}\nu^{(q)}||\lambda^{(r)}\sigma^{(s)}\right) = \left(\mu^{(0)}\nu^{(q)}|\lambda^{(r)}\sigma^{(s)}\right) - \frac{1}{2}\left(\mu^{(0)}\sigma^{(s)}|\lambda^{(r)}\nu^{(q)}\right), \tag{7.10}$$

with

$$\left(\mu^{(0)}\nu^{(q)}|\lambda^{(r)}\sigma^{(s)}\right) = \int\int \chi_{\mu}^{(0)}(\mathbf{r}_1)\chi_{\nu}^{(q)}(\mathbf{r}_1) \frac{1}{r_{12}} \chi_{\lambda}^{(r)}(\mathbf{r}_2)\chi_{\sigma}^{(s)}(\mathbf{r}_2) d\mathbf{r}_1 d\mathbf{r}_2. \tag{7.11}$$

Using the matrices defined above, we can write the expression for the HF total energy per unit cell as

$$E_{\text{HF}} = \sum_{\mu,\nu}\sum_{q} P_{\mu\nu}^{(q)} H_{\mu\nu}^{(q)} + \frac{1}{2}\sum_{\mu,\nu}\sum_{\lambda,\sigma}\sum_{q,r,s} P_{\mu\nu}^{(q)} P_{\lambda\sigma}^{(s-r)} \left(\mu^{(0)}\nu^{(q)}||\lambda^{(r)}\sigma^{(s)}\right) + E_{\text{NR}}, \tag{7.12}$$

where E_{NR} is the nuclear repulsion energy per unit cell. The expression for the HF energy gradients with respect to an in-phase nuclear displacement x is written as [6,7]

$$\frac{\partial E_{\text{HF}}}{\partial x} = \sum_{\mu,\nu}\sum_{q} P_{\mu\nu}^{(q)} \frac{\partial H_{\mu\nu}^{(q)}}{\partial x} + \frac{1}{2}\sum_{\mu,\nu}\sum_{\lambda,\sigma}\sum_{q,r,s} P_{\mu\nu}^{(q)} P_{\lambda\sigma}^{(s-r)} \frac{\partial}{\partial x}\left(\mu^{(0)}\nu^{(q)}||\lambda^{(r)}\sigma^{(s)}\right) + \frac{\partial E_{\text{NR}}}{\partial x} - \sum_{\mu,\nu}\sum_{q} W_{\mu\nu}^{(q)} \frac{\partial S_{\mu\nu}^{(q)}}{\partial x}, \tag{7.13}$$

where $W^{(q)}$ is the energy-weighted density matrix [43,44], whose elements are defined as

$$W_{\mu\nu}^{(q)} = \frac{2}{K} \sum_{j}^{\text{occ.}} \sum_{k}^{\text{BZ}} \epsilon_j^{[k]} C_{\mu j}^{[k]*} C_{\nu j}^{[k]} \exp(ikqa). \tag{7.14}$$

In Eq. (7.13), the terms involving the derivatives of density matrix elements are eliminated by making use of the orthonormality condition (7.2).

In-phase nuclear displacements include the translational period a. The first derivative of energy with respect to a can be calculated by using Eq. (7.13) and the following relation [6,7,9]

$$\frac{\partial}{\partial a} = \sum_A \sum_q q \frac{\partial}{\partial z_A^{(q)}}, \tag{7.15}$$

where $z_A^{(q)}$ denotes the z-coordinate of nucleus A in unit cell q and we assume that the chain axis is parallel to the z-axis.

7.2.2 CPHF equation

As we shall show in the next subsection, the formula for the MP2 gradients has dependence on the first derivatives of crystal orbital coefficients $\partial C_{\mu n}^{[k]}/\partial x$. These derivatives are obtained as solutions to the polymer version of the CPHF equation [8], which is an extension of the molecular CPHF equation first derived by Gerratt and Mills [45]. Following the notation of Pople *et al.* [44], the molecular CPHF equation is written as

$$(\epsilon_i - \epsilon_a)\, u_{ai}^{(1)} = Q_{ai}^{(1)} + 2 \sum_b^{\text{virt.}} \sum_j^{\text{occ.}} \{ u_{bj}^{(1)*}\, (ai||bj) + u_{bj}^{(1)}\, (ai||jb) \}. \tag{7.16}$$

Here the derivatives of molecular orbital coefficients are expanded by the molecular orbital coefficient vectors with the expansion coefficients being the solution vectors $u_{ai}^{(1)}$ of the CPHF equation [44–46]

$$\frac{\partial C_{\mu n}}{\partial x} = \sum_m^{\text{all}} C_{\mu m} u_{mn}^{(1)}. \tag{7.17}$$

Here we use i,j,h,l for occupied orbitals and a,b,c for virtual orbitals. We also use m,n for the entire set of molecular (or crystal) orbitals. The polymer version of the CPHF equation can be obtained from Eqs. (7.16) and (7.17) by the replacements

$$C_{\mu n} \;\rightarrow\; \frac{1}{\sqrt{K}} C_{\mu n}^{[k]} \exp(ikqa), \tag{7.18}$$

$$\psi_n(\mathbf{r}) \;\rightarrow\; \psi_n^{[k]}(\mathbf{r}), \tag{7.19}$$

$$\chi_\mu(\mathbf{r}) \;\rightarrow\; \chi_\mu^{(q)}(\mathbf{r}), \tag{7.20}$$

and so forth. The CPHF equation obtained by these replacements is, however, highly redundant; because of the translational invariance of molecular integrals we can substantially reduce the dimension of the matrices and vectors appearing in the equation. Eliminating the redundancy, we obtain the polymer CPHF equation in the following form:

$$\left(\epsilon_i^{[k_1]} - \epsilon_a^{[k_1]}\right) u_{ai}^{(1)[k_1]} = Q_{ai}^{(1)[k_1]} + 2 \sum_b^{\text{virt.}} \sum_j^{\text{occ.}} \sum_{k_2}^{\text{BZ}} \left\{ u_{bj}^{(1)[k_2]*} \left(a^{[k_1]} i^{[k_1]} || b^{[k_2]} j^{[k_2]} \right) \right.$$

$$+ u_{bj}^{(1)[k_2]} \left(a^{[k_1]} i^{[k_1]} || j^{[k_2]} b^{[k_2]} \right) \Big\}, \tag{7.21}$$

with

$$Q_{ai}^{(1)[k_1]} = \mathcal{H}_{ai}^{(1)[k_1]} + \mathcal{J}_{ai}^{(1)[k_1]} - \epsilon_i^{[k_1]} \mathcal{S}_{ai}^{(1)[k_1]} - 2 \sum_{h,l}^{\text{occ.}} \sum_{k_2}^{\text{BZ}} \mathcal{S}_{hl}^{(1)[k_2]} \left(a^{[k_1]} i^{[k_1]} || l^{[k_2]} h^{[k_2]} \right). \tag{7.22}$$

The readers can find in Chapter 6 the derivation of these equations starting from the molecular counterparts. Equation (7.17) is likewise generalized to give the derivatives of crystal orbital coefficients as

$$\frac{\partial C_{\mu n}^{[k]}}{\partial x} = \sum_{m}^{\text{all}} C_{\mu m}^{[k]} u_{mn}^{(1)[k]}, \tag{7.23}$$

where x denotes an in-phase nuclear displacement. Note that the two-electron integrals over crystal orbitals appearing in Eqs. (7.21) and (7.22) have only two independent k-indices, and are of the type

$$\begin{aligned} \left(a^{[k_1]} i^{[k_1]} || m^{[k_2]} n^{[k_2]} \right) &= \frac{1}{K} \sum_{\mu,\nu,\lambda,\sigma} \sum_{q,r,s} C_{\mu a}^{[k_1]*} C_{\nu i}^{[k_1]} C_{\lambda m}^{[k_2]*} C_{\sigma n}^{[k_2]} \\ &\quad \times \exp\{i(k_1 q - k_2 r + k_2 s)a\} \left(\mu^{(0)} \nu^{(q)} || \lambda^{(r)} \sigma^{(s)} \right). \end{aligned} \tag{7.24}$$

The matrices introduced in Eq. (7.22) are the so-called skeleton (core) derivative integral matrices [46], whose elements are defined as [8]

$$\mathcal{H}_{mn}^{(1)[k]} = \sum_{\mu,\nu} \sum_{q} C_{\mu m}^{[k]*} C_{\nu n}^{[k]} \frac{\partial H_{\mu\nu}^{(q)}}{\partial x} \exp(ikqa), \tag{7.25}$$

and

$$\mathcal{J}_{mn}^{(1)[k]} = \sum_{\mu,\nu} \sum_{\lambda,\sigma} \sum_{q,r,s} C_{\mu m}^{[k]*} C_{\nu n}^{[k]} P_{\lambda\sigma}^{(s-r)} \frac{\partial}{\partial x} \left(\mu^{(0)} \nu^{(q)} || \lambda^{(r)} \sigma^{(s)} \right) \exp(ikqa), \tag{7.26}$$

and

$$\mathcal{S}_{mn}^{(1)[k]} = \sum_{\mu,\nu} \sum_{q} C_{\mu m}^{[k]*} C_{\nu n}^{[k]} \frac{\partial S_{\mu\nu}^{(q)}}{\partial x} \exp(ikqa). \tag{7.27}$$

It may be adequate to define here another skeleton (core) derivative integral matrix for later use:

$$\begin{aligned} \mathcal{F}_{mn}^{(1)[k_1]} &= \mathcal{H}_{mn}^{(1)[k_1]} + \mathcal{J}_{mn}^{(1)[k_1]} - 2 \sum_{h,l}^{\text{occ.}} \sum_{k_2}^{\text{BZ}} \mathcal{S}_{hl}^{(1)[k_2]} \left(m^{[k_1]} n^{[k_1]} || l^{[k_2]} h^{[k_2]} \right) \\ &\quad + 2 \sum_{a}^{\text{virt.}} \sum_{l}^{\text{occ.}} \sum_{k_2}^{\text{BZ}} \Big\{ u_{al}^{(1)[k_2]*} \left(m^{[k_1]} n^{[k_1]} || a^{[k_2]} l^{[k_2]} \right) \\ &\quad + u_{al}^{(1)[k_2]} \left(m^{[k_1]} n^{[k_1]} || l^{[k_2]} a^{[k_2]} \right) \Big\}. \end{aligned} \tag{7.28}$$

7.2.3 MP2 part of the total energy and gradients

According to Rayleigh–Schrödinger perturbation theory, the exact ground-state wave function Ψ and energy E for a system described by the Hamiltonian $H + \lambda H'$ can be expanded in powers of λ,

$$\Psi = \Psi^{(0)} + \lambda\Psi^{(1)} + \lambda^2\Psi^{(2)}\cdots, \tag{7.29}$$

$$E = E^{(0)} + \lambda E^{(1)} + \lambda^2 E^{(2)}\cdots. \tag{7.30}$$

The complete Hamiltonian is a sum of two parts—the zeroth-order Hamiltonian H and the perturbation $\lambda H'$. Employing the Møller–Plesset partition scheme [47], we take the zeroth-order Hamiltonian as a sum of Fock operators. Truncating the energy expression, Eq. (7.30), at second order and setting $\lambda = 1$, we obtain the expression for the MP2 energy as

$$E_{\mathrm{MP2}} = E^{(0)} + E^{(1)} + E^{(2)}, \tag{7.31}$$

where $E^{(0)} + E^{(1)}$ is identical to the HF energy E_{HF}.

In the molecular orbital formalism, the MP2 correlation correction $E^{(2)}$ is written as [48,49]

$$E^{(2)} = \sum_{i,j}^{\text{occ.}}\sum_{a,b}^{\text{virt.}} \frac{2\,|(ia|jb)|^2 - (ia|jb)\,(ib|ja)}{\epsilon_i + \epsilon_j - \epsilon_a - \epsilon_b}. \tag{7.32}$$

The corresponding expression for infinite one-dimensional lattices is obtained by replacements (7.18)–(7.20) as

$$\begin{aligned} E^{(2)} = \frac{1}{K}\sum_{i,j}^{\text{occ.}}\sum_{a,b}^{\text{virt.}}\sum_{k_1,k_2,k_3,k_4}^{\mathrm{BZ}} \Big\{ & 2\left|\left(i^{[k_1]}a^{[k_2]}|j^{[k_3]}b^{[k_4]}\right)\right|^2 \\ & - \mathrm{Re}\left[\left(i^{[k_1]}a^{[k_2]}|j^{[k_3]}b^{[k_4]}\right)\left(i^{[k_1]}b^{[k_4]}|j^{[k_3]}a^{[k_2]}\right)^*\right]\Big\}\,\Delta_{ij}^{ab}(k_1,k_2,k_3,k_4), \end{aligned} \tag{7.33}$$

with

$$\Delta_{ij}^{ab}(k_1,k_2,k_3,k_4) = \left(\epsilon_i^{[k_1]} + \epsilon_j^{[k_3]} - \epsilon_a^{[k_2]} - \epsilon_b^{[k_4]}\right)^{-1}. \tag{7.34}$$

Here $E^{(2)}$ denotes the MP2 correlation correction per unit cell, and two-electron integrals over crystal orbitals are defined as

$$\begin{aligned} \left(i^{[k_1]}a^{[k_2]}|j^{[k_3]}b^{[k_4]}\right) &= \frac{1}{K^2}\sum_{\mu,\nu,\lambda,\sigma}\sum_{p,q,r,s} C_{\mu i}^{[k_1]*}C_{\nu a}^{[k_2]}C_{\lambda j}^{[k_3]*}C_{\sigma b}^{[k_4]} \\ &\quad \times \exp\{i(-k_1p + k_2q - k_3r + k_4s)a\}\left(\mu^{(p)}\nu^{(q)}|\lambda^{(r)}\sigma^{(s)}\right) \\ &= \frac{1}{K^2}\sum_{p}\exp\{i(-k_1 + k_2 - k_3 + k_4)pa\} \end{aligned}$$

$$\times \sum_{\mu,\nu,\lambda,\sigma} \sum_{q,r,s} C_{\mu i}^{[k_1]*} C_{\nu a}^{[k_2]} C_{\lambda j}^{[k_3]*} C_{\sigma b}^{[k_4]}$$
$$\times \exp[i\{k_2(q-p) - k_3(r-p) + k_4(s-p)\}a]$$
$$\times \left(\mu^{(p)}\nu^{(q)}|\lambda^{(r)}\sigma^{(s)}\right). \tag{7.35}$$

The summation $\sum_p \exp\{i(-k_1 + k_2 - k_3 + k_4)pa\}$ can be carried out separately, and it gives K if $(-k_1 + k_2 - k_3 + k_4)a$ is an integral multiple of 2π; otherwise the summation vanishes. If we confine k-points in the first Brillouin zone, there is always one and only one k_1, which gives a non-vanishing result for this summation, for any given k_2, k_3, and k_4. Thus, we can drop one of the four k-indices in the summation in Eq. (7.33). This is equivalent to writing [12]

$$E^{(2)} = \frac{1}{K} \sum_{i,j}^{\text{occ.}} \sum_{a,b}^{\text{virt.}} \sum_{k_2,k_3,k_4}^{\text{BZ}} \left\{ 2 \left| \left(i^{[k_1]}a^{[k_2]}|j^{[k_3]}b^{[k_4]}\right) \right|^2 \right.$$
$$\left. - \text{Re}\left[\left(i^{[k_1]}a^{[k_2]}|j^{[k_3]}b^{[k_4]}\right) \left(i^{[k_1]}b^{[k_4]}|j^{[k_3]}a^{[k_2]}\right)^* \right] \right\} \Delta_{ij}^{ab}(k_2,k_3,k_4), \tag{7.36}$$

with

$$\Delta_{ij}^{ab}(k_2,k_3,k_4) = \left(\epsilon_i^{[k_1]} + \epsilon_j^{[k_3]} - \epsilon_a^{[k_2]} - \epsilon_b^{[k_4]}\right)^{-1}. \tag{7.37}$$

Now the definition of two-electron integrals over crystal orbitals becomes

$$\left(i^{[k_1]}a^{[k_2]}|j^{[k_3]}b^{[k_4]}\right) = \frac{1}{K} \sum_{\mu,\nu,\lambda,\sigma} \sum_{q,r,s} C_{\mu i}^{[k_1]*} C_{\nu a}^{[k_2]} C_{\lambda j}^{[k_3]*} C_{\sigma b}^{[k_4]}$$
$$\times \exp\{i(k_2 q - k_3 r + k_4 s)a\} \left(\mu^{(0)}\nu^{(q)}|\lambda^{(r)}\sigma^{(s)}\right). \tag{7.38}$$

In these equations, k_1 is determined uniquely for each set of (k_2, k_3, k_4) by

$$k_1 = k_2 - k_3 + k_4, \tag{7.39}$$

and if k_1 is out of the first Brillouin zone, we can move it back into the zone by the replacements

$$k_1 \leftarrow k_1 - 2\pi/a \qquad (\text{if } k_1 > \pi/a), \tag{7.40}$$
$$k_1 \leftarrow k_1 + 2\pi/a \qquad (\text{if } k_1 \le -\pi/a). \tag{7.41}$$

The expression for the gradients of $E^{(2)}$ with respect to an in-phase nuclear displacement x can be obtained by generalizing the corresponding expression for molecules [44] as

$$\frac{\partial E^{(2)}}{\partial x} = \frac{4}{K} \sum_{i,j}^{\text{occ.}} \sum_{a,b}^{\text{virt.}} \sum_{k_2,k_3,k_4}^{\text{BZ}} \text{Re}\left[a_{ij}^{ab}(k_2,k_3,k_4) X_{ij}^{ab}(k_2,k_3,k_4) \right], \tag{7.42}$$

where we used the first-order Møller–Plesset wave function coefficients

$$a_{ij}^{ab}(k_2,k_3,k_4) = \left(i^{[k_1]}a^{[k_2]}||j^{[k_3]}b^{[k_4]}\right)^* \Delta_{ij}^{ab}(k_2,k_3,k_4), \tag{7.43}$$

and

$$\begin{aligned}
X_{ij}^{ab}(k_2,k_3,k_4) &= \frac{1}{K}\sum_{\mu,\nu,\lambda,\sigma}\sum_{q,r,s} C_{\mu i}^{[k_1]*} C_{\nu a}^{[k_2]} C_{\lambda j}^{[k_3]*} C_{\sigma b}^{[k_4]} \\
&\times \exp\{i(k_2 q - k_3 r + k_4 s)a\}\frac{\partial}{\partial x}\left(\mu^{(0)}\nu^{(q)}|\lambda^{(r)}\sigma^{(s)}\right) \\
&+ \sum_{l}^{\text{occ.}}\left\{2u_{la}^{(1)[k_2]}\left(i^{[k_1]}l^{[k_2]}|j^{[k_3]}b^{[k_4]}\right) - \left(\mathcal{F}_{il}^{(1)[k_1]} - \epsilon_i^{[k_1]}\mathcal{S}_{il}^{(1)[k_1]}\right)\right. \\
&\times \left.\left(l^{[k_1]}a^{[k_2]}|j^{[k_3]}b^{[k_4]}\right)\Delta_{lj}^{ab}(k_2,k_3,k_4) - \mathcal{S}_{il}^{(1)[k_1]}\left(l^{[k_1]}a^{[k_2]}|j^{[k_3]}b^{[k_4]}\right)\right\} \\
&+ \sum_{c}^{\text{virt.}}\left\{2u_{ci}^{(1)[k_1]*}\left(c^{[k_1]}a^{[k_2]}|j^{[k_3]}b^{[k_4]}\right) + \left(\mathcal{F}_{ac}^{(1)[k_2]*} - \epsilon_c^{[k_2]}\mathcal{S}_{ac}^{(1)[k_2]*}\right)\right. \\
&\times \left.\left(i^{[k_1]}c^{[k_2]}|j^{[k_3]}b^{[k_4]}\right)\Delta_{ij}^{cb}(k_2,k_3,k_4) - \mathcal{S}_{ac}^{(1)[k_2]*}\left(i^{[k_1]}c^{[k_2]}|j^{[k_3]}b^{[k_4]}\right)\right\}.
\end{aligned} \tag{7.44}$$

The occupied-virtual-block vectors $u_{la}^{(1)[k_2]}$ in Eq. (7.44) are obtained from the solution vectors of the CPHF equation $u_{al}^{(1)[k_2]}$ by virtue of the relation [44–46]

$$u_{la}^{(1)[k_2]} = -u_{al}^{(1)[k_2]*} - \mathcal{S}_{al}^{(1)[k_2]*}. \tag{7.45}$$

Equations (7.42)–(7.44) can be derived alternatively by directly differentiating Eq. (7.36). The derivation is parallel to that of the molecular counterparts, which can be found in the paper of Salter *et al.* [50]. However, considerable care must be exercised not to confuse the complex quantities with their conjugate values, since in the formulation for molecular systems molecular orbital coefficients and molecular integrals are usually assumed to be real. With the aid of Eq. (7.15), we can also compute the gradients with respect to the translational period $\partial E^{(2)}/\partial a$ without modifying the CPHF equation (7.21) and the gradient formulas (7.42)–(7.44) just described.

7.3 Computer implementation

We used the standard STO-3G [51] and 6-31G [52] basis sets as atomic orbitals. One- and two-electron integrals and their first derivatives were evaluated by using the sixth and ninth neighbor approximations, respectively, for the STO-3G and 6-31G calculations. We employed the Namur cutoff procedure [53,54] without long-range correction. Only the two-electron integrals and their derivatives whose absolute values were larger than the

threshold of 10^{-8} were computed, and then stored in the external storage. The criterion for the convergence of density matrix was set to 10^{-8}. The number of evenly spaced momentum sampling points in the first Brillouin zone was 20 (only one of the two points at the zone boundaries was counted).

The CPHF equation was solved in an iterative manner using a set of trial vectors [44]. The solution vectors were expanded by these trial vectors, and the expansion coefficients were determined by the DIIS (direct inversion in the iterative subspace) method [44,55]. The convergence criterion for the solutions was set to 10^{-9}, and typically 9 to 11 trial vectors were necessary to obtain this convergence. In each iteration of DIIS, we had to form the product vectors of two-electron integral over crystal orbitals and a trial vector. This product formation was carried out conveniently by using the atomic-orbital-based algorithm [56,57], the details of which have been given in Chapter 6. Thus, we could avoid, at this point, the integral transformation of two-electron integrals. As we shall show in the next section, the step of solving the CPHF equation requires only a small fraction of the total execution time, and hence we did not employ here more advanced algorithms such as the Z-vector method of Handy and Schaefer [58]. Therefore, the CPHF equation was solved for each of $3n+1$ nuclear degrees of freedom, where n is the number of nuclei in the unit cell and one degree of freedom is associated with the translational period a.

The MP2 correlation correction $E^{(2)}$ and its gradient contributions $\partial E^{(2)}/\partial x$ were evaluated in the following three steps. (1) The two-electron integrals over atomic orbitals were transformed to those over crystal orbitals. Transformation was performed stepwise. Outermost loop was over the virtual crystal orbitals $\psi_b^{[k_4]}(\mathbf{r})$, and the transformed two-electron integrals of the type $\left(m^{[k_1]}n^{[k_2]}|j^{[k_3]}b^{[k_4]}\right)$ were stored in core memory. This step required $\mathcal{O}(N^3K^2)$ memory, where N is the number of basis functions per unit cell and K is the number of momentum sampling points. Two-electron integrals over atomic orbitals were restored from the external storage for each pair of b and k_4. Thus, the I/O operations in this step totaled VK, where V is the number of virtual energy bands. (2) By using the current transformed integrals $\left(m^{[k_1]}n^{[k_2]}|j^{[k_3]}b^{[k_4]}\right)$ for a (b, k_4) pair, we incremented $E^{(2)}$ and obtained the first-order Møller–Plesset wave function coefficients $a_{ij}^{ab}(k_2,k_3,k_4)$. Here we have included the carbon 1s orbitals among the occupied orbitals; the frozen core approximation was not used. With the current transformed integrals, the second and third terms of Eq. (7.44) were computed and contracted with $a_{ij}^{ab}(k_2,k_3,k_4)$ to give

gradient contributions. The CPHF solutions and the skeleton (core) derivative matrices were $\mathcal{O}(VOK)$ and $\mathcal{O}(N^2K)$ quantities, respectively, and were stored in core memory. (3) The final step was to obtain the gradient contributions due to the two-electron integral derivatives over atomic orbitals, i.e., the first term of Eq. (7.44). This has conveniently been accomplished by using the (non-separable) two-particle density matrix [59–61]:

$$\begin{aligned}\Gamma_{\mu\nu\lambda\sigma}(q,r,s) &= \frac{1}{K}\sum_{i,j}^{\text{occ.}}\sum_{a,b}^{\text{virt.}}\sum_{k_2,k_3,k_4}^{\text{BZ}} C_{\mu i}^{[k_1]*}C_{\nu a}^{[k_2]}C_{\lambda j}^{[k_3]*}C_{\sigma b}^{[k_4]}a_{ij}^{ab}(k_2,k_3,k_4) \\ &\quad \times \exp\{i(k_2 q - k_3 r + k_4 s)a\}. \end{aligned} \tag{7.46}$$

Since we had $a_{ij}^{ab}(k_2,k_3,k_4)$ only for a (b, k_4) pair, we could obtain $\Gamma'_{\mu\nu\lambda b}(q,r,k_4)$ by carrying out three quarter back-transformations for pairs (i,k_1), (a,k_2), and (j,k_3):

$$\Gamma'_{\mu\nu\lambda b}(q,r,k_4) = \sum_{i,j}^{\text{occ.}}\sum_{a}^{\text{virt.}}\sum_{k_2,k_3}^{\text{BZ}} C_{\mu i}^{[k_1]*}C_{\nu a}^{[k_2]}C_{\lambda j}^{[k_3]*}a_{ij}^{ab}(k_2,k_3,k_4)\exp\{i(k_2 q - k_3 r)a\}. \tag{7.47}$$

This step again required $\mathcal{O}(N^3K^2)$ memory. The fourth quarter back-transformation for a (b,k_4) pair was performed last:

$$\Gamma_{\mu\nu\lambda\sigma}(q,r,s) = \frac{1}{K}\sum_{b}^{\text{virt.}}\sum_{k_4}^{\text{BZ}} C_{\sigma b}^{[k_4]}\Gamma'_{\mu\nu\lambda b}(q,r,k_4)\exp(ik_4 sa). \tag{7.48}$$

The contribution of the current (b,k_4) pair to $\Gamma_{\mu\nu\lambda\sigma}(q,r,s)$ was obtained and was immediately contracted with two-electron integral derivatives to give gradient contributions [61]. Two-electron integral derivatives were restored from the external storage for each (b,k_4) pair, and hence the total number of I/O operations in this step was again VK.

Geometry optimizations were carried out for all-*trans* polyacetylene by using the analytical energy gradients at the HF and MP2 levels. Threshold for the residual energy gradients was set to 2×10^{-4} hartree/bohr. GDIIS extrapolation [62] was adopted to accelerate the convergence of the geometry optimizations. At the HF level, vibrational frequency calculations were performed by using the analytical second derivatives [8]. At the MP2 level, the force constants were evaluated by numerical differentiation of the analytical energy gradients. The step size for the numerical differentiation was 0.02 bohr (each nucleus was displaced from the equilibrium position by ± 0.01 bohr in the x, y, and z directions). In order to obtain all the symmetrically distinct force constants, we have carried out energy gradient calculations at 10 different structures. The frequencies of $k = 0$ vibrations were computed with these force constants in the Cartesian coordinate basis according to the method described in Refs. [63,64].

7.4 Illustrative calculations

The analytical-derivative methods at the MP2 level as well as at the HF level have been used to calculate the equilibrium structures and harmonic vibrational frequencies of all-*trans* polyacetylene. The results are given in Tables 7.1 and 7.2.

In order to obtain correct MP2 energies, it is essential to use a suitably converged HF wave functions and energy band structures. In the first two columns of Table 7.1, the structural parameters and total energies calculated at the HF/STO-3G level by using our crystal orbital program are compared with those estimated from the oligomer (cluster) calculations. We have carried out geometry optimizations for oligoenes with 28 and 26 carbon atoms using the GAUSSIAN 94 program [65]. The structural parameters given in the second column of Table 7.1 are extracted from the central part of the longer oligoene, and the total energy is obtained as the energy difference between these two oligoenes. The results obtained by these two different methods agree with each other completely. We point out that the numerical accuracy of the crystal orbital calculations at the HF/STO-3G level is strongly influenced by the cutoff criterion of the long-range Coulomb and exchange summation [66]. The Namur cutoff criterion [53,54] adopted here has been shown to give the fastest convergence for total energy and other properties [66]. In his thorough investigation of this convergence behavior [66], Teramae has optimized the geometry of all-*trans* polyacetylene using several different cutoff criteria. The structural parameters and total energy obtained with the Namur cutoff criterion by Teramae are also in complete agreement with our results. Optimized geometry obtained in this study as well as that obtained by Teramae is also in reasonable agreement with the results previously reported by Karpfen and Petkov [67], by Karpfen and Höller [68], and by Teramae [69].

In the third and fourth columns of Table 7.1 are given the structural parameters and total energies calculated at the MP2/STO-3G level using the crystal orbital and the oligomer (cluster) methods. The structural parameters obtained by these two methods agree with each other to the first four significant figures. This result not only ensures the accuracy of the present analytical-gradient method but also indicates that the structural parameters of oligoenes with 28 carbon atoms converge at the corresponding values of an infinite chain. The MP2 correction $E^{(2)}$ obtained from the crystal orbital calculations is in agreement within 2×10^{-5} hartree with the value obtained as the finite difference of the oligomer results. The structural parameters obtained from our MP2/STO-3G calculations

Table 7.1 Optimized structural parameters and HF and MP2 energies of all-*trans* polyacetylene. Bond lengths in Å bond angles in degrees, and energies in hartree.

	STO-3G				6-31G	
	HF[a,b]	HF[c]	MP2[a]	MP2[c]	HF[a]	MP2[a]
C=C length	1.326	1.326	1.371	1.371	1.339	1.377
C–C length	1.477	1.477	1.485	1.485	1.451	1.449
C–H length	1.084	1.084	1.103	1.103	1.077	1.097
CCC angle	124.0	124.0	123.7	123.7	124.3	124.2
C=CH angle	119.8	119.8	119.3	119.3	119.1	118.5
E_{HF}	−75.94793	−75.94794	−75.94459	−75.94458	−76.86132	−76.85945
$E^{(2)}$	...	...	−0.12325	−0.12323	...	−0.17990

[a] Crystal orbital calculations. [b] See also Refs. [66–69]. [c] Oligomer (cluster) calculations.

are also in reasonable agreement with those reported previously by Suhai [14], but the C=CH angle he obtained is smaller than our optimized value by about 1 degree.

The structural parameters and total energies obtained at the HF/6-31G and MP2/6-31G levels are also given in Table 7.1. The results obtained at the HF/6-31G level are consistent with the structural parameters of a long oligoene ($C_{22}H_{24}$) reported by Villar *et al.* [70]. As has already been established [12], electron correlation reduces the degree of bond alternation (C–C bond length minus C=C bond length). From the results of the 6-31G calculations, it is seen that the C=C bond length increases substantially upon inclusion of electron correlation, while the C–C bond length decreases only by 0.002 Å. The C=C and C–C bond lengths optimized at the MP2/6-31G level (1.377 and 1.449 Å) are in reasonable agreement with the values (1.36 and 1.44 Å) measured by nutation NMR technique [71]. Effects of electron correlation on the bond alternation of all-*trans* polyacetylene have also been investigated by Suhai [12,18].

In Table 7.2, the calculated frequencies of the infrared- and Raman-active ($k = 0$) vibrations are compared with the observed frequencies taken from Refs. [29,34,72]. Here we assign weak infrared bands at 1170 and 861 cm^{-1} to the ν_6 modes of normal and perdeuterated species, respectively, according to our previous studies [9,41]. Teramae [66] has reported the calculated frequencies of $k = 0$ vibrations at the HF/STO-3G level using the analytical energy gradients. The frequencies given in Table 7.2, which are calculated by using the analytical second derivatives, agree with those obtained by Teramae within 2 cm^{-1}. At the HF/6-31G level, Cui *et al.* [73] extrapolated the vibrational frequencies of an infinite chain from those of a long oligoene ($C_{22}H_{24}$). The frequencies estimated by Cui *et al.* are also in agreement with our results within 5 cm^{-1}.

Table 7.2 Calculated and observed frequencies (in units of cm^{-1}) of the infrared- and Raman-active modes of all-*trans* polyacetylene and its perdeuterated analog. The values in parentheses are the percentage deviations from the observed frequencies.

Species	Mode[a]		Obs.[b]	STO-3G				6-31G			
				HF[c]		MP2		HF		MP2	
t-$(C_2H_2)_x$	a_g	ν_1	2990	3713	(24)	3490	(17)	3320	(11)	3122	(4)
		ν_2	1457	2005	(38)	1729	(19)	1846	(27)	1569	(8)
		ν_3	1294	1547	(20)	1418	(10)	1464	(13)	1344	(4)
		ν_4	1066	1352	(27)	1247	(17)	1306	(23)	1189	(12)
	b_u	ν_5	3013	3693	(22)	3490	(16)	3330	(11)	3133	(4)
		ν_6	1170	1380	(18)	1281	(9)	1340	(15)	1253	(7)
	a_u	ν_7	1012	1255	(24)	1146	(13)	1172	(16)	1017	(0)
	b_g	ν_8	884	1086	(23)	926	(5)	1090	(23)	825	(−7)
t-$(C_2D_2)_x$	a_g	ν_1	2230	2777	(25)	2603	(17)	2472	(11)	2319	(4)
		ν_2	1347	1950	(45)	1662	(23)	1789	(33)	1489	(11)
		ν_3	1201	1387	(15)	1283	(7)	1332	(11)	1237	(3)
		ν_4	852	1037	(22)	962	(13)	995	(17)	918	(8)
	b_u	ν_5	2231	2711	(22)	2563	(15)	2445	(10)	2300	(3)
		ν_6	861	1013	(18)	941	(9)	984	(14)	920	(7)
	a_u	ν_7	746	921	(23)	841	(13)	861	(15)	747	(0)
	b_g	ν_8	816	974	(19)	830	(2)	978	(20)	740	(−9)

[a] The normal modes are classified under the factor group isomorphous to the point group C_{2h}.
[b] References [29,34,72]. [c] See also Ref. [66].

The frequencies calculated at the HF level are invariably higher than the observed with the deviations being 15 – 45 % in the STO-3G result and 10 – 33 % in the 6-31G result. The largest deviations can be found for the ν_2 modes of the normal and perdeuterated species. These modes are the so-called "in-phase C=C stretching modes," which give rise to intense Raman bands. The in-phase C=C stretching mode is approximately regarded as a linear combination of the C=C bond stretch and the C–C bond shrinkage. Since the highest occupied orbital of polyacetylene has bonding character for the C=C bonds and antibonding character for the C–C bonds and the lowest unoccupied orbital is C=C antibonding and C–C bonding, the energy levels of these orbitals strongly couple with the in-phase C=C stretching vibrations. Electron correlation has profound effects on the frequencies of these vibrations since correlation mixes the HF ground-state wave function with the double-excitation configuration in which electrons are promoted from the highest occupied orbital to the lowest unoccupied orbital. Specifically, electron correlation lowers the frequencies of the in-phase C=C stretching modes [9,40,41]. The reduction of the magnitude of bond alternation upon inclusion of electron correlation can likewise be accounted for in terms of the highest occupied and lowest unoccupied orbitals.

It is seen from Table 7.2 that the inclusion of electron correlation at the MP2 level

significantly lowers the frequencies and improves the agreement between the calculations and experiments. The differences between the frequencies calculated at the MP2/STO-3G level and the observed are roughly one half of those found in the HF/STO-3G results. As expected from the above consideration, the largest improvement can be seen in the in-phase C=C stretching (ν_2) modes; the calculated frequencies of ν_2 modes of the normal and perdeuterated species shift to lower frequencies by as large as 276 and 288 cm^{-1}, respectively, on going from HF theory to MP2 theory. Nevertheless, the frequencies of these modes calculated at the MP2/STO-3G level are still overestimated by about 20 %. The use of 6-31G basis set leads to substantially improved agreement between the calculated and observed frequencies. At the HF/6-31G level, the percentage deviations for the in-phase C=C stretching modes are 27 and 33 % for normal and perdeuterated species, respectively. Inclusion of electron correlation at the MP2 theory accounts for about 70 % of these errors and as a result the calculated frequencies at this level of theory are in reasonable agreement with the observed frequencies for all the normal modes including the in-phase C=C stretching modes. Electron correlation effects are larger on the frequencies calculated with the 6-31G basis set than those obtained with the STO-3G basis set, probably because the number of virtual orbitals used in correlation correction increases as the basis set becomes larger. The percentage deviations of the frequencies calculated at the MP2/6-31G level are not uniform unlike the results obtained with hybrid HF/density functional theory with a comparable basis set [9]; overall, the MP2/6-31G theory overestimates the frequencies of the in-plane modes by $3 - 12$ %, while it underestimates the frequencies of the out-of-plane modes by $0 - 9$ %. This is consistent with the results of the MP2 calculations on all-*trans* oligoenes [41,74].

The execution times for the various steps of MP2 energy and gradient calculations are given in Table 7.3. The evaluation of energy gradients takes 8.6 times the execution time required to calculate the total energy alone. This ratio is substantially larger than those obtained by using the disk-based [44] or semi-direct [75] MP2 gradient schemes for molecules, primarily because we are currently using old algorithms for the evaluation of two-electron integral derivatives and the transformation of integrals. Nevertheless, the analytical-gradient method, as implemented in this study, has the advantage over the use of finite differences of total energies in the vibrational frequency calculations of polymers. The number of total energy calculations required to obtain energy gradients at a given structure by using the finite-difference method is $6n$ where n is the number of nuclei in

Table 7.3 Execution times (the sum of CPU and I/O times in seconds) for all-*trans* polyacetylene at the MP2/STO-3G level. All the calculations have been performed on an HP Exemplar workstation of our laboratory with the compile options "+DS2.0a +DA2.0N +O3 +Onolimit +Odataprefetch".

Step	Energy	Gradients
Two-electron integrals	148	148
SCF	13	13
First derivatives of two-electron integrals	...	2327
CPHF equation	...	359
Integral transformation + accumulation of $E^{(2)}$ and $\partial E^{(2)}/\partial x$	582	3403
Total[a]	745	6393

[a] Total execution times include small steps which have not been tabulated separately.

the unit cell. Therefore, for the vibrational frequency calculations of polyacetylene at the MP2/STO-3G level, our analytical-gradient method will be roughly twice as efficient as the finite-difference method. It is also expected that higher accuracy is obtained for the force fields and vibrational frequencies by the analytical-gradient method than by the finite-different method [49,76].

7.5 Conclusion

We have developed an analytical-gradient method in ab initio MP2 crystal orbital theory of polymers. We have applied the method to the geometry optimizations and vibrational analyses of all-*trans* polyacetylene. Inclusion of electron correlation at the MP2/6-31G level accounts for about 70 % of the differences between the frequencies calculated at the HF/6-31G level and the observed ones for the in-phase C=C stretching modes. Comparison of the execution times between the single point energy calculation and the gradient calculation indicates that the analytical-gradient method is more efficient than the finite-difference method in the vibrational frequency calculations of polymers. In order to extend the applicability of the MP2 analytical-gradient method to polymers with larger unit cells, we will have to invoke the direct [61,77] or semi-direct [75] techniques, which will require less disk space than the present algorithm. The authors believe that the present implementation serves as a basis for such extension.

References

[1] D. I. Bower and W. F. Maddams, *The Vibrational Spectroscopy of Polymers* (Cambridge University Press, Cambridge, 1989).

[2] G. Del Re, J. Ladik, and G. Biczó, Phys. Rev., **155,** 997 (1967).

[3] J. M. André, J. Chem. Phys., **50,** 1536 (1969).

[4] M. Kertész, Adv. Quantum Chem., **15,** 161 (1982).

[5] J. J. Ladik, *Quantum Theory of Polymers as Solids* (Plenum, New York, 1988).

[6] H. Teramae, T. Yamabe, C. Satoko, and A. Imamura, Chem. Phys. Lett., **101,** 149 (1983).

[7] H. Teramae, T. Yamabe, and A. Imamura, J. Chem. Phys., **81,** 3564 (1984).

[8] Chapter 6 of the present thesis.

[9] Chapter 3 of the present thesis.

[10] J.-Q. Sun and R. J. Bartlett, J. Chem. Phys., **108,** 301 (1998).

[11] Chapter 4 of the present thesis.

[12] S. Suhai, Chem. Phys. Lett., **96,** 619 (1983); Phys. Rev. B, **27,** 3506 (1983).

[13] S. Suhai, Int. J. Quantum Chem., **23,** 1239 (1983).

[14] S. Suhai, Int. J. Quantum Chem., **42,** 193 (1992).

[15] S. Suhai, J. Chem. Phys., **84,** 5071 (1986).

[16] S. Suhai, Int. J. Quantum Chem. Quantum Chem. Symp., **27,** 131 (1993).

[17] S. Suhai, J. Chem. Phys., **101,** 9766 (1994).

[18] S. Suhai, Phys. Rev. B, **51,** 16553 (1995).

[19] S. Suhai, Phys. Rev. B, **52,** 1674 (1995).

[20] C.-M. Liegener, J. Chem. Phys., **88,** 6999 (1988).

[21] Y.-J. Ye, W. Förner, and J. Ladik, Chem. Phys., **178,** 1 (1993).

[22] J.-Q. Sun and R. J. Bartlett, J. Chem. Phys., **104,** 8553 (1996).

[23] J.-Q. Sun and R. J. Bartlett, Phys. Rev. Lett., **77,** 3669 (1996).

[24] J.-Q. Sun and R. J. Bartlett, J. Chem. Phys., **106,** 5554 (1997).

[25] W. Förner, R. Knab, J. Čížek, and J. Ladik, J. Chem. Phys., **106,** 10248 (1997).

[26] J.-Q. Sun and R. J. Bartlett, J. Chem. Phys., **107,** 5058 (1997).

[27] J.-Q. Sun and R. J. Bartlett, Phys. Rev. Lett., **80,** 349 (1998).

[28] J. C. W. Chien, *Polyacetylene: Chemistry, Physics, and Material Science* (Academic, Orlando, 1984).

[29] H. Shirakawa and S. Ikeda, Polym. J., **2,** 231 (1971).

[30] H. Shirakawa, T. Ito, and S. Ikeda, Polym. J., **4,** 460 (1973).

[31] I. Harada, M. Tasumi, H. Shirakawa, and S. Ikeda, Chem. Lett., **1978,** 1411.

[32] S. Lefrant, L. S. Lichtmann, H. Temkin, D. B. Fitchen, D. C. Miller, G. E. Whitwell, II, and J. M. Burlitch, Solid State Commun., **29,** 191 (1979).

[33] I. Harada, Y. Furukawa, M. Tasumi, H. Shirakawa, and S. Ikeda, J. Chem. Phys., **73,** 4746 (1980).

[34] H. Kuzmany, Phys. Status Solidi B, **97,** 521 (1980).

[35] F. B. Schügerl and H. Kuzmany, J. Chem. Phys., **74,** 953 (1981).

[36] P. Piaggio, G. Dellepiane, L. Piseri, R. Tubino, and C. Taliani, Solid State Commun., **50,** 947 (1984).

[37] M. Gussoni, C. Castiglioni, and G. Zerbi, in *Spectroscopy of Advanced Materials,* edited by R. J. H. Clark and R. E. Hester (Wiley, 1991), p. 251.

[38] Y. Furukawa, in *The Chemistry of Dienes and Polyenes,* edited by Z. Rappoport (Wiley, 1997), p. 149.

[39] F. Inagaki, M. Tasumi, and T. Miyazawa, J. Raman Spectrosc., **3,** 335 (1975); M. Tasumi, J. Raman Spectrosc., **13,** 202 (1982).

[40] M. Kofranek, H. Lischka, and A. Karpfen, J. Chem. Phys., **96,** 982 (1992).

[41] S. Hirata, H. Torii, and M. Tasumi, J. Chem. Phys., **103,** 8964 (1995).

[42] Chapter 2 of the present thesis.

[43] P. Pulay, Mol. Phys., **17,** 197 (1969); **18,** 473 (1970).

[44] J. A. Pople, R. Krishnan, H. B. Schlegel, and J. S. Binkley, Int. J. Quantum Chem. Quantum Chem. Symp., **13,** 225 (1979).

[45] J. Gerratt and I. M. Mills, J. Chem. Phys., **49,** 1719 (1968); **49,** 1730 (1968).

[46] Y. Yamaguchi, Y. Osamura, J. D. Goddard, and H. F. Schaefer III, *A New Dimension to Quantum Chemistry: Analytic Derivative Methods in Ab Initio Molecular Electronic Structure Theory* (Oxford University Press, New York, 1994).

[47] C. Møller and M. S. Plesset, Phys. Rev., **46,** 618 (1934).

[48] A. Szabo and N. S. Ostlund, *Modern Quantum Chemistry: Introduction to Advanced Electronic Structure Theory* (Macmillan, New York, 1982).

[49] W. J. Hehre, L. Radom, P. v. R. Schleyer, and J. A. Pople, *Ab Initio Molecular Orbital Theory* (Wiley, New York, 1986).

[50] E. A. Salter, G. W. Trucks, G. Fitzgerald, and R. J. Bartlett, Chem. Phys. Lett., **141,** 61 (1987).

[51] W. J. Hehre, R. F. Stewart, and J. A. Pople, J. Chem. Phys., **51,** 2657 (1969).

[52] W. J. Hehre, R. Ditchfield, and J. A. Pople, J. Chem. Phys., **56,** 2257 (1972).

[53] J. Delhalle, L. Piela, J.-L. Brédas, and J.-M. André, Phys. Rev. B, **22,** 6254 (1980).

[54] J. M. André, D. P. Vercauteren, V. P. Bodart, and J. G. Fripiat, J. Comput. Chem., **5,** 535 (1984).

[55] P. Pulay, J. Chem. Phys., **78,** 5043 (1983).

[56] Y. Osamura, Y. Yamaguchi, and H. F. Schaefer, III, J. Chem. Phys., **77,** 383 (1982).

[57] M. Frisch, M. Head-Gordon, and J. Pople, Chem. Phys., **141,** 189 (1990).

[58] N. C. Handy and H. F. Schaefer, III, J. Chem. Phys., **81,** 5031 (1984).

[59] N. C. Handy, R. D. Amos, J. F. Gaw, J. E. Rice, and E. D. Simandiras, Chem. Phys. Lett., **120,** 151 (1985).

[60] J. E. Rice and R. D. Amos, Chem. Phys. Lett., **122,** 585 (1985).

[61] M. J. Frisch, M. Head-Gordon, and J. A. Pople, Chem. Phys. Lett., **166,** 275 (1990).

[62] P. Császár and P. Pulay, J. Mol. Struct., **114,** 31 (1984).

[63] M. Tasumi and T. Shimanouchi, J. Chem. Phys., **43,** 1245 (1965).

[64] L. Piseri and G. Zerbi, J. Mol. Spectrosc., **26,** 254 (1968).

[65] GAUSSIAN 94, Revision E.2, M. J. Frisch, G. W. Trucks, H. B. Schlegel, P. M. W. Gill, B. G. Johnson, M. A. Robb, J. R. Cheeseman, T. Keith, G. A. Petersson, J. A. Montgomery, K. Raghavachari, M. A. Al-Laham, V. G. Zakrzewski, J. V. Ortiz, J. B. Foresman, J. Cioslowski, B. B. Stefanov, A. Nanayakkara, M. Challacombe, C. Y. Peng, P. Y. Ayala, W. Chen, M. W. Wong, J. L. Andres, E. S. Replogle, R. Gomperts, R. L. Martin, D. J. Fox, J. S. Binkley, D. J. Defrees, J. Baker, J. P. Stewart, M. Head-Gordon, C. Gonzalez, and J. A. Pople, Gaussian, Inc., Pittsburgh PA, 1995.

[66] H. Teramae, Theor. Chim. Acta, **94,** 311 (1996).

[67] A. Karpfen and J. Petkov, Theor. Chim. Acta, **53,** 65 (1979).

[68] A. Karpfen and R. Höller, Solid State Commun., **37,** 179 (1981).

[69] H. Teramae, J. Chem. Phys., **85,** 990 (1986).

[70] H. O. Villar, M. Dupuis, J. D. Watts, G. J. B. Hurst, and E. Clementi, J. Chem. Phys., **88,** 1003 (1988).

[71] C. S. Yannoni and T. C. Clarke, Phys. Rev. Lett., **51,** 1191 (1983).

[72] H. Takeuchi, T. Arakawa, Y. Furukawa, I. Harada, and H. Shirakawa, J. Mol. Struct., **158,** 179 (1987).

[73] C. X. Cui, M. Kertesz, and M. Dupuis, J. Chem. Phys., **93,** 5890 (1990).

[74] S. Hirata, H. Yoshida, H. Torii, and M. Tasumi, J. Chem. Phys., **103,** 8955 (1995).

[75] M. J. Frisch, M. Head-Gordon, and J. A. Pople, Chem. Phys. Lett., **166,** 281 (1990).

[76] R. F. Hout, Jr., B. A. Levi, and W. J. Hehre, J. Comput. Chem., **3,** 234 (1982).

[77] J. Almlöf, K. Faegri, Jr., and K. Korsell, J. Comput. Chem., **3,** 385 (1982).

Chapter 8

Summary and general conclusion

In the present study, analytical-derivative methods have been developed within the framework of ab initio crystal orbital theory of one-dimensional lattices (polymers). Analytical energy gradients of hybrid HF/density functional energy and second-order Møller–Plesset perturbation energy and analytical second derivatives of the HF energy have been formulated and implemented for the first time. The analytical-derivative methods developed in this study have proven useful in determining the equilibrium structures and studying the normal vibrations of π-electron conjugated and non-conjugated hydrocarbon polymers and a consecutively hydrogen-bonded polymer. Since the structural parameters and vibrational frequencies of conjugated oligomers and hydrogen-bonded oligomers strongly depend on the chain length, crystal orbital theory is virtually the only means to derive reliable energetic, structural, and vibrational information for the infinite analogs of them. The results of the present study are summarized in the following.

In Chapter 2, we have implemented the self-consistent-field procedure of LCAO density functional crystal orbital theory. We have examined the exchange-correlation-functional dependence of the structures of polyacetylene isomers. The crystal orbital calculations indicate that exact-exchange mixing is essential in describing the electronic and structural properties of polyacetylene; the exchange-correlation functionals without exact-exchange mixing lead to unrealistic potential energy curves along the bond-alternation coordinate. The structural parameters and photoelectron spectra of *trans*- and *cis*-polyacetylene calculated using the B3LYP functional, in which the exact-exchange matrix elements are admixed, are in reasonably good agreement with the experimental results. The B3LYP functional correctly predicts the total energies of polyacetylene isomers in the order expected from experiment.

In Chapter 3, we have described the formulas and computer implementation of analytical-gradient method for density functional and hybrid HF/density functional crystal orbital theories. We have found that the formula for the energy gradient with respect to the translational period contains a two-dimensional integral. This two-dimensional integral can be transformed to three-dimensional integrals by virtue of Gauss theorem, and the latter integrals are evaluated conveniently by Becke's atomic partitioning scheme. We have carried out geometry optimizations and harmonic vibrational frequency calculations of *trans*- and *cis*-polyacetylene and *anti*- and *syn*-polymethineimine using the B3LYP functional. The calculated frequencies of polyacetylene agree very well with the experimental results. This result implies that the density functional calculations using the hybrid

exchange-correlation functionals can reproduce the vibrational spectra of a variety of conjugated polymers with considerable accuracy. We have found that the total energy of the *syn* isomer of polymethineimine is lower than that of the *anti* isomer by 15.6 kJ mol^{-1}. The calculated frequencies also appear to be in reasonable agreement with the observed frequencies if we assume that the polymer samples synthesized by Wöhrle consist of the *syn* isomer. However, because of a limited number of observed frequencies available, we could not conclude unambiguously which isomer the actual samples of polymethineimine consist of. The present calculations, nevertheless, indicate that the previous assumption that polymethineimine takes the *anti* form is ungrounded.

In Chapter 4, we have applied the analytical-gradient methods to the calculations of the infrared- and Raman-active vibrations, phonon dispersion curves, and inelastic neutron scattering spectra for all-*trans* polyethylene using SVWN, BLYP, and B3LYP functionals. We have found that the basis-set dependence is more important for the calculated structural parameters and vibrational frequencies than the choice of exchange-correlation functional. This result is in striking contrast with the results obtained for polyacetylene (Chapters 2 and 3). The calculated frequencies, phonon dispersion curves, and inelastic neutron scattering spectra are in reasonably good agreement with the experimental results. In the simulation of inelastic neutron scattering spectra, we have taken into account the effects of Debye–Waller factors and phonon wings.

Crystalline hydrogen fluoride consists of planar zigzag hydrogen-bonded chains of hydrogen fluoride molecules, which have only weak interchain interactions. In Chapter 5, we have presented the structural parameters, binding energies, and vibrational frequencies of an infinite hydrogen fluoride polymer calculated by using the BLYP and B3LYP density functional theory as well as HF theory with the 6-311++G(d,p) basis set. We have concluded that the HF level seriously underestimates the cooperative binding effects of consecutive hydrogen bonds, whereas the density functional methods slightly overestimate this property. Assignment of the librational modes of crystalline hydrogen fluoride has been made with greater certainty on the basis of the calculated frequencies.

In Chapter 6, we have introduced an analytical-second-derivative method for ab initio HF crystal orbital theory of polymers. We have derived the polymer version of coupled perturbed Hartree–Fock (CPHF) equation, which has been implemented in the direct atomic-orbital-based algorithms and in the conventional crystal-orbital-based algorithms. We have shown that the number of independent wavevector indices of two-electron inte-

grals in polymer CPHF equation can be reduced to two. Our analytical-second-derivative method has turned out to be less expensive than the finite-difference method in the vibrational frequency calculations of polymers. The second derivative calculation using the atomic-orbital-based algorithm is only 1.3 times as costly as that using the crystal-orbital-based algorithm. Considering the intensive use of the external storage in the latter algorithm, we conclude that there is no advantage in using the crystal-orbital-based algorithm instead of using the atomic-orbital-based algorithm for the vibrational frequency calculations of polymers.

In Chapter 7, we have described the formalism and computer implementation of an analytical-gradient method for ab initio MP2 crystal orbital theory. The CPHF equation has been solved iteratively using the atomic-orbital-based algorithms. Although the two-electron integrals and their first derivatives have to be stored externally, the integral transformation of the first derivatives has been avoided with the aid of the two-particle density matrix. The method has been applied to the geometry optimization and vibrational frequency calculations of *trans*-polyacetylene. The inclusion of electron correlation at the MP2/6-31G level accounts for about 70 % of the differences between the frequencies calculated at the HF level and the observed frequencies.

Acknowledgment

The present research program has been conducted under the supervision of Professor Suehiro Iwata of Institute for Molecular Science. The author would like to express his sincere gratitude for Professor Iwata's kind guidance and encouragement. The studies on polyacetylene isomers described in Chapter 2 have been carried out in collaboration with Professor Mitsuo Tasumi and Dr. Hajime Torii at The University of Tokyo. The author gratefully acknowledges their guidance and helpful discussions. The author would like to thank all the members of Professor Iwata's laboratory for numerous advises and technical help. The present work was financially supported by the Research Fellowship of the Japan Society for the Promotion of Science for Young Scientists.